Base-Induced Elimination Reactions

An Experimental and Theoretical Study on Gas-Phase Reactions

Base-Induced Elimination Reactions

An Experimental and Theoretical Study
on Gas-Phase Reactions

ACADEMISCH PROEFSCHRIFT

ter verkrijging van de graad van doctor
aan de Universiteit van Amsterdam,
op gezag van de Rector Magnificus
Prof. Dr. P.W.M. de Meijer
in het openbaar te verdedigen in de Aula der Universiteit
(Oude Lutherse Kerk, ingang Singel 411, hoek Spui),
op woensdag 17 februari 1993 te 15.00 uur

door

Friedrich Matthias Bickelhaupt

geboren te Amstelveen

Promotor: Prof. Dr. N.M.M. Nibbering
Co-Promotor: Prof. Dr. E.J. Baerends

The research reported in this thesis was carried out at the Instituut voor Massaspectrometrie, Faculteit Scheikunde, Universiteit van Amsterdam and at the Afdeling Theoretische Chemie, Faculteit Scheikunde, Vrije Universiteit te Amsterdam. Part of this work was financially supported by the Stichting Nationale Computer Faciliteiten (NCF) of the Nederlandse Organisatie voor Wetenschappelijk Onderzoek (NWO).

Meinen Eltern
Para Célia

Contents

1 General Introduction

Base-induced alkene-forming 1,2-elimination reactions (Equation 1) constitute one of the basic types of reaction in organic chemistry.[1]

$$B^- + H\text{-}C^{\beta}R_2\text{-}C^{\alpha}R_2\text{-}L \longrightarrow B\text{-}H + CR_2{=}CR_2 + L^- \qquad (1)$$

They are involved in the synthesis of many important and interesting compounds. Sometimes, base-induced elimination reactions play a key role in the formation of the compound of interest, as in the synthesis of [n]metacyclophanes[2,3] (**1**, Scheme I); in many other cases, like in the synthesis of chlorophyll[4,5] (**2**), they are less conspicuous, but nevertheless indispensable for success. Their importance is further illustrated by the key role they play in fundamental processes of life as, for example, Vitamin B_6 catalyzed conversions of α-amino and α-keto acids.[6]

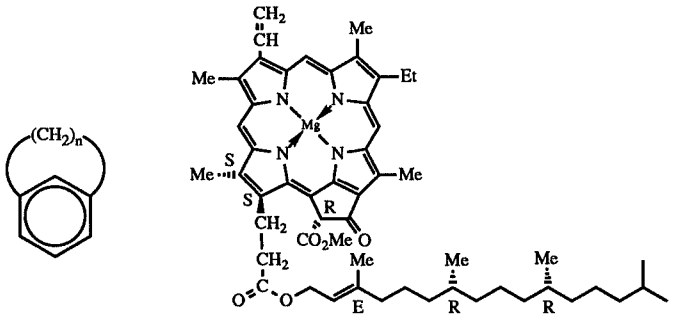

1 **2**

Scheme I

Another interesting perspective of elimination reactions is that they are the reverse counterpart of addition reactions[1] (Equation 2) and knowledge of the former also contributes to the

understanding of the latter.

$$B\text{-}Z + CR_2{=}CR_2 + Nu^- \longrightarrow B^- + Z\text{-}CR_2\text{-}CR_2\text{-}Nu \quad (2)$$

Finally, in explaining the importance of base-induced elimination reactions it should also be mentioned that they can occur as unwanted side-reactions which are very often in competition with the important reaction type of nucleophilic substitution[1] (Equation 3).

$$B^- + H\text{-}C^{\beta}R_2\text{-}C^{\alpha}R_2\text{-}L \longrightarrow H\text{-}C^{\beta}R_2\text{-}C^{\alpha}R_2\text{-}B + L^- \quad (3)$$

From the foregoing discussion it appears that a profound understanding of base-induced elimination reactions is of great importance in organic chemistry. Since in 1927 Ingold[7,8] introduced the concept of "base-promoted olefine-forming elimination reactions", many experimental investigations have been performed on this class of reactions in the condensed phase[9-18] as well as in the gas phase.[19–28] Considerable experience has been gathered concerning the parameters which determine the reaction rates, the product distribution and the stereochemistry. The nature of base-induced alkene-forming 1,2-elimination reactions is now well understood and interpreted in terms of the concept of the Variable Transition State (VTS).[29] In this concept, reactions are classified according to the geometry of the transition state (TS), which is conceived as being located at one point in a continuous spectrum of mechanistic possibilities (Figure 1). The VTS theory comprises the Bunnet E2H-spectrum,[14,15] i.e. E1cb(-like), central or ideal synchronous E2, and E1(-like) eliminations involving linear proton transfer, as well as the Winstein-Parker E2H-E2C-spectrum[16–18] in which bent proton transfer may occur with a certain degree of base/C^{α} covalent interaction. From theoretical investigations it follows, that stereoelectronic arguments account for the preference of TS structures in which the base and the leaving group are anti- or syn-*periplanar* (Figure 1).[30-33]

Still, however, a number of fundamental and interesting aspects concerning base-induced elimination reactions exist which have received only very little attention in mechanistic studies. It is the purpose of the work described in this thesis to investigate these aspects in order to achieve a more complete understanding of the nature of this class of reactions. This is accomplished in a

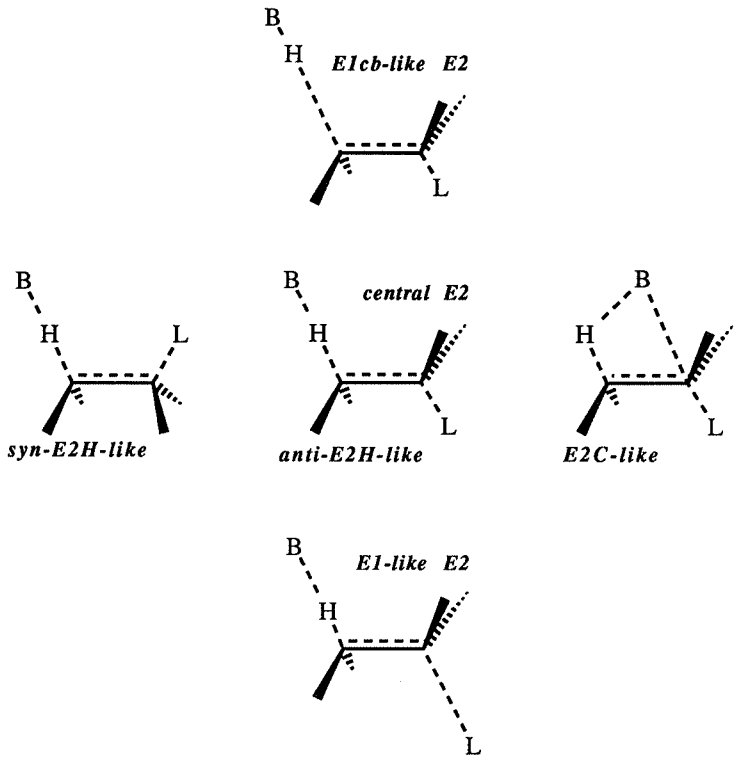

***Figure 1**. Mechanistic spectrum of transition states of base-induced 1,2-elimination reactions.*

combined Fourier Transform Ion Cyclotron Resonance (FT-ICR) mass spectrometric[34] and density-functional (DF) theoretical[35,36] approach. The experimental (FT-ICR)[34] and quantum theoretical (DF)[35,36] methods employed are described in chapter 2. In chapter 3 the effect of replacement of the $C^{\alpha}R_2$ group of the substrate (Equation 1) by $N^{\alpha}R$ (Equation 4) is studied through investigation of the base-induced heteroalkene-forming 1,2-eliminations of N,O-dimethylhydroxylamine (DHA) in the gas phase.

$$B^- + H\text{-}C^{\beta}R_2\text{-}N^{\alpha}R\text{-}L \longrightarrow B\text{-}H + CR_2{=}NR + L^- \qquad (4)$$

In chapter 4 the effect of integration of the C^{α}-L bond into a cyclic structure on the reactivity pattern of base-induced alkene-forming 1,2-eliminations is investigated using tetrahydrofuran

(THF) as the substrate. An interesting item that is addressed concerns the question on the origin of the [H_2O, OH^-] cluster that is formed as a secondary product anion in the reaction system OH^- + THF + H_2O. Next, in chapter 5, the multi-step processes in the gas-phase reactions of halomethyl anions XCH_2^- (X = Cl, Br) with CH_3X and NH_3 are studied. The occurrence of secondary base-induced ethene-forming 1,2-elimination reactions which proceed from a relatively long-lived intermediate anion/molecule complex is discussed. Finally, chapter 6 presents the results of a DF theoretical investigation on the model reaction system F^- + CH_3CH_2F which has also been studied by Minato and Yamabe.[31,32] In the present theoretical study the 2-dimensional reaction energy surface E[d(C^β-H),d(C^α-F)] is explored for the fluoride-induced 1,2-elimination in which the C^β-H and C^α-F bonds are broken. Besides a quantitative description the main objective of this study is a qualitative understanding of the nature of base-induced 1,2-elimination reactions. In particular the role of the base as a catalyst for the elimination of HF from fluoroethane is discussed.

References

1. Carey, F.A.; Sundberg, R.J. *Advanced Organic Chemistry*, Part A; Plenum Press: New York, 1984.
2. Turkenburg, L.A.M.; Blok, P.M.L.; Wolf, W.H. de; Bickelhaupt, F. *Tetrahedron Lett.* **1981**, 22, 3317.
3. Kraakman, P.A.; Valk, J.-M.; Niederländer, H.A.G.; Brouwer, D.B.E.; Bickelhaupt, F.M.; Wolf, W.H. de; Bickelhaupt, F.; Stam, C.H. *J. Am. Chem. Soc.* **1990**, 112, 6638.
4. Woodward, R.B.; Ayer, W.A.; Beaton, J.M.; Bickelhaupt, F.; Bonnett, R.; Buchschacher, P.; Closs, G.L.; Dutler, H.; Hannah, J.; Hauck, F.P.; Itô, S.; Langemann, A.; Le Goff, E.; Leimgruber, W.; Lwowski, W.; Sauer, J.; Valenta, Z.; Volz, H. *J. Am. Chem. Soc.* **1960**, 82, 3800.
5. Woodward, R.B.; Ayer, W.A.; Beaton, J.M.; Bickelhaupt, F.; Bonnett, R.; Buchschacher, P.; Closs, G.L.; Dutler, H.; Hannah, J.; Hauck, F.P.; Itô, S.; Langemann, A.; Le Goff, E.; Leimgruber, W.; Lwowski, W.; Sauer, J.; Valenta, Z.; Volz, H. *Tetrahedron* **1990**, 22, 7599.

6. Martell, A.E. *Acc. Chem. Res.* **1989**, 22, 115.
7. Hanhart, W.; Ingold, C.K. *J. Chem. Soc.* **1927**, 997.
8. Hughes, E.D.; Ingold, C.K. *Trans. Faraday Soc.* **1941**, 37, 657.
9. Gandler, J.R. in *The Chemistry of Double-Bonded Functional Groups*, Vol. 2, Part I; Patai, S. Ed.; Wiley: New York, 1989.
10. Bartsch, R.A.; Závada, J. *Chem. Rev.* **1980**, 80, 453.
11. Saunders, W.H., Jr. *Acc. Chem. Res.* **1976**, 9, 19.
12. Bartsch, R.A. *Acc. Chem. Res.* **1975**, 8, 239.
13. Saunders, W.H., Jr.; Cockerill, A.F. *Mechanisms of Elimination Reactions*; Wiley: New York, 1973.
14. Bunnett, J.F. *Angew. Chem.* **1962**, 74, 731.
15. Bartsch, R.A.; Bunnett, J.F. *J. Am. Chem. Soc.* **1968**, 90, 408.
16. Parker, A.J.; Ruane, M.; Biale, G.; Winstein, S. *Tetrahedron Lett.* **1968**, 2113.
17. Biale, G.; Cook, D.; Lloyd, D.J.; Parker, A.J.; Stevens, I.D.R.; Takahashi, J.; Winstein, S. *J. Am. Chem. Soc.* **1971**, 93, 4735.
18. McLennan, D.J. *Tetrahedron* **1975**, 31, 2999.
19. Koning, L.J. de; Nibbering, N.M.M. *J. Am. Chem. Soc.* **1987**, 109, 1715.
20. Berkel, W.W. van; Koning, L.J. de; Nibbering, N.M.M. *J. Am. Chem. Soc.* **1987**, 109, 7602.
21. Koning, L.J. de; Nibbering, N.M.M. *J. Am. Chem. Soc.* **1988**, 110, 2066.
22. Ridge, D.P.; Beauchamp, J.L. *J. Am. Chem. Soc.* **1974**, 96, 637.
23. Sullivan, S.A.; Beauchamp, J.L. *J. Am. Chem. Soc.* **1976**, 98, 1160.
24. Sullivan, S.A.; Beauchamp, J.L. *J. Am. Chem. Soc.* **1977**, 99, 5017.
25. Doorn, R. van; Jennings, K.R. *Org. Mass Spectrom.* **1981**, 16, 397.
26. DePuy, C.H.; Bierbaum, V.M. *J. Am. Chem. Soc.* **1981**, 103, 5034.
27. DePuy, C.H.; Beedle, E.C.; Bierbaum, V.M. *J. Am. Chem. Soc.* **1982**, 104, 6483.
28. Bierbaum, V.M.; Filley, J.; DePuy, C.H.; Jarrold, M.F.; Bowers, M.T. *J. Am. Chem. Soc.* **1985**, 107, 2818.
29. Lowry, T.H.; Richardson, K.S. *Mechanism and Theory in Organic Chemistry*, 2nd ed.; Harper and Row: New York, 1981.
30. Bach, R.D.; Badger, R.C.; Lang, T.J. *J. Am. Chem. Soc.* **1979**, 101, 2845.

31. Minato, T.; Yamabe, S. *J. Am. Chem. Soc.* **1985**, 107, 4621.

32. Minato, T.; Yamabe, S. *J. Am. Chem. Soc.* **1988**, 110, 4586.

33. Albright, T.A.; Burdett, J.K.; Whangbo, M.-H. *Orbital Interactions in Chemistry*, Wiley: New York, 1985.

34. Nibbering, N.M.M. *Acc. Chem. Res.* **1990**, 23, 279.

35. Parr, R.G.; Yang, W. *Density-Functional Theory of Atoms and Molecules*, Oxford University Press: New York, 1989.

36. Baerends, E.J.; Ros, P. *Int. J. Quantum Chem., Quantum Chem. Symp.* **1978**, S12, 169.

2 Experimental and Theoretical Methods

2.1 Introduction

This chapter briefly describes the experimental and quantum theoretical methods which have been employed in the studies of this thesis. In the following section, 2.2, an overview is given of the Fourier Transform Ion Cyclotron Resonance (FT-ICR) mass spectrometric method and its basic equations. Furthermore, a typical FT-ICR experiment is described and the essential features of gas-phase ion/molecule reactions are discussed. Next, section 2.3 deals with the fundamental concepts of density-functional theory (DFT) and with the procedure in which bonding mechanisms are evaluated in the Amsterdam Density-Functional (ADF) program system.

2.2 Fourier Transform Ion Cyclotron Resonance

The Principle

Fourier Transform Ion Cyclotron Resonance (FT-ICR) mass spectrometry[1-5] is based on the movement of ions in combined static magnetic and electric fields according to their equation of motion:[6]

$$m\frac{d^2\vec{r}}{dt^2} = q\left(\frac{d\vec{r}}{dt} \times \vec{B} + \vec{E}\right) - m\zeta\frac{d\vec{r}}{dt} \qquad (1)$$

where $\vec{r} = x\,\vec{e}_x + y\,\vec{e}_y + z\,\vec{e}_z$, m and q are the position, the mass and the charge of the ion, respectively, and $\vec{B}$ and $\vec{E}$ represent the magnetic induction and the electric field strength. Through the effective friction constant ζ the effect of momentum transfer due to ion/molecule collisions is introduced.

The principle of FT-ICR is best explained for a homogeneous magnetic field with $\vec{B} = B\,\vec{e}_z$ in the absence of an electric field ($\vec{E} = 0$) in which case the solution of Equation 1 is given by:

$$R(t) = x(t) + i\,y(t) = R(0)\,e^{-\zeta t}\,e^{i\omega_C t} \tag{2 a}$$

with $$\omega_C = \frac{q\,B}{m} \tag{2 b}$$

and $$z(t) = z(0) + \frac{v_z(0)}{\zeta}\left(1 - e^{-\zeta t}\right) \tag{2 c}$$

From Equations 2 it follows that the motion of the ions is constrained to circular orbits in the xy-plane perpendicular to the magnetic field. The amplitude of this so-called cyclotron motion exponentially decays with time due to ion/molecule collisions. Furthermore, the cyclotron frequency ω_C depends inversely proportional on m/q, i.e. the mass over charge ratio of the ion. In principle, therefore, the information for a mass spectrum of the ions trapped in the xy-plane is contained in their combined electromagnetic signals $I_t(t)$ as a function of time:

$$I_t(t) = k\sum_j N_j\,R_j(t) = k\sum_j N_j\,R_j(0)\,e^{-\zeta_j t}\,e^{i\,\omega_{C,j} t} \tag{3}$$

This time-domain signal is proportional to the cyclotron radii of all ions. In Equation 3 the summation runs over ions of different $\omega_{C,j}$ and N_j is the number of ions with this cyclotron frequency, where it has been assumed that all ions with the same cyclotron frequency have the same cyclotron radius at $t = 0$. This situation is achieved in a cubic FT-ICR cell (Figure 1a) when the ions are generated in the center of the cell, e.g. by electron impact (EI), and subsequently coherently excited for all $\omega_{C,j}$ via application of a radio-frequent electric field on the transmitter plates (Figure 1a) which sweeps in a short time (1-2 ms) through the appropriate frequency interval $\Delta\nu = \Delta\omega/2\pi$. The measurement of $I_t(t)$ then is analogously performed via detection of the image current that is induced in the receiver plates (Figure 1b). At this point, it should be stressed that de-phasing of the originally coherently orbiting ion ensemble is a very important reason for the decay of the measured signal, too. Finally, a frequency-domain signal and thus a mass spectrum is obtained through Fourier transformation (FT) of the transient time-domain signal $I_t(t)$:

$$I_\omega(\omega) = S \int_0^\infty I_t(t)\, e^{i\,\omega t}\, dt \qquad (4)$$

where S is a normalization constant. The complex spectrum $I_\omega(\omega) = I_A(\omega) + i\, I_D(\omega)$ is composed of the absorption spectrum $I_A(\omega)$, i.e. the cosine transform of $I_t(t)$, and the dispersion spectrum $I_D(\omega)$, i.e. the sine transform of $I_t(t)$. Very often an FT-ICR mass spectrum is represented by its magnitude spectrum $I_M(\omega)$ which is the absolute value of $I_\omega(\omega)$:

$$I_M(\omega) = |I_\omega(\omega)| = \sqrt{I_A(\omega)^2 + I_D(\omega)^2} \qquad (5)$$

Finally, it should be mentioned that the motion in a homogeneous magnetic field with $\vec{B} = B\,\vec{e}_z$ is unrestricted in the z-direction parallel to this field, except for a factor that leads to exponen-

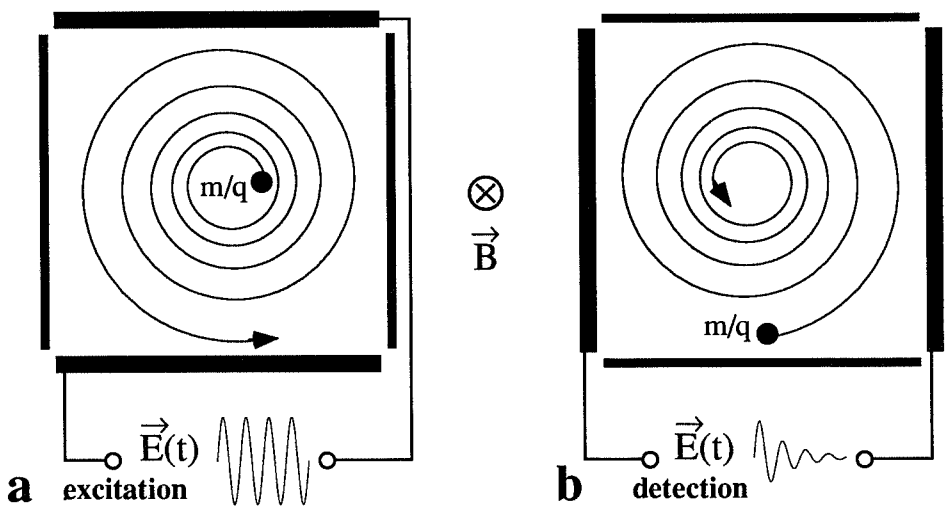

Figure 1. *xy-Cross section through the center of a cubic FT-ICR cell: (a) resonant excitation of the ion cyclotron motion through application of an appropriate oscillating electric field on the transmitter plates, (b) measurement of the decaying ion cyclotron motion of a heavy ion ($m_{ion} >> m_{molecule}$ from cell atmosphere) via detection of the image current induced in the receiver plates.*

tial decay due to collisional friction (Equation 2 c). Therefore, in order to prevent the ions to escape from the FT-ICR cell along the z-direction the cell is "closed" by two trapping plates (Figure 2). The trapping plates are kept at a trapping potential V_T which is positive with respect to the potential V_0 of the transmitter and receiver plates when cations have to be trapped ($V_T - V_0 > 0$) and negative in the case of negative ions ($V_T - V_0 < 0$). As a result, the ions are repelled from the trapping plates into the center of the cell. The introduction of an electric field $\vec{E}(\vec{r})$ due to the potential difference $V_T - V_0$ also considerably complicates the xy-motion: the cyclotron frequency is slightly shifted and a very low-frequent circular magnetron motion is superimposed on the cyclotron motion. Nevertheless, the principle and the essential features of FT-ICR are not affected. For more details the reader is referred to the literature.[3,4]

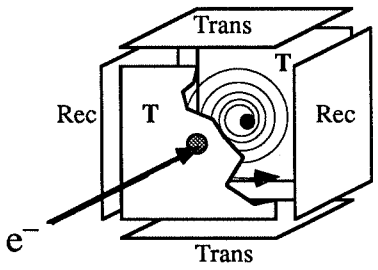

Figure 2**. Schematic representation of a cubic FT-ICR cell with trapping plates (T***) transmitter plates (*Trans*), receiver plates (*Rec*), ion in cyclotron orbit (●) and electron beam (e^-) for electron impact (EI) ionization.*

The Experiment

In the previous subsection the principles of ion trapping, manipulation and detection in FT-ICR mass spectrometry have been briefly discussed. In this subsection a short description of a typical FT-ICR experiment is presented.[3,4] This description is summarized in the flow scheme of Figure 3. At this point it is stressed that in FT-ICR mass spectrometry one is restricted to the observation of ***ionic*** reactants and ***ionic*** products which may be formed via ion/molecule reactions.

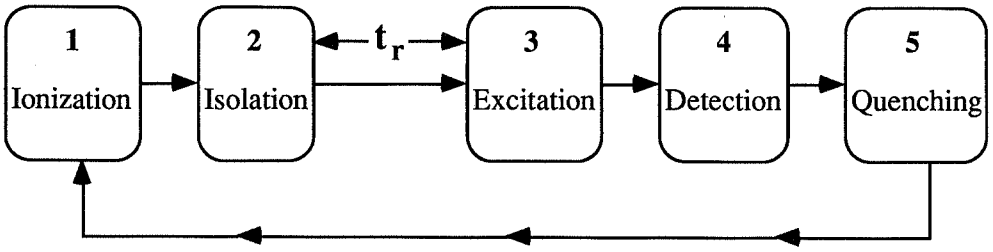

***Figure 3**. Flow scheme for the different steps in an FT-ICR experiment.*

The FT-ICR cell is continuously evacuated and a background pressure of circa 10^{-7} Pa is achieved. A number of reactant gases can be introduced into the cell with a total pressure which is kept constant (normally below 10^{-5} Pa) through continuous introduction. After ionization (step 1, Figure 3), e.g. by electron impact (EI), ions of specific m/z (m/q in amu/au) can be isolated (step 2) through ejection of all other ions that have been formed. The ejection of ions is achieved by resonant excitation of their cyclotron motion until they hit the cell wall, and are discharged and removed from the cell. Subsequently, the isolated ions are allowed to react with neutral molecules. After a certain reaction time t_r the cyclotron motion of all reactant and product ions present in the cell is excited (step 3) in order to detect their time-domain signal (step 4). Finally, the potential difference $V_T - V_0$ is reversed as a result of which all ions are attracted to and hit the trapping plates, and are discharged and removed from the cell (quenching, step 5). Steps 1 to 5 are repeated and the individual time-domain signals are accumulated until a satisfying signal-to-noise ratio has been achieved after which Fourier transformation (FT) results in an FT-ICR mass spectrum.

Gas-Phase Ion/Molecule Reactions

An essential feature of gas-phase ion/molecule reactions is that they involve ion/molecule complexes which are loosely bound by ion/(induced)dipole interactions and eventually by hydrogen bonds.[3,4,7] The reaction proceeds via association of the ion A^- and the neutral B in a reactant complex $[A^-, B]^*$ (Equation 6). The reactant complex is transformed in a chemical reaction into a product complex $[C^-, D]^*$ which dissociates into the separated products.

$$A^- + B \underset{\text{association}}{\rightleftharpoons} [A^-, B]^* \underset{\text{reaction}}{\rightleftharpoons} [C^-, D]^* \underset{\text{dissociation}}{\rightleftharpoons} C^- + D \qquad (6)$$

Under the low pressure conditions of an FT-ICR cell ($p < 10^{-5}$ Pa) termolecular processes are very improbable and can be neglected.[3,4] Therefore, the energy gained upon association or released in an exothermic reaction cannot be lost by collisional cooling and remains in the ion/molecule complex as rovibrational internal energy, unless photon emission[8] occurs (Figure 4). This internal energy thus is available for redissociation of the ion/molecule complex (typical lifetime is circa 10^{-6} s)[7] or to overcome reaction barriers. The isolated situation of the ion/molecule complexes furthermore implies that they cannot absorb energy from their surroundings. Consequently, overall endothermic reaction channels are in principle not energetically accessible. However, as in general the reactants have some internal energy, processes which are overall slightly endothermic (1 - 5 kcal/mol) may sometimes occur.

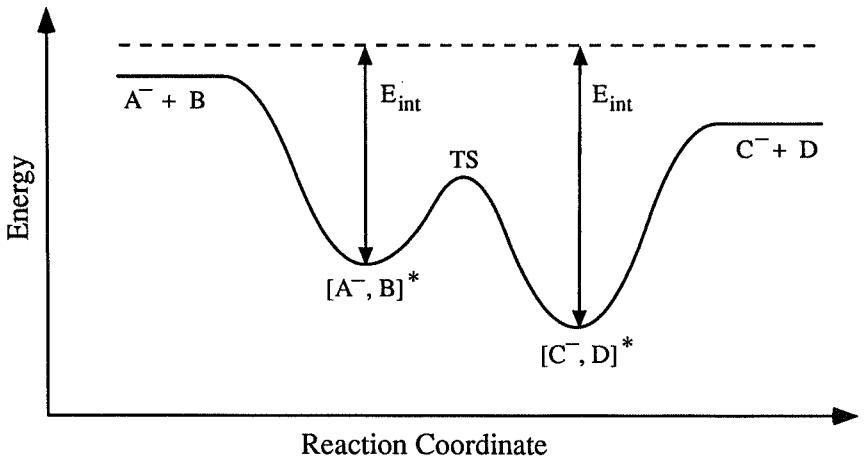

Figure 4. *Schematic representation of the reaction energy profile of a gas-phase ion/molecule reaction.*

2.3 Density Functional Theory

The Principle

Density Functional Theory[9] (DFT) is based on the Hohenberg-Kohn theorem[10] which states that the ground state energy E of an electronic system is a unique functional of the electron density $\rho(\vec{r})$. According to the Kohn-Sham theorem,[11] the exact energy functional can be expressed as:

$$E[\rho] = T_S[\rho] + E_n[\rho] + E_C[\rho] + E_{XC}[\rho] \tag{7}$$

where the exact electron density is given by a summation over orbital densities:

$$\rho(\vec{r}) = \sum_i n_i \, |\phi_i(\vec{r})|^2 \tag{8}$$

with orbital occupation numbers n_i. In Equation 7 $T_S[\rho]$ represents the kinetic energy of the electrons of a non-interacting reference system. $E_n[\rho]$ is the electron/nucleus attraction and for molecular systems also includes the internuclear repulsion. $E_C[\rho]$ is the Coulomb interaction between two electronic charge distributions $\rho(\vec{r})$. The last term in Equation 7, $E_{XC}[\rho]$, is the exchange-correlation energy which accounts for exchange and Coulomb correlation between electrons and also includes corrections to the kinetic energy $T_S[\rho]$. The Kohn-Sham orbitals $\{\phi_i(\vec{r})\}$ are obtained from the effective one-electron Kohn-Sham equation:

$$h_{eff}\,\phi_i = \varepsilon_i\,\phi_i \tag{9 a}$$

where

$$h_{eff} = \frac{\delta E}{\delta \rho} = -\tfrac{1}{2}\vec{\nabla}^2 + V_n + V_C + V_{XC} \tag{9 b}$$

is the effective one-electron hamiltonian which is the functional derivative of E with respect to ρ. In Equation 9 b, $-\tfrac{1}{2}\vec{\nabla}^2$ is the kinetic energy operator, V_n is the external potential due to the nuclear frame, V_C is the effective Coulomb potential due to the electronic charge distribution $\rho(\vec{r})$ and

$$V_{XC} = \frac{\delta E_{XC}[\rho(\vec{r})]}{\delta\rho(\vec{r})} \tag{10}$$

is the exchange-correlation potential. The exchange-correlation potential is not known exactly. However, local (depending on $\rho(\vec{r})$) and also non-local approximations (depending on $\rho(\vec{r})$ and $\vec{\nabla}^n\rho(\vec{r})$) have been developed which have resulted in very accurate calculations of chemically important quantities like bond energy, geometry and activation energy.[12] The simplest and probably the most widely employed approximation to V_{XC} is Slaters local Xα potential:[13]

$$V_{X\alpha}[\rho(\vec{r})] = -3\alpha\left(\frac{3}{8\pi}\right)^{\frac{1}{3}}\rho(\vec{r})^{\frac{1}{3}} \tag{11}$$

which is based on the homogeneous electron gas expression for the exchange part of V_{XC}. The DF method which employs this Xα potential is called the Xα- or Hartree-Fock-Slater (HFS) method. In the Amsterdam Density Functional (ADF) program package[14-17] this and more advanced local[18,19] as well as non-local[20,21] density-functionals are available. For more details, the reader is referred to the literature.

Analysis of Bonding Mechanisms

An important feature of the Kohn-Sham approach in DFT is the combination of quantitative accuracy and preservation of the independent electron picture. As a result quantitative results can be interpreted in terms of concepts from the orbital interaction model as, for example, Pauli repulsion, pair bonding and donor/acceptor interaction between physically meaningful fragments (Scheme I).[22]

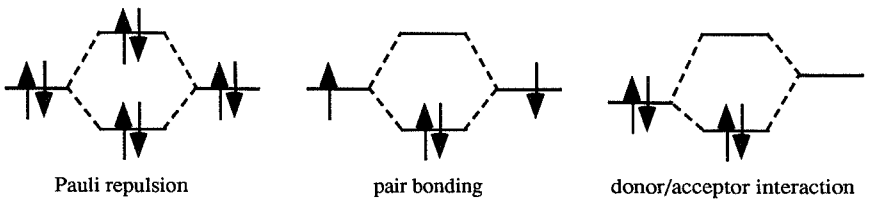

Scheme I

The Amsterdam Density Functional (ADF) program system makes use of these possibilities by a bond energy decomposition scheme[23,24] which is described in the following and illustrated by Figure 5. The bond energy of two closed shell fragments A and B in a closed shell molecule AB is defined as the energy difference between the separated fragments and the molecule:

$$\Delta E = E(AB) - E(A) - E(B) \tag{12}$$

and can be decomposed into a steric part ΔE^0 and a relaxation part ΔE_{oi}, similar to the procedure suggested by Morokuma:[25,26]

$$\Delta E = \Delta E^0 + \Delta E_{oi} \tag{13}$$

The steric interaction ΔE^0 is defined as the energy difference between the separated fragments and the hypothetical system AB^0 which can be described by the wavefunction Ψ^0, the anti-symmetrized product of the overlapping fragment orbitals:[23]

$$\Delta E^0 = E(AB^0) - E(A) - E(B) \tag{14 a}$$

$$\Psi^0 = |(\text{closed shells})_A(\text{closed shells})_B| \tag{14 b}$$

In AB^0 occupied orbitals of A and B interact and can mix but no mixing between occupied and virtual orbitals is allowed (Figure 5). The steric interaction is composed of the classical electrostatic interaction of the unperturbed interpenetrating charge distributions of A and B, ΔE_{elstat}, and the Pauli or overlap repulsion, ΔE_{Pauli}, which is the consequence of the anti-symmetry requirement for Ψ^0.

$$\Delta E^0 = \Delta E_{elstat} + \Delta E_{Pauli} \tag{15}$$

It is interesting to note that ΔE_{elstat} is normally attractive near the equilibrium bond distance of A and B and the overall steric repulsion is entirely due to the rise in kinetic energy of the electrons contained in ΔE_{Pauli}.[27]

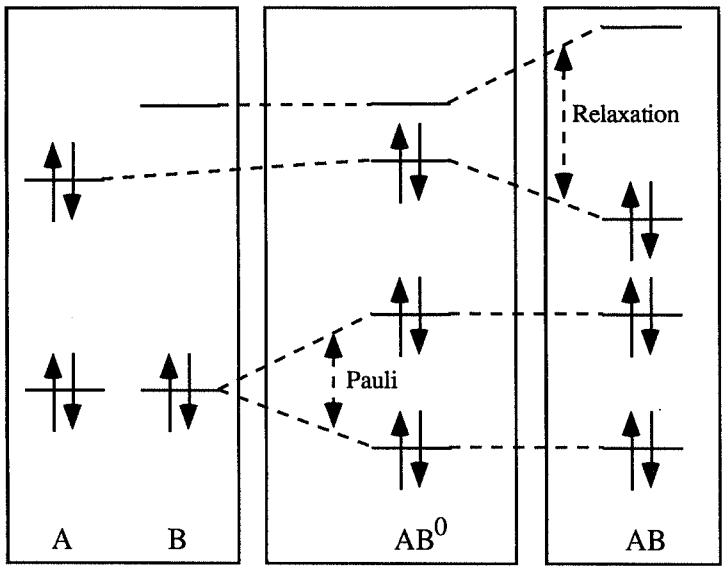

***Figure 5**. Orbital interaction diagram for the interaction of two closed shell fragments, A and B, in an overall system AB.*

The orbital interaction ΔE_{oi} is defined as the energy difference between the hypothetical system AB^0 with Ψ^0 and the final molecule AB in which Ψ^0 is allowed to relax to the final SCF wavefunction Ψ_{SCF} by admixing virtual orbitals into the occupied spectrum:[23]

$$\Delta E_{oi} = E(AB) - E(AB^0) \tag{16}$$

The orbital interaction comprises charge transfer, i.e., donor/acceptor interactions, polarization of one fragment due to the presence of the other and relief of steric repulsion, and can be symmetry decomposed according to the irreducible representations of the molecular point group of AB:[24]

$$\Delta E_{oi} = \sum_{\Gamma} \Delta E_{oi}(\Gamma) \tag{17}$$

References

1. Comisarow, M.B.; Marshall, A.G. *Chem. Phys. Lett.* **1974**, 25, 282.
2. Comisarow, M.B.; Marshall, A.G. *Can. J. Chem.* **1974**, 52, 1997.
3. Nibbering, N.M.M. *Adv. Phys. Org. Chem.* **1988**, 24, 1, and references cited therein.
4. Nibbering, N.M.M. *Acc. Chem. Res.* **1990**, 23, 279, and references cited therein.
5. Koning, L.J. de *Thesis*, University of Amsterdam, 1989.
6. Goldstein, F. *Classical Mechanics*, Addison-Wesley: Reading, 1980.
7. Lias, S.G.; Ausloos, P. *Ion-Molecule Reactions*, American Chemical Society: Washington, 1975.
8. Dunbar, R.C.; *Mass Spectrom. Rev.* **1992**, 11, 309.
9. Parr, R.G.; Yang, W. *Density-Functional Theory of Atoms and Molecules*, Oxford University Press: New York, 1989.
10. Hohenberg, P.; Kohn, W. *Phys. Rev.* **1964**, 136, B864.
11. Kohn, W.; Sham, L.J. *Phys. Rev.* **1965**, 140, A1133.
12. Ziegler, T. *Chem. Rev.* **1991**, 91, 651, and references cited therein.
13. Slater, J.C. *Quantum Theory of Molecules and Solids*, Vol. 4, McGraw-Hill: New York, 1974.
14. Baerends, E.J.; Ellis, D.E.; Ros, P. *Chem. Phys.* **1973**, 2, 41.
15. Boerrigter, P.M.; Velde, G. te; Baerends, E.J. *Int. J. Quantum Chem.* **1988**, 33, 87.
16. Baerends, E.J.; Ros, P. *Chem. Phys.* **1975**, 8, 412.
17. Baerends, E.J.; Ros, P. *Int. J. Quantum Chem., Quantum Chem. Symp.* **1978**, S12, 169.
18. Stoll, H.; Golka, E.; Preus, H. *Theoret. Chim. Acta* **1980**, 55, 29.
19. Vosko, S.H.; Wilk, L.; Nusair, M. *Can. J. Phys.* **1980**, 58, 1200.
20. Becke, A.D. *Int. J. Quantum. Chem.* **1983**, 23, 1915.
21. Becke, A.D. *J. Chem. Phys.* **1986**, 85, 7184.
22. Albright, T.A.; Burdett, J.K.; Whangbo, M.-H. *Orbital Interactions in Chemistry*, Wiley: New York, 1985.
23. Bickelhaupt, F.M.; Nibbering, N.M.M.; Wezenbeek, E.M. van; Baerends, E.J. *J. Phys. Chem.* **1992**, 96, 4864, and references cited therein.

24. Ziegler, T.; Rauk, A. *Theoret. Chim. Acta* **1977**, 46, 1.

25. Morokuma, K. *J. Chem. Phys.* **1971**, 55, 1236.

26. Kitaura, K.; Morokuma, K. *Int. J. Quantum Chem.* **1976**, 10, 325.

27. Hoek, P.J. van den; Kleyn, A.W.; Baerends, E.J. *Comments At. Mol. Phys.* **1989**, 23, 93.

3 Base-Induced Imine-Forming 1,2-Elimination Reactions in the Gas Phase

Abstract

The gas-phase reactivity of N,O-dimethylhydroxylamine (DHA) and O-methylhydroxylamine (MHA) towards a series of anionic bases has been studied using the method of Fourier Transform Ion Cyclotron Resonance (FT-ICR) mass spectrometry. Both DHA and MHA undergo a competing proton abstraction from and nucleophilic substitution reaction on the nitrogen atom. The competition between these processes is governed by the strength of the base used.

Unexpectedly, the nucleophilic attack on the nitrogen atom leading to the substitution of the methoxy group is found to be a relatively facile process. This is especially evident in the substitution reactions with O-methylhydroxylamine, NH_2-O-CH_3, where the formation of methoxide ions is much more efficient than in the highly inefficient substitution reactions of dimethylether, CH_3-O-CH_3. Apparently, substitution reactions on the nitrogen atom do not suffer from a very unfavorable activation barrier which is assumed to hamper nucleophilic substitution reactions on carbon atoms in the gas phase. This seems to be supported by high-level density-functional (DF) calculations which indicate that the nucleophilic substitution reactions on the nitrogen atom proceed via an entropically favored less tight, S_N1-like transition state.

However, in the reactions of N,O-dimethylhydroxylamine, CH_3NH-O-CH_3, the proton abstraction and substitution processes unfavorably compete with a base-induced imine-forming 1,2-elimination. The efficiency of the imine-forming elimination reactions of CH_3NH-O-CH_3 can be compared favorably with that of base-induced alkene-forming 1,2-elimination reactions of corresponding simple ethers such as CH_3CH_2-O-C_2H_5.

3.1 Introduction

Base-induced alkene-forming 1,2-elimination reactions (Equation 1) constitute one of the basic types of reaction in organic chemistry.[1] Since in 1927 Ingold[2,3] introduced the concept of "base-promoted olefine-forming elimination reactions", many experimental investigations have been performed on this class of reactions in the condensed phase[4-13] as well as in the gas phase.[14–23]

$$B^- + H\text{-}C^{\beta}R_2\text{-}C^{\alpha}R_2\text{-}L \longrightarrow B\text{-}H + CR_2{=}CR_2 + L^- \quad (1)$$

Considerable experience has been gathered concerning the parameters which determine the reaction rates, the product distribution and the stereochemistry. The nature of base-induced alkene-forming 1,2-elimination reactions is now well understood and interpreted in terms of the concept of the Variable Transition State (VTS).[1,24] In this concept, reactions are classified according to the geometry of the transition state (TS), which is conceived as being located at one point in a continuous spectrum of mechanistic possibilities. The VTS theory comprises the Bunnet E2H-spectrum,[9,10] i.e. E1cb(-like), synchronous E2, and E1(-like) eliminations involving linear proton transfer, as well as the Winstein-Parker E2H-E2C-spectrum[11-13] in which bent proton transfer may occur with a certain degree of base/C^{α} covalent interaction. Furthermore, stereoelectronic arguments account for the preference of TS structures in which the base and the leaving group are anti- or syn-*periplanar*.[25-27]

In contrast, base-induced heteroalkene-forming 1,2-eliminations have received little attention both in condensed[28-33] and in gas phase[34-36] mechanistic studies, although in synthetic organic chemistry they represent an important tool to introduce a π-bond between a carbon and a hetero atom or between two hetero atoms.[28-33] As an exception, the base-induced *imine*-forming 1,2-elimination reaction (Equation 2) has been investigated extensively in the condensed phase during the past decade.[37-43]

$$B^- + H\text{-}C^{\beta}R_2\text{-}N^{\alpha}R\text{-}L \longrightarrow B\text{-}H + CR_2{=}NR + L^- \quad (2)$$

Extensive studies have been performed on base-induced imine-forming 1,2-eliminations of N-chloramines in the condensed phase.[43] These studies provide convincing evidence that these imine-forming 1,2-elimination reactions are of E2 type. For example, alkoxide-induced imine-forming 1,2-elimination reactions of N-chloro-N-methylbenzylamines exhibit overall bimolecular kinetics. Hammett studies indicate that the electron density increases at the β-carbon in going to the transition state (TS). Furthermore, stretching of the C^{β}-H and N^{α}-L bonds in the activated complex is revealed by a considerable primary kinetic H/D isotope and a large leaving group element effect, respectively.[37,38]

However, there are some significant differences between imine- and alkene-forming 1,2-elimination reactions. In the former, a C-N π-bond is formed which is circa 10 kcal/mol[24,44] stronger than the C-C π-bond which results from the latter. Furthermore, the N-L single bond which has to be broken is about 31 kcal/mol (L = Cl)[24,44] weaker than the C-L single bond. As a result, base-induced imine-forming 1,2-eliminations are considerably more exothermic and have a lower activation enthalpy ($\Delta H^{\neq}$) than their alkene-forming analogues (the $\Delta S^{\neq}$ values are comparable).[43] Consequently, the reaction rate constants for the imine-forming eliminations of N-chloramines are found to be a factor of about 10^4 higher than the alkene-forming eliminations of the corresponding chloroalkanes.[37,43]

On the basis of the results from Hammett studies it is suggested that the E2 transition state is shifted from E1cb-like for alkene-forming eliminations towards a more central E2 for analogous imine-forming eliminations.

In the present study the feasibility of gas-phase base-induced imine-forming 1,2-eliminations in comparison with competing substitution processes has been explored. To this end the reactivity of N,O-dimethylhydroxylamine (DHA) and O-methylhydroxylamine (MHA) towards a series of anionic bases has been studied as a function of the strength of the base, under the low pressure conditions of a Fourier Transform Ion Cyclotron Resonance (FT-ICR) mass spectrometer where association of solvent molecules and/or counter ions is avoided.[45,46] This experimental study is supplemented with quantum chemical calculations using a high-level density-functional (DF) method.[47-52]

3.2 Experimental

The experiments were performed with a Fourier transform ion cyclotron resonance (FT-ICR) mass spectrometer constructed at the University of Amsterdam and equipped with a 1.4 T electromagnet and a cubic inch cell (De Koning and Nibbering,[14] and references cited therein). The Segmented Fourier Transform (SEFT) procedure[53] was employed to obtain relative ion abundances with an accuracy of better than 1%. General operating and experimental procedures have been described previously.[14]

The temperature in the cell was around 333 K as measured by a thermocouple on the trapping plate opposite the filament. The total pressure in the different experiments was normally kept below 10^{-4} Pa with a background pressure lower than 5×10^{-7} Pa. The pressure was measured with an ionization gauge placed in a side arm of the main pumping line.

The ionization gauge was calibrated for methane by fitting our rate constant for the reaction $CH_4^{+\bullet} + CH_4 \rightarrow CH_5^+ + CH_3^\bullet$ to the average literature value of $(1.11 \pm 0.04) \cdot 10^{-9}$ $cm^3molecule^{-1}s^{-1}$.[54] Absolute pressures were obtained by correction for the sensitivities R_x of the ionization gauge for gases x relative to methane, using the relationship $R_x = 0.36\alpha + 0.30$ of Bartmess and Georgiadis[55] and polarizabilities α from Miller.[56] The determination of overall bimolecular rate constants $k(B^-)$ for the reactions of B^- with the substrate was complicated by the formation of CN^-, probably due to proton abstraction from traces of HCN, which are considered to result from pyrolysis of nitrogen containing compounds on the hot filament. This complication can lead to an overestimation of the determined overall rate constants. Therefore, rate constants could be determined only for relatively efficient reactions (Tables I and III).

NH_2^- was generated via dissociative resonant capture of electrons with a kinetic energy of 5 eV by NH_3. $C_6H_5^-$ was produced via proton abstraction from benzene by NH_2^-. OH^- was generated via dissociative resonant capture of electrons with a kinetic energy of 6 eV by H_2O (OH^- is formed via H^-). CH_3O^- was generated via reaction of NH_2^- with N,O-dimethylhydroxylamine or via reaction of OH^- with O-methylhydroxylamine and was selected as the ^{13}C isotopomer (m/z 32) in order to distinguish the reactant from the product methoxide. $C_2H_5O^-$ was formed via proton abstraction from ethanol by OH^-. F^- was generated via dissociative resonant capture of electrons with a kinetic energy of 6 eV by CF_4. Cl^- was made in a S_N2 substitution of NH_2^- and CH_3Cl. Finally, CN^- was obtained by proton abstraction from HCN (contamination, *vide supra*).

Chemicals

Gaseous O-methylhydroxylamine was generated from its hydrochloric salt by treating it with an excess of grained sodium hydroxide under high vacuum in the inlet system of the FT-ICR. N,O-Dimethylhydroxylamine (DHA) and the hydrochloric salt of O-methylhydroxylamine (MHA•HCl) were a gift from Professor F. Bickelhaupt of the Scheikundig Laboratorium, Vrije Universiteit, Amsterdam. All other chemicals were commercially available. GC analysis (Reoplex, 60 °C) of the DHA sample indicated that the purity was better than 98%. MS analysis (MAT 90, Finnigan MAT, Bremen, Germany) indicated that the MHA•HCl was free from methanol, while no significant amount of methanol was detected in the gaseous MHA sample which was introduced to the FT-ICR cell as described above.

3.3 Theoretical

Quantum chemical calculations were performed using a high-level density-functional (DF) method, as implemented in the Amsterdam Density-Functional (ADF) program system.[47-52] The MOs were expanded in a large set of Slater type orbitals (STOs). The basis is of double-ζ quality (two STOs per nl shell). A polarization function was added on each atom: 2p on H, 3d on N, O, and F. Geometries were optimized with the simple Xα exchange-correlation potential[47] using gradient techniques.[57] The energy data reported for stable structures have been obtained in the optimum geometry with more sophisticated density-functionals (DF) for exchange and correlation. Exchange is described with Slater's $\rho^{1/3}$ potential (Xα with $\alpha = 2/3$), with a non-local correction due to Becke.[58-60] According to the suggestion by Stoll et al.,[61] only correlation between electrons of different spin is introduced, for which electron gas data (in the Vosko-Wilk-Nusair[62] parametrization) are used.

It has been noticed before that the complexation energy of fluorine containing anion/molecule complexes depends very critically on the quality of the basis set.[63] Therefore, after the geometries were optimized with the double-ζ basis, DFT calculations for the anion/molecule complexes $[MHA, F^-]_N$ and $[MHA, F^-]_C$ (*vide infra*) and their fragments MHA and F^- were performed with an extra large triple-ζ basis augmented with two polarization functions on each atom (3d and 4f on F, N, O, C; 2p and 3d on H). However, the gross Mulliken population

analysis[64] (see charges in Figure 1 and Table VI) has been performed using the smaller double-ζ basis set to avoid problems associated with the application of this method in the case of very large basis sets containing diffuse functions.[65]

Considerable experience shows that with the DF approach interaction energies in systems involving main group elements and/or metals can be calculated with an accuracy of better than 5 kcal/mol.[57,63,66–72]

Thermochemistry

The proton affinity (PA) of NH_2O^- (Table V) has been obtained by anchoring the calculated energy difference ΔE for the reaction $NH_2OH + F^- \rightarrow NH_2O^- + HF$ to the literature value for the proton affinity of F^-,[73] using the relation $PA(NH_2O^-) = PA(F^-) + \Delta E + \Delta ZPE$ and assuming that $\Delta ZPE \approx 0$ for the proton transfer. The proton affinity of CH_3NHO^- has been estimated using the relation $PA(CH_3NHO^-) = PA(NH_2O^-) + [PA(CH_3NHO^-) - PA(NH_2O^-)]$ and assuming that $[PA(CH_3NHO^-) - PA(NH_2O^-)] \approx [PA(C_2H_5O^-) - PA(CH_3O^-)]$, where the PA values for methoxide and ethoxide have been obtained from the literature.[73] The heat of formation (ΔH_f) of NH_2F (Table V) has been obtained by anchoring the calculated energy difference ΔE for the reaction $F^- + NH_2OCH_3 \rightarrow NH_2F + CH_3O^-$ to the literature values for the heats of formation of F^- and NH_2OCH_3,[73] using the relation $\Delta H_f(NH_2F) = \Delta H_f(F^-) + \Delta H_f(NH_2OCH_3) - \Delta H_f(CH_3O^-) + \Delta E + \Delta ZPE$ and asuming that $\Delta ZPE \approx 0$ for the substitution reaction.

3.4 Results and Discussion

General

The experimental results and thermochemical data are summarized in Tables I to V. Tables I and III show the primary product anion distribution for the reactions of B^- with N,O-dimethyl-hydroxylamine (DHA) and O-methylhydroxylamine (MHA), respectively. The corresponding thermicities for a number of conceivable processes (Equations 3a-f) are listed in Tables II and IV, respectively. The results of the quantum chemical DF calculations are shown in Tables V and VI and in Figure 1.

Table I. Primary product anion distributions (%) and overall bimolecular rate constants, $k(B^-)$ (10^{-9} $cm^3s^{-1}molecule^{-1}$), for reactions of B^- with N,O-dimethylhydroxylamine (DHA).

B^-	$k(B^-)$	Product anion distribution[a]			
		$(DHA–H)^-$	CH_3O^-	$[CH_3O^-, HB]$	$CH_2=N^-$
NH_2^-	2.9±0.4[b]	11	56	—	33
$C_6H_5^-$	c	17	49	—	34
OH^-	3.9±1.4[b]	9	72	—	19
CH_3O^-	c	—	100	—	—
$C_2H_5O^-$	c	—	100	—	—
F^-	c	—	96	4	—
CN^-	0.0	—	—	—	—
Cl^-	0.0	—	—	—	—

[a] See Equations 3a-f.

[b] Deviation from average over two independent experiments.

[c] Rate constant determination complicated (see experimental section).

Table II. Reaction enthalpies (ΔH_r, kcal/mol) for reactions of B^- with N,O-dimethylhydroxylamine (DHA).[a]

B^-	$PA(B^-)$[b]	ΔH_r					
		PT[c]	$S_N2(N)$[c]	$S_N2(C)$[c]	1,2-E[c]	1,2-E_{solv}[c]	1,2-E/PT[c]
NH_2^-	403.7	–18	–29	–19	–45	–55	–37
$C_6H_5^-$	400.8	–15	–59	–29	–42	–52	–34
OH^-	390.8	–5	–4	–2	–32	–56	–24
CH_3O^-	380.5	6	0	3	–22	–51	–14
$C_2H_5O^-$	377.4	9	—	6	–19	–39	–11
F^-	371.4	15	—	14	–13	–43	–5
CN^-	351.1	35	—	13	7	–9	15
Cl^-	333.4	53	48	48	25	11	33

[a] Calculated using data of Lias et al.[73] and Benson[74]. For formaldimine, CH_2=NH, we have used the revised heat of formation of 17 kcal/mol determined in our group,[76] and the accordingly adjusted heat of formation of 40 kcal/mol for the imide $CH_2=N^-$: $\Delta H_f(CH_2=N^-) = \Delta H_f(CH_2=NH)$[76] + $PA(CH_2=N^-)$[73] + $\Delta H_f(H^+)$[73]. Thermochemical data for $(DHA–H)^-$, CH_3NHO^-, and NH_2F have been determined in this work (see Table V).

[b] The gas-phase proton affinity (PA) is defined as the enthalpy change associated with the reaction $BH \rightarrow B^- + H^+$ (see reference 73).

[c] See Equations 3a-f.

Table III. Primary product anion distributions (%) and overall bimolecular rate constants, $k(B^-)$ (10^{-9} $cm^3s^{-1}molecule^{-1}$), for reactions of B^- with O-methylhydroxylamine (MHA).

B^-	$k(B^-)$	Product anion distribution[a]	
		$(MHA–H)^-$	CH_3O^-
NH_2^-	1.7	49	51
$C_6H_5^-$	b	30	70
OH^-	1.3	45	55
CH_3O^-	b	—	100
$C_2H_5O^-$	0.0	—	—
F^-	b	—	100

[a] See Equations 3a-c.

[b] Rate constant determination complicated (see experimental section).

Table IV. Reaction enthalpies (ΔH_r, kcal/mol) for reactions of B^- with O-methylhydroxylamine (MHA).[a]

B^-	PA	ΔH_r			
		PT[b]	$S_N2(N)$[b]	$S_N2(C)$[b]	1,1-E[c]
NH_2^-	403.7	–18	–31	–17	25
$C_6H_5^-$	400.8	–15	–61	–27	28
OH^-	390.8	–5	–5	0	38
CH_3O^-	380.5	6	0	5	48
$C_2H_5O^-$	377.4	9	3	8	51
F^-	371.4	15	5	16	57

[a] Calculated using data of Lias et al.[73] and Benson[74].

Thermochemical data for $(MHA–H)^-$, NH_2O^-, and NH_2F have been determined in this work (see Table V).

[b] See Equations 3a-c.

[c] See Equation 4.

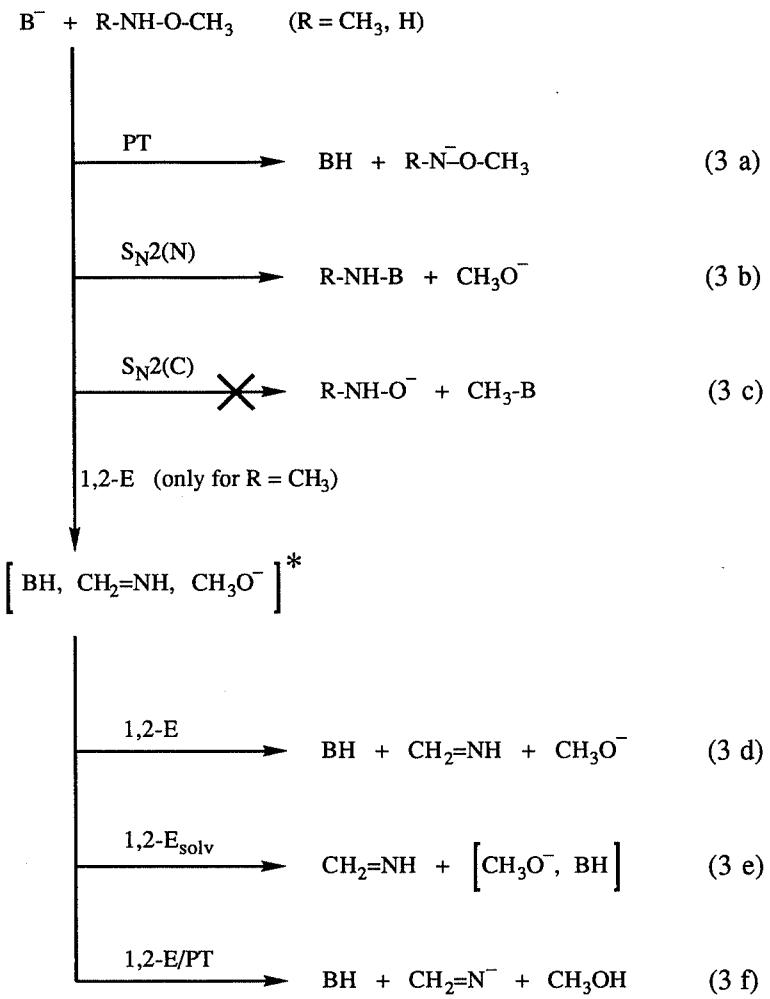

In the various reactions of B^- (B^- = NH_2^-, $C_6H_5^-$, OH^-, MeO^-, EtO^-, F^-, CN^-, and Cl^-) with DHA, the competing formation of four types of primary product anions is observed, namely $(DHA–H)^-$, CH_3O^-, $[CH_3O^-, HB]$, and $CH_2=N^-$ (Table I). The relatively weak bases CN^- and Cl^- appear to be unreactive towards DHA. This can be ascribed to the relatively unfavorable thermicity of the conceivable reactions listed in Table II. For all other reaction systems, CH_3O^- appears to be the dominant product anion.

In the reactions of B^- (B^- = NH_2^-, $C_6H_5^-$, OH^-, MeO^-, EtO^-, and F^-) with MHA the competing formation of two types of primary product anions is observed, namely $(MHA–H)^-$ and

CH_3O^- (Table III). The efficiency of the reactions involving MHA is significantly lower than for the reactions involving DHA. This trend continues for the reaction of $C_2H_5O^-$ with MHA, where no product anion was formed at all. However, for all other bases CH_3O^- appears to be the most abundant product anion as in the reactions with DHA.

The Formation of (DHA–H)$^-$ and (MHA–H)$^-$

The formation of $(DHA–H)^-$ and $(MHA–H)^-$ is considered to proceed via a proton abstraction from DHA and MHA at the nitrogen atom, leading to $(CH_3)(CH_3O)N^-$ and CH_3ONH^-, respectively (Equation 3a). This proton transfer (PT) is observed in the reactions of NH_2^-, $C_6H_5^-$, and OH^- (PA = 390.8 kcal/mol) but not for MeO^- (PA = 380.5 kcal/mol), EtO^-, F^-, CN^-, and Cl^- (Tables I and III). Assuming that entropy changes associated with the studied proton transfers are small, the proton affinity (PA) of both $(CH_3)(CH_3O)N^-$ and CH_3ONH^- is bracketed between the proton affinities of hydroxide and methoxide and, hence, amounts to 386 ± 5 kcal/mol (Table V).

Table V. Selected proton affinities (PA, kcal/mol) and heats of formation (ΔH_f, kcal/mol) obtained from proton transfer bracketing experiments and DFT calculations.

System	Quantity	Value	Method
$(DHA–H)^-$	PA	386 ± 5	experimental bracketing[a]
$(MHA–H)^-$	PA	386 ± 5	experimental bracketing[a]
NH_2O^-	PA	385	DFT[b]
CH_3NHO^-	PA	382	estimated[b]
NH_2F	ΔH_f	–27	DFT[b]

[a]PA bracketed between PA of OH^- and CH_3O^- (see Tables I and III).

[b]See theoretical section.

The Formation of CH_3O^-

The formation of methoxide in the reactions of B^- with MHA can be associated with a nucleophilic substitution on the nitrogen atom ($S_N2(N)$; Equation 3b). The possibility of an 1,1-elimination (1,1–E; Equation 4) leading to the formation of the highly energetic nitrene N-H (ΔH_f = 90 kcal/mol)[73] can be excluded as this process is very endothermic for all bases used (Table IV).

$$B^- + NH_2\text{-}OCH_3 \xrightarrow{1,1\text{-}E} \not\rightarrow \quad B\text{-}H + {}^{\cdot}\underline{\bar{N}}\text{–}H + CH_3O^- \qquad (4)$$

However, the formation of methoxide in the reactions of B^- with DHA may proceed via both $S_N2(N)$ (Equation 3b) and a base-induced imine-forming 1,2-elimination (1,2-E, Equation 3d). The $S_N2(N)$ reaction of DHA is expected to be less efficient than the $S_N2(N)$ reaction of MHA due to the steric shielding of the nitrogen center by the methyl substituent. Nonetheless, both the proportion of the reactions resulting in methoxide ions and the overall reaction rate constants, $k(B^-)$, are significantly larger for the reactions with DHA than for the corresponding reactions with MHA (Tables I and III), implying that the formation of methoxide ions is much more efficient in the reactions with DHA. This leads to the conclusion that the formation of methoxide anions in the reactions with DHA dominantly (if not exclusively) proceeds via an 1,2-E process (Equation 3d) which is considered to be much more efficient than the competing $S_N2(N)$ process (Equation 3b). One arrives at an upper limit of 20% and 15% for the proportion of methoxide ions which are formed via a $S_N2(N)$ substitution in the reactions DHA with NH_2^- and OH^-, respectively, if it is assumed that the branching ratios of the proton transfer (PT) and the $S_N2(N)$ substitution are similar for DHA and MHA.

An interesting question that remains is why the nucleophilic substitution on the nitrogen atom resulting in methoxide ions ($S_N2(N)$, Equation 3b) is not in competition with the nucleophilic substitution on the carbon atom of the methoxy group ($S_N2(C)$, Equation 3c), which is anticipated to result in the formation of unobserved CH_3NHO^- and NH_2O^- ions in the reactions with DHA and MHA, respectively. At first sight one might expect that nucleophilic substitution on the more electronegative nitrogen ($Q_{N\ in\ MHA}$ = –0.32 electrons) would be less effective than nucleophilic

substitution on carbon ($Q_{C\ in\ MHA}$ = +0.10 electrons; Figure 1). From the results in Tables II and IV it appears that the observed $S_N2(N)$ process always is favored energetically over the corresponding $S_N2(C)$ process. According to Hammonds postulate,[75] an increase of the exothermicity of a reaction leads to a decrease of the activation barrier. This effect may partly compensate for the effect of the electron distribution which shields the nitrogen center from nucleophilic attack. Theoretical calculations[26] show that gas-phase $S_N2(C)$ reactions are hampered by a tight transition state (TS) which can be considered as an "entropy bottleneck". As a result, $S_N2(C)$ reactions very unfavorably compete with less exothermic 1,2-E processes.[14,21] The apparent prevalence of $S_N2(N)$ over $S_N2(C)$ may have the same origin. The average homolytic bond strength of the N-O single bond (43 kcal/mol) is nearly two times smaller than that of the C-O single bond (84 kcal/mol).[44] Furthermore, the DF theoretical investigation (Figure 1) shows that the N-O bond (140.5 pm) in MHA is slightly longer than the C-O bond (139.9 pm).

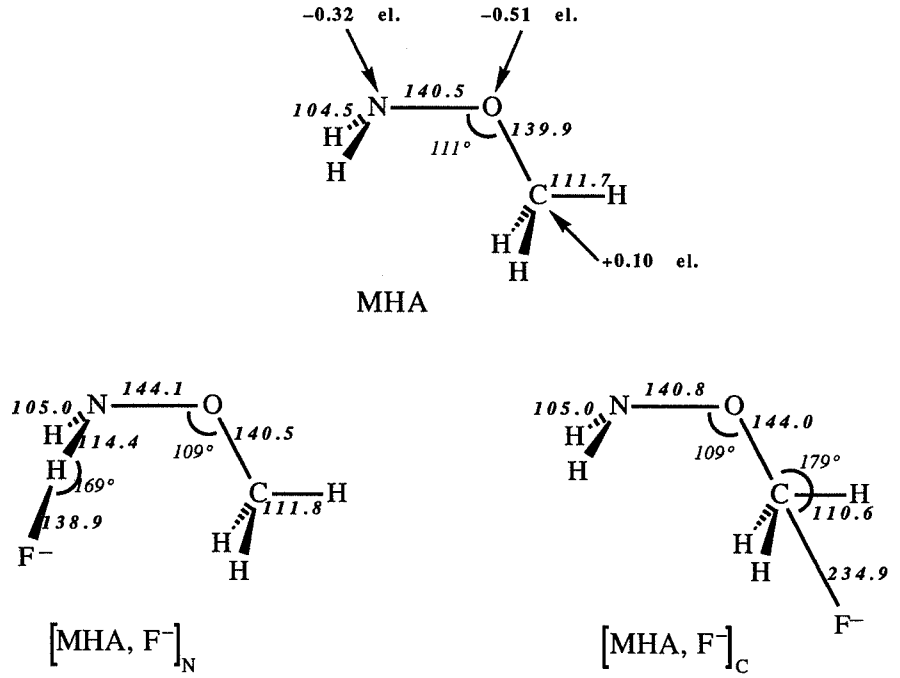

Figure 1. *Calculated minimum energy structures (pm) of O-methylhydroxylamine (MHA) and its complexes with F^- and gross Mulliken atom charges (electrons) for MHA.*

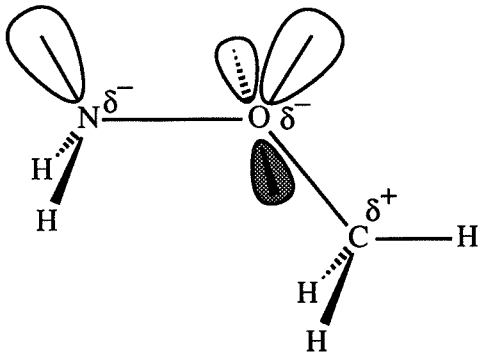

Figure 2. *Schematic representation of lone pair orbitals in O-methylhydroxylamine (MHA).*

The relatively large N-O bond distance is probably the result of the mutual Pauli repulsion between the nitrogen and oxygen atoms which both have a lone pair in the same plane (Figure 2). This contrasts the situation for the slightly positively charged methoxy carbon in MHA which has no lone pair.

The above considerations may lead to the conclusion that the $S_N2(N)$ substitution proceeds via a TS in which N-O bond rupture is more advanced than C-O bond rupture in the TS of the $S_N2(C)$ substitution. This implies that relative to $S_N2(C)$, $S_N2(N)$ proceeds via a less tight, S_N1-like TS associated with a higher density of states and, thus, a more favorable activation entropy. Further support for this hypothesis comes from the DF calculations on the anion/molecule complexes of MHA and F^- (Table VI, Figure 1).

Table VI. Complexation energies $\Delta E_{complex}$ (kcal/mol), and gross Mulliken charges Q (electrons) which the fragments acquire in the complexes of O-methylhydroxylamine (MHA) and fluoride obtained from DFT calculations.[a]

System	$\Delta E_{complex}$	Q(F^-)	Q(MHA)
$[MHA, F^-]_N$	–22.1	–0.68	–0.32
$[MHA, F^-]_C$	–11.4	–0.75	–0.25

[a]See Figure 1 for calculated minimum energy structures.

Association of MHA (calculated dipole moment of 2.623 D) and F^- can lead to the formation of two different anion/molecule complexes in which the base is bonded to the amino or to the methyl group of MHA, i.e. $[MHA, F^-]_N$ and $[MHA, F^-]_C$, respectively (Figure 1). In $[MHA, F^-]_C$ the fluoride anion is bound by circa 11.4 kcal/mol to the "backside" of the methyl group of MHA and thus has an appropriate configuration for an $S_N2(C)$ substitution. The complexation is accompanied by a charge transfer of –0.25 electrons from F^- to MHA, and a lengthening of the C-O bond by 4.1 to 144.0 pm. The amino bonded complex $[MHA, F^-]_N$ appears to be considerably more stable than the methyl bonded complex $[MHA, F^-]_C$ (Table VI). In $[MHA, F^-]_N$ the fluoride anion is bound by 22.1 kcal/mol to MHA which now has acquired a charge of –0.32 electrons. In contrast to the situation for $[MHA, F^-]_C$, the fluoride anion in $[MHA, F^-]_N$ is hydrogen bonded to one of the N-H bonds of MHA. This N-H bond has been extended by about 10 pm from 104.5 in the free MHA to 114.4 pm, while the F-H bond length amounts to 138.9 pm. In fact, no stable conformation for a "backside" $S_N2(N)$ attack could be found. Nevertheless, the formation of $[MHA, F^-]_N$ is accompanied by a significant lengthening of the weak N-O bond in MHA by 3.6 to 144.1 pm. This suggests that in the $S_N2(N)$ TS the N-B bond formation lags behind N-O bond breaking more than the C-B bond formation lags behind the C-O bond breaking in the $S_N2(C)$ TS. Furthermore, the DF calculations show that upon formation of the reaction complex only a slight deviation (6° at d(F-C) = 281 pm) from the F^- approach coaxial with the C-O axis results in a collapse of the reaction complex to $[MHA, F^-]_N$ rather than to $[MHA, F^-]_C$. Although this cannot directly be related to the relative energies of the transition states for $S_N2(N)$ and $S_N2(C)$, it suggests that F^- is captured in the vicinity of nitrogen and thus is predisposed for attack at this center. Summarizing, association of MHA and F^- preferentially leads to the formation of the more stable $[MHA, F^-]_N$ reaction complex leading to $S_N2(N)$ substitution with a relatively loose, S_N1-like TS.

The Formation of $[CH_3O^-, HB]$

The formation of the HB solvated methoxide, i.e. the $[CH_3O^-, HB]$ anion/molecule complex, in the reaction between B^- and DHA can unambiguously be associated with a mechanistic pathway in which a base-induced imine-forming 1,2-elimination (1,2-E) takes place followed by evaporation of formaldimine, CH_2=NH, from the product complex $[BH, CH_2=NH, CH_3O^-]^*$ ($1,2\text{-}E_{solv}$; Equation 3e). The formation of HB solvated methoxide is observed only for

the reaction induced by F^-, probably because the reaction enthalpy gained in the 1,2-E process of F^- ($\Delta H_{1,2\text{-}E}(F^-) = -13$ kcal/mol, see Table II) is the lowest for the reaction systems studied and may be insufficient to fuel the very endothermic desolvation of the methoxide anion from HB ($\Delta H_{complex} = -30$ kcal/mol[73] for [CH_3O^-, HF]). It may be supposed that formation of CH_3O^- and [CH_3O^-, HF] proceed via two stereochemically distinct elimination mechanisms, i.e. anti- and syn-1,2-E, respectively, as has been suggested for analogous gas-phase base-induced alkene-forming 1,2-elimination reactions of simple ethers[14] and thioethers.[15]

The Formation of $CH_2{=}N^-$

The formation of the imide ion $CH_2{=}N^-$ in the reactions between B^- and DHA can be associated with a mechanism that initiates with a 1,2-E reaction step. As discussed above, this results in the formation of the [BH, CH_2=NH, CH_3O^-]* product complex. Prior to the dissociation of this intermediate reaction complex a proton is transferred from formaldimine to methoxide leading to the formation of $CH_2{=}N^-$ (1,2-E/PT; Equation 3f). The PT step, which is about 8 kcal/mol[73] endothermic, has to be fueled by the reaction enthalpy gained in the preceding 1,2-E reaction step. If the 1,2-E reaction step becomes less exothermic, the reaction enthalpy gained may be insufficient for the overall 1,2-E/PT process to occur (Table II). In agreement with this, the formation of $CH_2{=}N^-$ is observed only in the reactions induced by the three strongest bases, i.e. NH_2^-, $C_6H_5^-$, and OH^- (Table I).

3.5 Conclusions

It appears that base-induced imine-forming 1,2-elimination reactions can be very efficient in the gas phase, as has been found for the reactions of N,O-dimethylhydroxylamine, CH_3NH-O-CH_3, with anionic bases. The efficiency of the imine-forming elimination reactions of CH_3NH-O-CH_3 can be compared favorably with the efficiency of base-induced alkene-forming 1,2-elimination reactions of corresponding simple ethers such as diethylether, CH_3CH_2-O-C_2H_5.[14]

Unexpectedly, nucleophilic attack on the nitrogen atom leading to the substitution of the methoxy group is found to be a relatively facile process. This is especially evident in the substitution reactions of anionic bases with O-methylhydroxylamine, NH_2-O-CH_3, where the

formation of methoxide anions is much more efficient than in the corresponding highly inefficient substitution reactions with dimethylether, CH_3-O-CH_3.[21] Apparently, substitution reactions on a nitrogen atom do not suffer from a very unfavorable activation entropy which is assumed to hamper nucleophilic substitution reactions on a carbon atom in the gas phase. This seems to be supported by high-level density-functional (DF) calculations which indicate that the nucleophilic substitution reactions on the nitrogen atom proceed via an entropically favored less tight, S_N1-like transition state.

References

1. Carey, F.A.; Sundberg, R.J. *Advanced Organic Chemistry*, Part A; Plenum Press: New York, 1984; Chapter 6.
2. Hanhart, W.; Ingold, C.K. *J. Chem. Soc.* **1927**, 997.
3. Hughes, E.D.; Ingold, C.K. *Trans. Faraday Soc.* **1941**, 37, 657.
4. Gandler, J.R. in *The Chemistry of Double-Bonded Functional Groups*, Vol. 2, Part I; Patai, S. Ed.; Wiley: New York, 1989.
5. Bartsch, R.A.; Závada, J. *Chem. Rev.* **1980**, 80, 453.
6. Saunders, W.H., Jr. *Acc. Chem. Res.* **1976**, 9, 19.
7. Bartsch, R.A. *Acc. Chem. Res.* **1975**, 8, 239.
8. Saunders, W.H., Jr.; Cockerill, A.F. *Mechanisms of Elimination Reactions*; Wiley: New York, 1973; Chapter 1.
9. Bunnett, J.F. *Angew. Chem.* **1962**, 74, 731.
10. Bartsch, R.A.; Bunnett, J.F. *J. Am. Chem. Soc.* **1968**, 90, 408.
11. Parker, A.J.; Ruane, M.; Biale, G.; Winstein, S. *Tetrahedron Lett.* **1968**, 2113.
12. Biale, G.; Cook, D.; Lloyd, D.J.; Parker, A.J.; Stevens, I.D.R.; Takahashi, J.; Winstein, S. *J. Am. Chem. Soc.* **1971**, 93, 4735.
13. McLennan, D.J. *Tetrahedron* **1975**, 31, 2999.
14. Koning, L.J. de; Nibbering, N.M.M. *J. Am. Chem. Soc.* **1987**, 109, 1715.
15. Berkel, W.W. van; Koning, L.J. de; Nibbering, N.M.M. *J. Am. Chem. Soc.* **1987**, 109, 7602.

16. Koning, L.J. de; Nibbering, N.M.M. *J. Am. Chem. Soc.* **1988**, 110, 2066.
17. Ridge, D.P.; Beauchamp, J.L. *J. Am. Chem. Soc.* **1974**, 96, 637.
18. Sullivan, S.A.; Beauchamp, J.L. *J. Am. Chem. Soc.* **1976**, 98, 1160.
19. Sullivan, S.A.; Beauchamp, J.L. *J. Am. Chem. Soc.* **1977**, 99, 5017.
20. Doorn, R. van; Jennings, K.R. *Org. Mass Spectrom.* **1981**, 16, 397.
21. DePuy, C.H.; Bierbaum, V.M. *J. Am. Chem. Soc.* **1981**, 103, 5034.
22. DePuy, C.H.; Beedle, E.C.; Bierbaum, V.M. *J. Am. Chem. Soc.* **1982**, 104, 6483.
23. Bierbaum, V.M.; Filley, J.; DePuy, C.H.; Jarrold, M.F.; Bowers, M.T. *J. Am. Chem. Soc.* **1985**, 107, 2818.
24. Lowry, T.H.; Richardson, K.S. *Mechanism and Theory in Organic Chemistry*, 3rd ed.; Harper and Row: New York, 1987; Chapter 7.
25. Bach, R.D.; Badger, R.C.; Lang, T.J. *J. Am. Chem. Soc.* **1979**, 101, 2845.
26. Minato, T.; Yamabe, S. *J. Am. Chem. Soc.* **1985**, 107, 4621.
27. Minato, T.; Yamabe, S. *J. Am. Chem. Soc.* **1988**, 110, 4586.
28. Dayagi, S.; Degani, Y. in *The Chemistry of Carbon-Nitrogen Double Bonds*; Patai, S., Ed.; Wiley: London, 1970; pp 121-124.
29. Cockerill, A.F.; Harrison, R.G. in *The Chemistry of Double Bonded Functional Groups*, Supplement A, Part 1; Patai, S., Ed.; Wiley: London, 1977; Chapter 4.
30. *Multiple Bonds and Low Coordination in Phosphorus Chemistry*; Regitz, M.; Scherer, O.J., Eds.; Georg Thieme Verlag: Stuttgart, 1990, in particular Chapter D.4 (Appel, R.), Chapter D.8 (Niecke, E.) and Chapter D.9 (Yoshifuji, M.).
31. Cullis, C.F.; Fish, A. in *The Chemistry of the Carbonyl Group*; Patai, S., Ed.; Wiley: London, 1966; pp 142-143.
32. Kice, J.L.; Kopczyk-Subotkowska, L. *J. Org. Chem.* **1990**, 55, 1523, and references cited therein.
33. Davy, M.B.; Douglas, K.T.; Loran, J.S.; Steltner, A.; Williams, A. *J. Am. Chem. Soc.* **1977**, 99, 1196, and references cited therein.
34. Thomas, D.A.; Bloor, J.E.; Bartmess, J.E. *J. Am. Soc. Mass Spectrom.* **1990**, 1, 295.
35. Grabowski, J.J.; Zhang, L. *J. Am. Chem. Soc.* **1989**, 111, 1193.
36. Noest, A.J.; Nibbering, N.M.M. *Adv. Mass Spectrom.* **1980**, 8A, 227.

37. Bartsch, R.A.; Cho, B.R. *J. Am. Chem. Soc.* **1979**, 101, 3587.
38. Cho, B.R.; Yoon, J.C.; Bartsch, R.A. *J. Org. Chem.* **1985**, 50, 4943.
39. Cho, B.R.; Namgoong, S.K.; Kim, T.R. *J. Org. Chem.* **1986**, 51, 1320.
40. Cho, B.R.; Maeng, J.H.; Yoon, J.C.; Kim, T.R. *J. Org. Chem.* **1987**, 52, 4752.
41. Bartsch, R.A.; Cho, B.R. *J. Am. Chem. Soc.* **1989**, 111, 2252.
42. Cho, B.R.; Suh, Y.W. *J. Org. Chem.* **1989**, 54, 2855.
43. Hoffman, R.V.; Bartsch, R.A.; Cho, B.R. *Acc. Chem. Res.* **1989**, 22, 211, and references cited therein.
44. Waser, J.; Trueblood, K.N.; Knobler, C.M. *Chem One*; McGraw-Hill: New York, 1976.
45. Nibbering, N.M.M. *Adv. Phys. Org. Chem.* **1988**, 24, 1.
46. Nibbering, N.M.M. *Acc. Chem. Res.* **1990**, 23, 279.
47. Slater, J.C. *Quantum Theory of Molecules and Solids*, Vol. 4; McGraw-Hill: New York, 1974.
48. Parr, R.G.; Yang, W. *Density-Functional Theory of Atoms and Molecules*, Oxford University Press: New York, 1989.
49. Baerends, E.J.; Ellis, D.E.; Ros, P. *Chem. Phys.* **1973**, 2, 41.
50. Boerrigter, P.M.; Velde, G. te; Baerends, E.J. *Int. J. Quantum Chem.* **1988**, 33, 87.
51. Baerends, E.J.; Ros, P. *Chem. Phys.* **1975**, 8, 412.
52. Baerends, E.J.; Ros, P. *Int. J. Quantum Chem., Quantum Chem. Symp.* **1978**, S12, 169.
53. Koning, L.J. de; Kort, C.W.F.; Pinkse, F.A.; Nibbering, N.M.M. *Int. J. Mass Spectrom. Ion Processes* **1989**, 95, 71.
54. W.T. Huntress, Jr., J.B. Laudenslager and R.F. Pinizzotto, Jr., *Int. J. Mass Spectrom. Ion Physics* **1974**, 13, 331.
55. J.E. Bartmess and R.M. Georgiadis, *Vacuum* **1983**, 33, 149.
56. K.J. Miller, *J. Am. Chem. Soc.* **112**, 8533 (1990).
57. Versluis, L.; Ziegler, T. *J. Chem. Phys.* **1988**, 88, 322.
58. Becke, A.D. *Int. J. Quantum. Chem.* **1983**, 23, 1915.
59. Becke, A.D. *J. Chem. Phys.* **1986**, 85, 7184.
60. Ziegler, T.; Tschinke, V.; Becke, A. *Polyhedron* **1987**, 6, 685.

61. Stoll, H.; Golka, E.; Preus, H. *Theoret. Chim. Acta* **1980**, 55, 29.
62. Vosko, S.H.; Wilk, L.; Nusair, M. *Can. J. Phys.* **1980**, 58, 1200.
63. Bickelhaupt, F.M.; Koning, L.J. de; Nibbering, N.M.M.; Baerends, E.J. *J. Phys. Org. Chem.* **1992**, 5, 179.
64. Mulliken, R.S. *J. Chem. Phys.* **1955**, 23, 1833.
65. Reed, A.E.; Weinstock, R.B.; Weinhold, F. *J. Chem. Phys.* **1985**, 83, 735.
66. Bickelhaupt, F.M.; Fokkens, R.H.; Koning, L.J. de; Nibbering, N.M.M.; Baerends, E.J.; Goede S.J.; Bickelhaupt, F. *Int. J. Mass Spectrom. Ion Processes* **1991**, 103, 157.
67. Bickelhaupt, F.M.; Nibbering, N.M.M.; Wezenbeek, E.M. van; Baerends, E.J. *J. Phys. Chem.* **1992**, 96, 4864.
68. Ziegler, T.; Tschinke, V.; Ursenbach, C. *J. Am. Chem. Soc.* **1987**, 109, 4825.
69. Ziegler, T.; Tschinke, V.; Versluis L.; Baerends, E.J. *Polyhedron* **1988**, 7, 1625.
70. Fan, L.; Ziegler, T. *J. Chem. Phys.* **1990**, 92, 3645.
71. Ziegler, T.; Rauk, A. *Theoret. Chim. Acta* **1977**, 46, 1.
72. Ziegler, T. *Chem. Rev.* **1991**, 91, 651.
73. Lias, S.G.; Bartmess, J.E.; Liebman, J.F.; Holmes, J.L.; Levin R.D.; Mallard, W.G. *J. Phys. Chem. Ref. Data* **1988**, 17, Suppl. Nr. 1.
74. Benson, S.W. *Thermochemical Kinetics*, 2nd Ed.; Wiley: New York, 1976.
75. Hammond, G.S. *J. Am. Chem. Soc.* **1955**, 77, 334.
76. Peerboom, R.A.L.; Ingemann, S.; Nibbering, N.M.M.; Liebman, J.F. *J. Chem. Soc., Perkin Trans. 2* **1990**, 1825.

4 Anionic Ether Cleavage of Tetrahydrofuran in the Gas Phase

Abstract

The gas phase reactivity of tetrahydofuran (THF) towards a series of anionic bases (B^- = NH_2^-, $C_6H_5^-$, OH^-, CH_2=CH–CH_2^-) has been investigated under the low pressure conditions of a Fourier Transform Ion Cyclotron Resonance (FT-ICR) mass spectrometer.

It appears that under the low pressure conditions the anionic base-induced reactions of THF predominantly proceed by 1,2-elimination. This elimination initially results in rovibrationally excited HB solvated but-3-ene-1-oxide ions. As a result of the absence of thermal interaction with the environment, HB is vaporized from these excited solvated ions. Depending on the nature of the base used, a proportion of the excited but-3-ene-1-oxide is found to eliminate molecular hydrogen or formaldehyde leading to overall exothermic formation of the resonance stabilized buta-1,3-diene-1-oxide ions and allyl anions, respectively.

Interestingly, reaction between the but-3-ene-1-oxide ion and water results in the very efficient formation of hydrated hydroxide ions, [H_2O, OH^-]. Isotopic labeling reveals that formation of this water solvated hydroxide ion is initiated by an endothermic proton transfer from water to but-3-ene-1-oxide which is followed by a reversible hydroxide-induced E1cb process, leading to the elimination of 1,3-butadiene and formation of the hydrated hydroxide ion. To our knowledge, this is the first example of a gas-phase anionic base-induced elimination in which hydroxide is involved as a leaving group. An interesting aspect of this 1,2-elimination reaction is that it provides an independent route to a type of intermediate which may also occur in base-induced diene-forming 1,4-elimination reactions.

4.1 Introduction

Many reactions in synthetic organic chemistry are carried out with ethers as solvents.[1,2] Already for a long time, it has been well known that these solvents are not always inert reaction media as they can undergo anionic ether cleavage. For example, organolithium compounds dissolved in ethers can induce protophilic 1,2-elimination,[3] 1,1-elimination,[4] 1,2'-elimination,[5] and Wittig-rearrangement (Scheme I).[2,5]

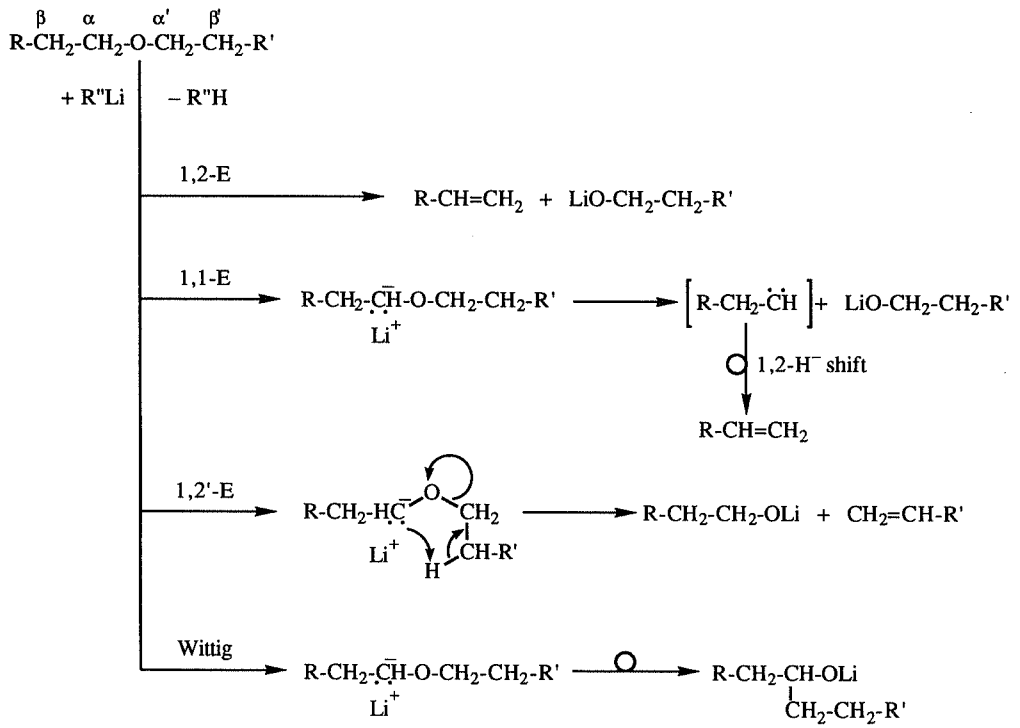

Scheme I

Nucleophilic cleavage is observed in the reaction with soft, resonance stabilized organolithium reagents as for example benzhydryllithium (Equation 1).[2]

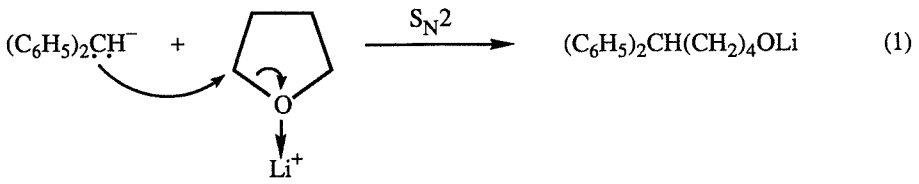

(1)

More recently, mechanistic studies on ether cleavage reactions have been performed from which it appears that a specific ether can decompose via different mechanisms.[2] These side reactions can lead to the formation of unexpected products. In some cases, they can be applied in synthesis, and it is important to understand their nature and occurrence.

Anionic ether cleavage reactions have also been studied in the gas phase by Ion Cyclotron Resonance (ICR)[6], Flowing Afterglow (FA)[7-10] and Fourier Transform Ion Cyclotron Resonance (FT-ICR)[11] techniques. In general, these studies indicate that base-induced 1,2-elimination reactions strongly prevail in the gas phase. In the studies on the gas-phase anionic base-induced reactions of ethers DePuy, Bierbaum and coworkers have found that under relatively high pressure FA conditions both NH_2^- and OH^- react with tetrahydrofuran (THF) under the competing formation of $(THF–H)^-$ and $[(THF–H)^-, HB]$.[8,9] Isotopic labeling has revealed that the formation of these primary product ions proceeds via a 1,2-elimination yielding but-3-ene-1-oxide (Equation 2a) as well as HB solvated but-3-ene-1-oxide ions (Equation 2b).

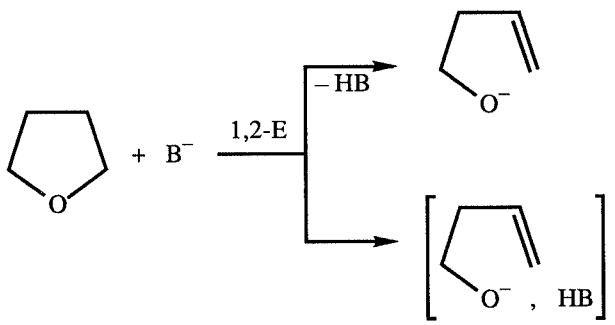

(2 a)

(2 b)

An interesting phenomenon seems to be the formation of hydrated hydroxide, $[H_2O, OH^-]$, detected as a secondary product ion in the reaction of OH^- and THF.[9] The authors[9] view this formation as a reaction of adventitious water molecules with the collisionally stabilized (by the He

carrier gas) loosely bound encounter complex (Equation 3a) or the product complex in which 1,2-elimination has occurred (Equation 3b).

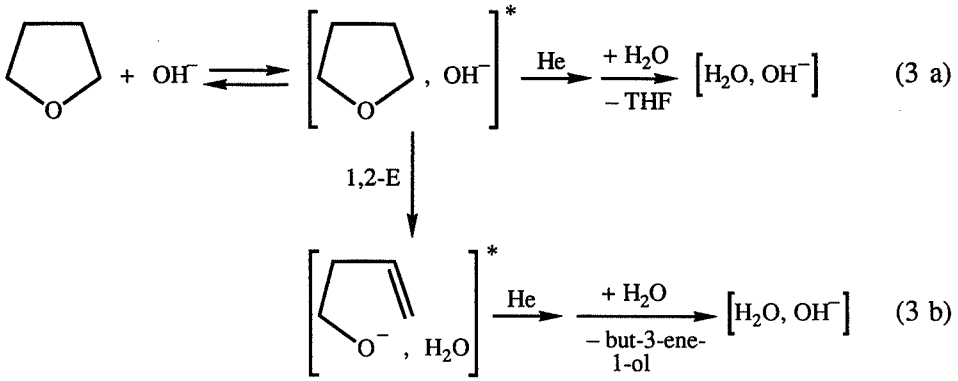

The present study is concerned with the reactivity of THF towards a series of anionic bases (NH_2^-, $C_6H_5^-$, OH^-, CH_2=CH–CH_2^-) under the relatively low pressure FT-ICR[12,13] conditions ($p < 10^{-4}$ Pa) where termolecular reactions and collisional stabilization of intermediate, loosely bound ion/molecule encounter and product complexes are highly restricted. It is the aim of this study to investigate what the effect is of the absence of collisional stabilization of intermediate ion/molecule complexes on the course of the reactions of THF. In particular, it is anticipated that the present study may reveal the origin of the hydrated hydroxide which is observed as a secondary product ion under the relatively high pressure FA conditions.

4.2 Experimental

The experiments were performed with a Fourier transform ion cyclotron resonance (FT-ICR) mass spectrometer constructed at the University of Amsterdam and equipped with a 1.4 T electromagnet and a cubic inch cell (De Koning and Nibbering,[11] and references cited therein). The Segmented Fourier Transform (SEFT) procedure[14] was employed to obtain relative ion abundances with an accuracy of better than 1%. General operating and experimental procedures have been described previously.[11]

The temperature in the cell was around 333 K as measured by a thermocouple on the

trapping plate opposite the filament. The total pressure in the different experiments was normally kept below 10^{-4} Pa with a background pressure lower than 5×10^{-7} Pa. The pressure was measured with an ionization gauge placed in a side arm of the main pumping line.

NH_2^- was generated via dissociative resonant capture of electrons with a kinetic energy of 5 eV by NH_3. OH^- was generated via dissociative resonant capture of electrons with a kinetic energy of 6 and 1.5 eV by H_2O (OH^- is formed via H^-) and N_2O (OH^- is formed via $O^{-\bullet}$ and $H^\bullet$ abstraction from the substrate), respectively. The allyl and phenyl anions were produced via proton abstraction by NH_2^- from propene and benzene, respectively. All chemicals were commercially available. The labeling content of $H_2{}^{18}O$ and D_2O amounts to circa 97 % and 94 %, respectively.

4.3 Results and Discussion

General

The gas phase reactivity of tetrahydrofuran (THF) towards the anionic bases B^- (B^- = NH_2^-, $C_6H_5^-$, OH^-, $CH_2{=}CH{-}CH_2^-$) has been investigated under relatively low pressure FT-ICR conditions. The experimental results and thermochemical data are summarized in Tables I, II, and III. Table I shows the primary product anion distribution for the reactions of THF with B^-. In the various reactions four types of primary product anions are formed, namely the allyl anion $CH_2{=}CH{-}CH_2^-$, $(THF{-}3H)^-$, $(THF{-}H)^-$, and $(THF{+}B)^-$ (Equation 4b-4e). In the reaction of OH^- with THF, in the presence of gaseous water, the hydrated hydroxide, $[H_2O, OH^-]$, is detected as a secondary product ion (Equation 4f).

All bases studied react with THF under the formation of a $(THF{-}H)^-$ ion (Equation 4b). As in the reactions under FA conditions,[8] the $(THF{-}H)^-$ ion is considered to be formed via a 1,2-elimination reaction in which proton abstraction from the β-position is associated with ring-opening, yielding but-3-ene-1-oxide ions (Equation 4b). Depending on the base used and, in the case of hydroxide, depending on the presence of water molecules in the reaction atmosphere, besides $(THF{-}H)^-$ one of the other above mentioned product anions is formed in the reaction with THF. This is discussed below for the various reaction systems.

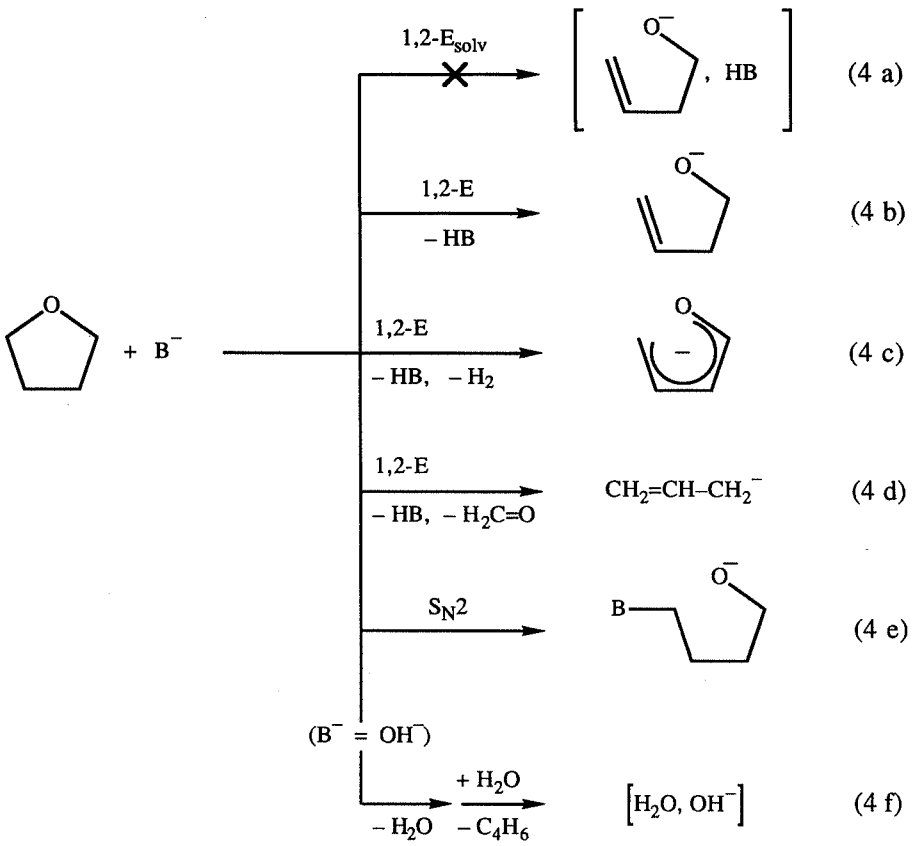

The $OH^-/N_2O/THF$ Reaction System

In a water free reaction atmosphere hydroxide reacts with THF under the formation of $(THF–H)^-$ (86%) and $(THF–3H)^-$ (14%; Table I). This is at variance with the FA results[9] which show formation of $(THF–H)^-$ (46%) and $[(THF–H)^-, H_2O]$ (54%), but no formation of $(THF–3H)^-$ ions (Equation 2). This can be rationalized by the absence of "collisional cooling" under the present low pressure conditions, as a result of which the reaction complex is rovibrationally more exited. The energy gained fuels the dissociation of the $[(THF–H)^-, H_2O]^*$ product complex, which cannot be detected (Equation 4a), leading to the formation of the but-3-ene-1-oxide, $(THF–H)^-$, ions (Equation 4b). However, in about 14% of the rovibrationally excited product complexes H_2 is lost from the but-3-ene-1-oxide, $(THF–H)^-$, prior to the

Table I. Primary product ion distributions for reactions of B^- with THF.

B^-	Product anion distribution (%)			
	CH_2=CH–CH_2^- [a]	$(THF–3H)^-$ [b]	$(THF–H)^-$ [c]	$(THF+B)^-$ [d]
NH_2^-	71	0	29	0
$C_6H_5^-$	0	0	100[e]	0
OH^-	0	14	86	0
CH_2=CH–CH_2^-	0	0	85[e]	15[e]

[a]Equation 4d. [b]Equation 4c. [c]Equation 4b. [d]Equation 4e.

[e]Analysis of primary product ion distribution hampered by the low conversion rate (see text).

Table II. Reaction enthalpies ΔH_r (kcal/mol) associated with reactions of B^- with THF.

B^-	$PA(B^-)$[a]	ΔH_r for the formation of[b]			
		CH_2=CH–CH_2^-[c]	$(THF–3H)^-$[d]	$(THF–H)^-$[e]	$(THF+B)^-$[f]
NH_2^-	403.7	10	–30	–20	–31
$C_6H_5^-$	400.8	13	–27	–17	–40
OH^-	390.8	23	–17	–7	–16
CH_2=CH–CH_2^-	390.8	23	–17	–7	–27

[a] The gas-phase proton affinity (PA) is defined as the enthalpy change associated with the reaction $BH \rightarrow B^- + H^+$ (see reference 15).

[b] Thermochemical data taken from or calculated from heats of formation of Lias et al.[15] or calculated using data from Benson.[23] The PA of $(THF–H)^-$ is estimated to equal the PA of n-butoxide (376 kcal/mol).[15] The heat of formation of S_N2 product ions was estimated using the relation $\Delta H_f(B\text{-}(CH_2)_4O^-) \approx \Delta H_f(B\text{-}(CH_2)_4OH)$[23] + $PA(n\text{-}BuO^-)$[15,24] – $\Delta H_f(H^+)$[15]

[c] Equation 4d. [d] Equation 4c. [e] Equation 4b. [f] Equation 4e.

dissociation of the complex leading to the formation of the buta-1,3-diene-1-oxide, $(THF–3)^-$, ion (Equation 4c, Table I). The loss of H_2 from rovibrationally exited alkoxide ions is a well known process.[16-18] Formally, the formation of the $(THF–3H)^-$ ion can be viewed as initiated by a

hydride transfer from the but-3-ene-1-oxide ion to the water molecule resulting in a complex between the hydrated hydride[19] and but-3-enal (Equation 5). Subsequent proton transfer from the but-3-enal ion to the hydrated hydride followed by dissociation of the product complex results in the formation of the strongly resonance stabilized buta-1,3-diene-1-oxide, $(THF–3H)^-$, ion. From the data in Table II it follows that formation of the ion is highly exothermic for all the bases used. Nonetheless, only in the reaction induced by OH^- this product ion is detected (Table I). This result shows that the loss of H_2 as represented by the mechanism in Equation 5 is best catalysed by a water molecule in the reaction complex, in agreement with the relatively higher hydride affinity (HA) of water (HA = 16 kcal/mol)[20] relative to, for instance, ammonia (HA = 8 kcal/mol).[20]

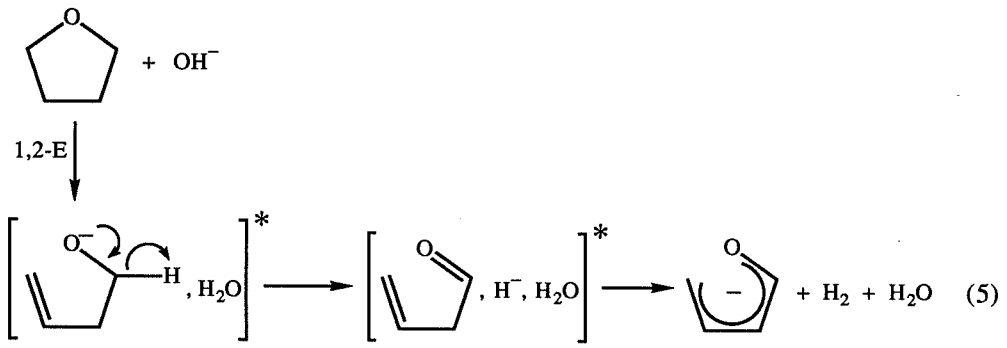

(5)

The $NH_2^-/NH_3/THF$ Reaction System

Amide reacts with THF under the present low pressure conditions under formation of $CH_2=CH–CH_2^-$ (71%) and $(THF–H)^-$ (29%; Table I). This is in contrast with the FA results[9] which show formation of $(THF–H)^-$ (93%) and $[(THF–H)^-, NH_3]$ (7%), but no formation of $CH_2=CH–CH_2^-$. Again the absence of collisional cooling can be held responsible for the nonappearance of the thermally labile solvated $(THF–H)^-$ (Equation 4a). The formation of the allyl anion can be interpreted in terms of a mechanism in which the $(THF–H)^-$ ion in the rovibrationally excited product complex $[(THF–H)^-, NH_3]^*$ fragments via the alternative pathway as presented in Equation 6. Compared to the situation for hydroxide (ΔH_r = 22.8 kcal/mol) this reaction channel is now considerably less endothermic (ΔH_r = 9.9 kcal/mol; Table II) due to the higher basicity of amide. Nevertheless, the formation of the allyl product anion can only be understood if it is

assumed that the reactants are already rovibrationally exited by a few kcal/mol. Apparently, collisional cooling prevents the formation of CH_2=CH–CH_2^- in the endothermic reaction between NH_2^- and tetrahydrofuran under FA conditions.[9] However, reaction of NH_2^- and the highly strained 2-methyloxetane does lead to the exothermic formation of CH_2=CH–CH_2^- via an analogous mechanism in which protophilic attack of NH_2^- on the methyl group of 2-methyloxetane induces subsequent 1,2-elimination, ring-opening, and fragmentation.[9,21]

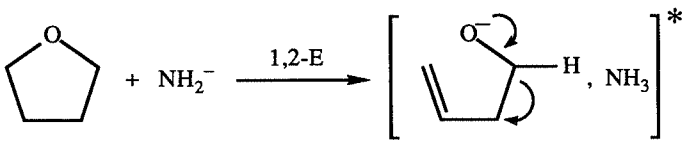

$$\left[\overline{CH_2}\text{–}CH\text{–}\overline{CH_2},\ H_2C{=}O,\ NH_3\right]^* \longrightarrow CH_2{=}CH\text{-}CH_2^- + H_2C{=}O + NH_3 \quad (6)$$

The $C_6H_5^-$/C_6H_6/THF and CH_2=CH-CH_2^-/CH_2=CH-CH_3/THF Reaction Systems

The reactions of THF induced by the carbon bases appear to be very inefficient, relative to those induced by the nitrogen and oxygen bases. The low conversion rate does not allow for an accurate analysis of the product ion distributions. Yet, it appears that the reaction of the phenyl anion with THF exclusively results in the formation of $(THF–H)^-$ ions. However, in the reaction of the allyl anion with THF, both $(THF–H)^-$ (85%) and $(THF+B)^-$ (15%) have been observed (Table I). In principle, $(THF+B)^-$ may be represented by [$(THF–H)^-$, HB] resulting from a 1,2-elimination (Equation 4a). However, this is highly unlikely since no [$(THF–H)^-$, HB] is detected in the reaction of hydroxide with THF, although the 1,2-elimination induced by CH_2=CH–CH_2^- and OH^- are isoenthalpic (Table II). Moreover, solvation of $(THF–H)^-$ by the polar water molecule is probably energetically favored over solvation by the less polar propene. Therefore, the $(THF+B)^-$ product ions formed in the reaction induced by CH_2=CH–CH_2^- can be best represented by CH_2=CH-$(CH_2)_5$-O^- resulting from a nucleophilic attack of the allyl anion on an

α-carbon of THF (S_N2, Equation 4e). It is assumed that this initially rovibrationally excited product ion is thermally less labile than the isomeric [$(THF–H)^-$, CH_2=CH–CH_3] complex ion so that the life-time of this product ion is sufficient to allow collisional stabilization, even under the present low pressure conditions. This gas-phase result parallels condensed phase observations[2] that only soft, resonance stabilized carbanions react with THF via S_N2 substitution.

The inefficiency of proton abstractions from carbon acids by carbanions seems to be a general phenomenon in the gas phase. Representatively, the very inefficient thermoneutral proton transfer from CH_3X (X = Cl, Br) to XCH_2^- is considered to be hindered by a tight transition state which acts as an entropy bottleneck associated with a low density of states.[22] For the allyl anion, the structural change that is caused by the localization of the double bond during the reaction probably enhances this effect.

The Formation of [H_2O, OH^-]

An interesting phenomenon is the efficient formation of the hydrated hydroxide [H_2O, OH^-] when OH^- is allowed to react with THF in the presence of gaseous water, i.e. in the OH^-/H_2O/THF reactant atmosphere rather than in the OH^-/N_2O/THF reactant atmosphere (Equation 4f). The formation of the [H_2O, OH^-] complex is due to a reaction of H_2O and a primary product anion which stems from the reaction between OH^- and THF.The efficient formation of the [H_2O, OH^-] product ions is highly unexpected because the mechanism suggested for the formation of this ion under FA conditions which involves collisional stabilization of the rovibrationally excited intermediate reaction complexes (Equation 3, *vide supra*) is not compatible with the present low pressure conditions. To elucidate the origin of this species, a more detailed mechanistic investigation has been carried out using the technique of oxygen-18 and deuterium isotopic labeling. The experimental results for the various reaction systems are summarized in Table III. Because the secondary reactions involving H_2O are considerably more efficient than the primary reaction between OH^- and THF, determination of the primary product ion distributions for the various reaction systems is hampered. Therefore, Table III shows the product ion distribution at an arbitrary reaction time which is fixed for all reaction systems studied.

Table III. Product anion distributions associated with some reaction systems involving isotopic labeling.[a]

Reaction system	Product anion distribution (%)							
	$D_2HO_2^{-}$[b]	$D_3O_2^{-}$[b]	$H_3{}^{18}OO^{-}$[b]	$H_3{}^{18}O_2^{-}$[b]	$(THF–3H)^{-}$	$(THF–4H+D)^{-}$	$(THF–H)^{-}$	$(THF–2H+D)^{-}$
$OH^{-}/N_2O/THF$	—	—	—	—	18	—	82	—
$^{18}OH^{-}/H_2{}^{18}O/THF$	—	—	9	43	16	—	32	—
$OD^{-}/D_2O/THF$	11	59	—	—	5	3	16	6
$(THF–H)^{-}/D_2O/THF$	38	62	—	—	—	—	c	—
$(THF–3H)^{-}/D_2O/THF$	—	—	—	—	c	—	—	—

[a]Because an accurate determination of the primary product ion distributions is hampered by the relatively highly efficient secondary reaction between the $(THF–H)^{-}$ ion and water, the product ion distributions are given at an arbitrary but fixed reaction time for all reaction systems studied.

[b]These product ions represent isotopomers of the hydrated hydroxide [H_2O, OH^{-}].

[c]Reactant ion.

The $^{18}OH^-/H_2{}^{18}O$/THF and OD^-/D_2O/THF Reaction Systems

The reaction of $^{18}OH^-$ in a $H_2{}^{18}O$/THF atmosphere leads to the formation of $H_3{}^{18}OO^-$ (9%), $H_3{}^{18}O_2^-$ (43%), $(THF–3H)^-$ (16%) and $(THF–H)^-$ (32%; Table III). Analogously, the reaction of OD^- in a D_2O/THF atmosphere leads to the formation of $D_2HO_2^-$ (11%), $D_3O_2^-$ (59%), $(THF–3H)^-$ (5%), $(THF–4H+D)^-$ (3%), $(THF–H)^-$ (16%) and $(THF–2H+D)^-$ (6%; Table III). A mechanism which rationalizes these observations is presented in Scheme II for the OD^-/D_2O/THF reaction system.

As discussed above, the primary $(THF–H)^-$ and $(THF–3H)^-$ ions are generated in an OD^- induced 1,2-elimination reaction of THF. Subsequent association of the but-3-ene-1-oxide, $(THF–H)^-$, ion with D_2O enables an about 15 kcal/mol endothermic deuteron transfer from D_2O to the but-3-ene-1-oxide (reaction step **A**),[15,24] resulting in a hydrogen bound intermediate complex between OD^- and but-3-enol (**2** in Scheme II). Close to thermoneutral proton abstraction from the relatively acidic allylic position of but-3-ene-1-ol by OD^- (reaction step **B**) yields a hydrogen bound intermediate complex between the resulting carbanion and HOD (**3** in Scheme II). HOD assisted cleavage of the C^{α}-OD bond leads to the elimination of 1,3-butadiene from the reaction complex (reaction step **C**) and formation of the observed [HOD, OD^-] product ion. The sequence of reaction steps **B** and **C** can be viewed as a reversible E1cb process, i.e. $(E1cb)_{rev}$. Further, HOD in the [HOD, OD^-] product ion can be exchanged for D_2O which ultimately results in the formation of [D_2O, OD^-]. The above described multi-step reaction between the $(THF–H)^-$ ion and water leading to the formation 1,3-butadiene and the hydrated hydroxide product ion is estimated to be exothermic by 4 kcal/mol.[15,23,24] The analogous formation of the unobserved ammonia solvated hydroxide, [NH_3, OH^-], in the reaction between the $(THF–H)^-$ ion and ammonia (reaction system NH_2^-/NH_3/THF) involves an about 28 kcal/mol[15,24] endothermic proton transfer from ammonia to $(THF–H)^-$ and is estimated to be overall endothermic by at least 8 kcal/mol.[15,23-25] Evidence for the intermediacy of the complex **3** between HOD and the resonance stabilized carbanion is obtained from the observation of the $(THF–4H+D)^-$ and $(THF–2H+D)^-$ product ions. These product ions can be viewed as the $(THF–3H)^-$ and $(THF–H)^-$ ions in which one deuterium has been incorporated. This incorporation can be considered to proceed via the intermediacy of complex **3** in which H/D exchange occurs between HOD and the resonance stabilized carbanion prior to the reverse reaction back to the reactants involving steps **D** and **E**.

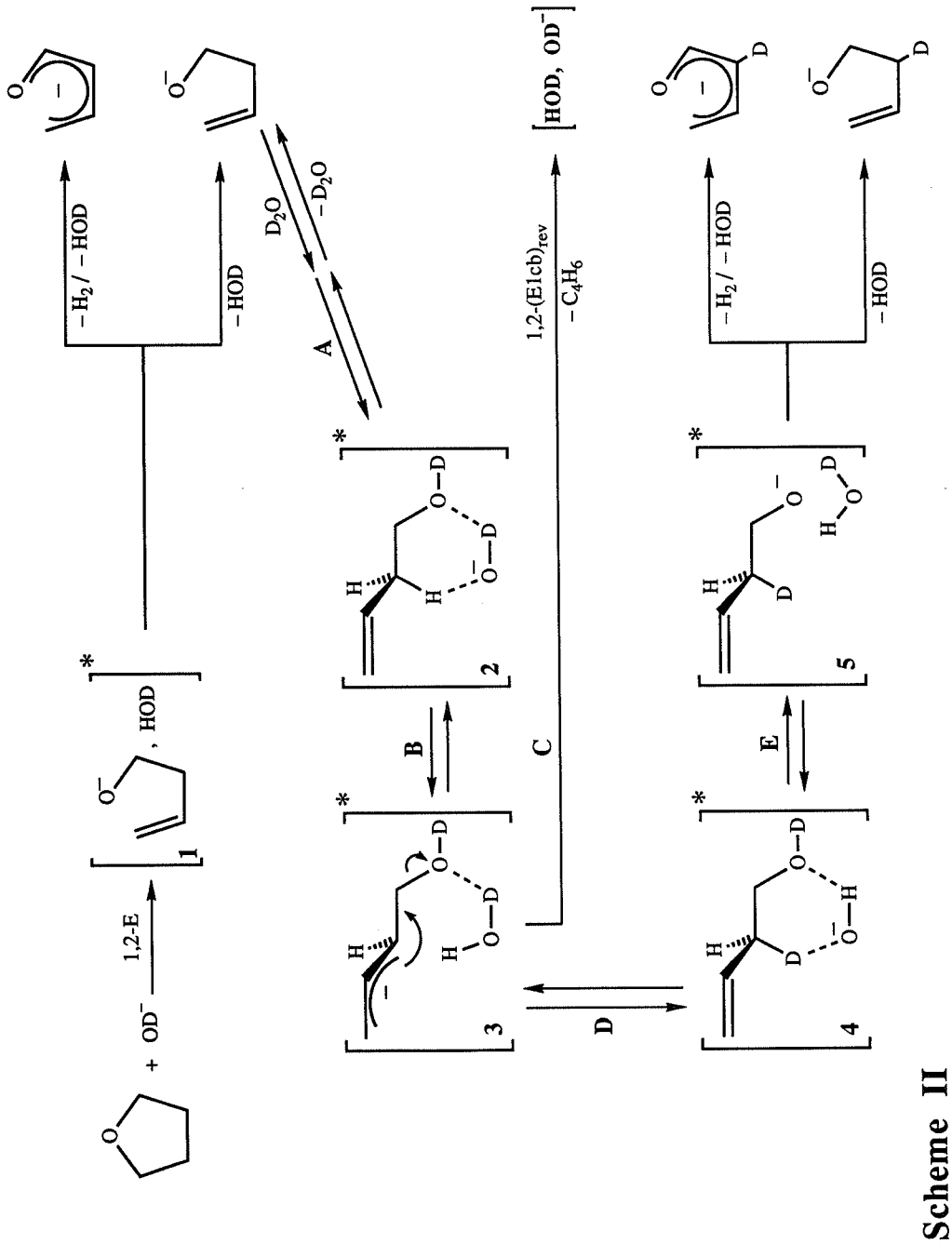

Scheme II

It thus appears that the hydrated hydroxide product ions are generated from a secondary association complex of the $(THF–H)^-$ primary product ions and water and *not* directly from the initial product complex **1** which is composed of the same fragments. This can be rationalized if it is considered that formation of the primary product complex **1** in the hydroxide-induced elimination of THF is more exothermic than formation of this complex via a simple association of the $(THF–H)^-$ product ion and water, because of the energy released in the elimination step (see Table II). As a result, the rovibrationally more excited complex **1** between $(THF–H)^-$ and water formed in the hydroxide-induced elimination of THF rather undergoes a simple entropy favored dissociation than a subsequent reaction towards formation of the hydrated hydroxide ion.

The $(THF–H)^-/D_2O/THF$ and $(THF–3H)^-/D_2O/THF$ Reaction Systems

The but-1,3-diene-1-oxide, $(THF–3H)^-$, ion generated in the hydroxide-induced reaction of THF (Equation 4c) appears to be unreactive in a D_2O/THF atmosphere (Table III). This demonstrates that formation of the $(THF–4H+D)^-$ ion in the OD^-/D_2O/THF reaction system (*vide supra*) is associated with the reaction between the $(THF–H)^-$ ion and D_2O, as suggested in Scheme II, rather than in the reaction between the strongly resonance stabilized $(THF–3H)^-$ ion and D_2O.

The but-3-ene-1-oxide, $(THF–H)^-$, ion, generated in the hydroxide-induced reaction of THF (Equation 4b), very efficiently reacts in the D_2O/THF atmosphere under formation of the isotopomers of the hydrated hydroxide ions (Table III). This clearly shows that these hydrated hydroxide ions result from the reaction between $(THF–H)^-$ and water, as suggested in Scheme II, rather than from the reaction between the hydroxide ion and THF. However, formation of the $(THF–2H+D)^-$, $(THF–4H+D)^-$ and $(THF–3H)^-$ ions observed in the OD^-/D_2O/THF reaction system is not detected in the $(THF–H)^-/D_2O$/THF reaction system (Table III). This demonstrates that the branching ratio of the elimination of 1,3-butadiene from the intermediate complex **3** in reaction step **C** in Scheme II and the hydrogen/deuterium exchange followed by the reverse reaction leading to incorporation of a deuterium atom in the $(THF–H)^-$ and $(THF–3H)^-$ ions (via reaction steps **D** and **E**) very critically depends on the internal energy of the intermediate complex **3**. Under the low pressure conditions the internal energies of the intermediate complexes are likely to differ slightly for the $(THF–H)^-/D_2O$/THF and OD^-/D_2O/THF reaction systems.

4.4 Conclusions

Under low pressure conditions ($p < 10^{-4}$ Pa) the anionic gas-phase base-induced reactions of tetrahydrofuran (THF) predominantly proceed via 1,2-elimination. This elimination initially results in rovibrationally excited, HB solvated but-3-ene-1-oxide ions. As a result of the absence of thermal interaction with the environment HB is vaporized from these solvated ions. Depending on the nature of the base used, a proportion of the excited but-3-ene-1-oxide ions eliminates molecular hydrogen or formaldehyde leading to the formation of the resonance stabilized but-1,3-diene-1-oxide ions and allyl anions, respectively.

Interestingly, reaction between the but-3-ene-1-oxide ion and water results in the very efficient formation of hydrated hydroxide ions. Isotopic labeling reveals that the formation of this hydrated hydroxide is initiated by an endothermic proton transfer from water to but-3-ene-1-oxide generating a complex between hydroxide and but-3-ene-1-ol. Subsequently, a reversible hydroxide-induced E1cb process leads to the elimination of 1,3-butadiene and formation of the hydrated hydroxide ion. To our knowledge, this is the first example of a gas-phase anionic base-induced elimination in which hydroxide is involved as a leaving group. Finally, it is pointed out that this 1,2-elimination provides an independent route to a type of intermediate, namely **2'**, which may also be involved in the mechanism of base-induced diene-forming 1,4-elimination reactions (Equation 7).[26]

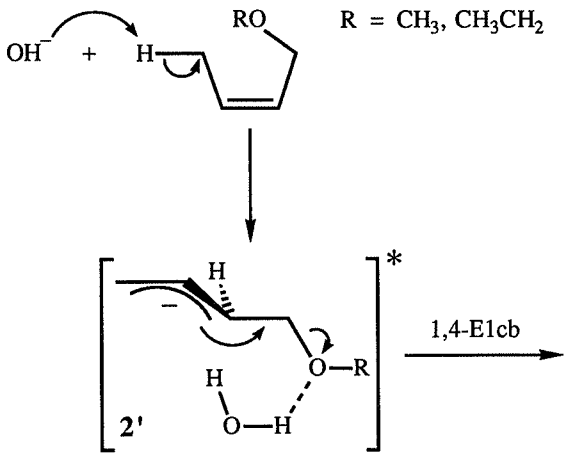

(7)

References

1. Carey, F.A.; Sundberg, R.J. *Advanced Organic Chemistry*, Part A; Plenum Press: New York, 1984.
2. Maercker, A. *Angew. Chem.* **1987**, 99, 1002.
3. Letsinger, R.; Schnizer, W.; Bobko, E. *J. Am. Chem. Soc.* **1951**, 73, 5708.
4. Ziegler, K.; Gellert, H.-G. *Justus Liebigs Ann. Chem.* **1950**, 567, 185.
5. Wittig, G.; Löhmann, L. *Justus Liebigs Ann. Chem.* **1942**, 550, 260.
6. Doorn, R. van; Jennings, K.R. *Org. Mass Spectrom.* **1981**, 16, 397.
7. Bierbaum, V.M.; DePuy, C.H.; Shapiro, R.H.; Stewart, J.H. *J. Am. Chem. Soc.* **1976**, 98, 4229.
8. DePuy, C.H.; Bierbaum, V.M. *J. Am. Chem. Soc.* **1981**, 103, 5034.
9. DePuy, C.H.; Beedle, E.C.; Bierbaum, V.M. *J. Am. Chem. Soc.* **1982**, 104, 6483.
10. Bierbaum, V.M.; Filley, J.; DePuy, C.H.; Jarrold, M.F.; Bowers, M.T. *J. Am. Chem. Soc.* **1985**, 107, 2818.
11. Koning, L.J. de; Nibbering, N.M.M. *J. Am. Chem. Soc.* **1987**, 109, 1715.
12. Nibbering, N.M.M. *Adv. Phys. Org. Chem.* **1988**, 24, 1.
13. Nibbering, N.M.M. *Acc. Chem. Res.* **1990**, 23, 279.
14. Koning, L.J. de; Kort, C.W.F.; Pinkse, F.A.; Nibbering, N.M.M. *Int. J. Mass Spectrom. Ion Processes* **1989**, 95, 71.
15. Lias, S.G.; Bartmess, J.E.; Liebman, J.F.; Holmes, J.L.; Levin R.D.; Mallard, W.G. *J. Phys. Chem. Ref. Data* **1988**, 17, Suppl. Nr. 1.
16. Hayes, R.N.; Sheldon, J.C.; Bowie, J.H.; Lewis, D.E. *Aust. J. Chem.* **1985**, 38, 1197.
17. Hayes, R.N.; Sheldon, J.C.; Bowie, J.H.; Lewis, D.E. *J. Chem. Soc., Chem. Commun.* **1984**, 1431.
18. Noest, A.J.; Nibbering, N.M.M. *Adv. Mass Spectrom.* **1980**, 8A, 227.
19. Kleingeld, J.C.; Nibbering, N.M.M. *Int. J. Mass Spectrom. Ion Phys.* **1983**, 49, 311.
20. Bartmess, J.E. in *Structure/Reactivity and Thermochemistry of Ions*; Ausloos, P.; Lias, S.G. (Eds.); Reidel: Dordrecht, 1987, p. 374, 375.
21. Ingemann, S.; Kleingeld, J.C.; Nibbering, N.M.M. in *Ionic Processes in the Gas Phase*; Almoster Ferreira, M.A. (Ed.); Reidel: Dordrecht: 1984, p. 98.

22. Bickelhaupt, F.M.; Koning, L.J. de; Nibbering, N.M.M.; Baerends, E.J. *J. Phys. Org. Chem.* **1992**, 5, 179.

23. Benson, S.W. *Thermochemical Kinetics*, 2nd Ed.; Wiley: New York, 1976.

24. The PA of but-3-ene-1-oxide, CH_2=CH-$(CH_2)_2O^-$, and of species B-$(CH_2)_4O^-$ (B- = NH_2-, C_6H_5-, HO-, CH_2=CH-CH_2-) is estimated to equal the PA of n-butoxide (376 kcal/mol).[15]

25. The complexation enthalpy of [NH_3, OH^-] is estimated to be less than or equal to that of [NH_3, NH_2^-] which amounts to –12 kcal/mol.[15]

26. Bickelhaupt, F.M.; Buisman, G.J.H.; Koning, L.J. de; Nibbering, N.M.M.; Baerends, E.J., to be published.

5 Multi-Step Processes in Gas-Phase Reactions of Halomethyl Anions XCH_2^- (X = Cl, Br) with CH_3X and NH_3

Abstract

A mechanistic investigation of the gas-phase reactivity of the halomethyl anions XCH_2^- (X = Cl, Br) towards a mixture of the corresponding halomethane and ammonia has been performed, using FT-ICR mass spectrometry. The interpretation of the experimental data is supported by high level density functional theoretical (DFT) calculations for the chlorine containing systems (X = Cl).

When the specific isotopomer $^{A}XCH_2^-$ ($^{A}X = {}^{35}Cl, {}^{79}Br$) is allowed to react in an atmosphere of CH_3X and NH_3, the exclusive formation of the isotope cluster of the halide anions $^{A}X^-$ and $^{B}X^-$ ($^{B}X = {}^{37}Cl, {}^{81}Br$) is observed. However, the intensity ratio $I(^{A}X^-)/I(^{B}X^-)$ exceeds significantly the value expected from the natural relative isotope abundances and depends linearly on the pressure ratio $p(NH_3)/p(CH_3X)$.

The experimental results are interpreted in terms of three competing reaction mechanisms: i) The by far dominating process is the more than 70 kcal/mol exothermic one-step S_N2 substitution of $^{A}XCH_2^-$ on CH_3X, generating haloethane $^{A}XCH_2CH_3$ and X^- isotopomers, the latter in the proportion of their natural abundances (direct S_N2). The experimentally observed excess of $^{A}X^-$ stems from two minor reaction pathways: ii) In a secondary reaction, the halide X^- in the primary product anion/molecule complex $[^{A}XCH_2CH_3 \cdots X^-]^*$ of the S_N2 substitution induces a 1,2-elimination, leading to the formation of the $^{A}X^-$ isotopomer (two-step $S_N2/E2$); iii) Finally, $^{A}XCH_2^-$ can react with ammonia by consecutive endothermic proton transfer (PT) from NH_3 to $^{A}XCH_2^-$ and a very exothermic S_N2 substitution of the resulting amide on $^{A}XCH_3$ leading to CH_3NH_2 and an excess of $^{A}X^-$ which depends linearly on $p(NH_3)/p(CH_3X)$ (PT/S_N2). Theoretical calculations show that in the case of $[ClCH_2^- \cdots NH_3]^*$, the PT/S_N2 reaction has no stable intermediate. Therefore, it is concluded that this reaction is *not* a two-step but a one-step process.

5.1 Introduction

In the past decade, a large number of gas-phase ion/molecule reactions has been studied by Fourier transform ion cyclotron resonance (FT-ICR) mass spectrometry, and it has been well established that the observed gas-phase ion/molecule reactions proceed via loose ion/molecule complexes which are bound by ion/dipole and ion/induced dipole interactions and hydrogen bonds.[1-2] A fascinating phenomenon is the possibility of secondary reactions taking place in relatively long lived product ion/molecule complexes of primary reactions, i.e., product ions can be formed via multiple consecutive reaction steps.[3-4]

In this context an interesting observation has been reported by our group in a study on the gas-phase reactivity of a number of carbanions bearing an α-heteroatom.[5] In that study, amongst others, the reactivity of the halomethyl anions $ClCH_2^-$ and $BrCH_2^-$ was investigated in an atmosphere of the corresponding halomethane and ammonia. When $^{35}ClCH_2^-$ was isolated and subsequently allowed to react, no $^{37}ClCH_2^-$ ions were formed. However, $^{35}Cl^-$ was produced more abundantly than expected from S_N2 substitution on chloromethane, i.e., the intensity ratio $I(^{35}Cl^-)/I(^{37}Cl^-)$ significantly exceeded the natural relative isotope abundance[6] of 3.13 (Equation 1).

$$^{35}ClCH_2^- \xrightarrow{CH_3Cl\ /\ NH_3} \begin{cases} \longrightarrow\ ^{35}Cl^- : {}^{37}Cl^- > 3 : 1 & \text{(1 a)} \\ \not\longrightarrow\ ^{37}ClCH_2^- & \text{(1 b)} \end{cases}$$

This was explained by proposing[5] a mechanism in which the chloromethyl anion, $^{35}ClCH_2^-$, reacts with ammonia via a two-step mechanism: i) In the first step the intermediate complex $[^{35}ClCH_3 \bullet\bullet\bullet NH_2^-]^*$ is formed by endothermic proton transfer (PT) from ammonia to $^{35}ClCH_2^-$; ii) in the second step the amide NH_2^- effects an S_N2 substitution under expulsion of the $^{35}Cl^-$ (Equation 2; R = H). Support for this mechanism comes from the observation that addition of a more acidic amine R_2NH leads to an increase of the excess of $^{35}Cl^-$. Similar results were obtained for $^{79}BrCH_2^-$ in an atmosphere of bromomethane and an amine.

$$^{35}ClCH_2^- + R_2NH \rightleftharpoons [^{35}ClCH_2^- \cdots R_2NH]^* \rightleftharpoons [^{35}ClCH_3 \cdots R_2N^-]^* \longrightarrow {}^{35}Cl^- + CH_3NR_2 \quad (2)$$

The purpose of the present paper is a quantitative elucidation of the different mechanisms which contribute to the above mentioned formation of the halide anion isotope cluster in a combined FT-ICR mass spectrometric and density-functional theoretical (DFT) approach. To this end, several a priori conceivable mechanisms are discussed in section 5.3 of this paper and a relationship is presented which expresses the isotope intensity ratio $I(^AX^-)/I(^BX^-)$ as a function of the pressure ratio $p(CH_3X)/p(NH_3)$. This relationship serves as the guide for the mass spectrometric experiments and for the interpretation of their results (sections 5.4 and 5.5).

Besides the elucidation and quantification of the mechanisms active in the chloride or bromide anion formation, the nature of these mechanisms is investigated by theoretical calculations, using a high level density-functional (DF) method as implemented in the Amsterdam DF program system.[7-12] One question which will be adressed concerns the character of the PT/S_N2 reaction: does a stable intermediate $[^{35}ClCH_3 \cdots R_2N^-]^*$ exist as postulated in equation 2 ? This might not be the case[13] for a proton transfer which is endothermic by 7.6 kcal/mol.[14] Furthermore, an explanation is presented for the observation that a thermoneutral PT in the reactant complex $[^{35}ClCH_2^- \cdots CH_3Cl]^*$ cannot compete with the S_N2 process. For economic reasons the theoretical investigations do not include the bromine containing systems.

5.2 Methods

Experimental

The experiments were performed with a "home-made" Fourier transform ion cyclotron resonance (FT-ICR) mass spectrometer equipped with a 1.2 T electromagnet and a cubic inch cell.[15] The Segmented Fourier transform (SEFT) procedure[16] was employed in all cases to obtain absolute peak intensities with an accuracy of better than 1%. General operating and experimental procedures have been described previously.[15]

The temperature in the cell was around 333 K as measured by a thermocouple on the trapping plate opposite the filament. The total pressure in the different experiments was kept

between 10^{-6} and 10^{-4} Pa with a background pressure lower than $5 \cdot 10^{-7}$ Pa. The pressures were measured with an ionization gauge manometer placed in a side arm of the main pumping line. The ionization gauge manometer was calibrated for methane by fitting our rate constant for the reaction $CH_4^{+\bullet} + CH_4 \rightarrow CH_5^+ + CH_3^\bullet$ to the average literature value of $(1.11 \pm 0.04) \cdot 10^{-9}$ $cm^3molecule^{-1}s^{-1}$.[17] Absolute pressures were obtained by correction for the relative sensitivities R_x of the ionization gauge manometer for gases x, using the relationship $R_x = 0.36\alpha + 0.30$ of Bartmess and Georgiadis[18] and polarizabilities α from Miller.[19]

NH_2^- was generated via dissociative resonant capture of electrons with a kinetic energy of 5 eV by NH_3. The halomethyl anions were formed through proton abstraction from the corresponding halomethane by NH_2^-. All the chemicals used were commercially available.

Theoretical

General

The MOs were expanded in a large set of Slater type orbitals (STOs). The basis is of double-ζ quality (two STOs per nl shell). A polarization function was added on each atom: 2p on H, 3d on C, N, and Cl. Geometries were optimized with the simple Xα exchange-correlation potential[7] using gradient techniques.[20] C_S point group symmetry was assumed for the ion/molecule complexes. The energy data reported for stable structures (energy minima) have been obtained in the optimum geometry with more sophisticated density-functionals (DF) for exchange and correlation. Exchange is described with Slater's $\rho^{1/3}$ potential (Xα with $\alpha = 2/3$), with a non-local correction due to Becke.[21-23] According to the suggestion by Stoll et al.,[24] only correlation between electrons of different spin is introduced, for which electron gas data (in the Vosko-Wilk-Nusair[25] parametrization) are used.

Accuracy of DF interaction energies

Table I compares our DFT results for the cluster energies (ΔE_{clust}) and enthalpies (ΔH_{clust}) of a number of small anion/molecule complexes with the results obtained by other theoretical and experimental methods. The DFT cluster *energies*, ΔE_{clust}, are in good agreement with the results obtained by conventional ab initio calculations. For the $H_2O{\cdots}OH^-$ and $CH_4{\cdots}CH_3^-$ systems incorporation of correlation into the conventional ab initio calculation leads to a strengthening of the

anion/molecule interaction and to a better agreement with the DFT values. The DFT cluster *enthalpies*, ΔH_{clust}, also compare well with those obtained experimentally. Deviations are in the order of 5 kcal/mol. The largest deviation is found for FH•••F$^-$, where the DFT value (–45.8 kcal/mol) is 7.1 kcal/mol more bonding than the experimental value (–38.7±2[36]). The cluster energy and enthalpy of the fluorine containing anion/molecule complex appear to depend very critically on the quality of the basis set. Therefore, the DFT calculation was performed with an extra large triple-ζ basis augmented with two polarization functions on each atom (3d and 4f on F, 2p and 3d on H). The difference of 7.1 kcal/mol between the DFT and experimental ΔH_{clust} might be further reduced if a quadruple-ζ basis is employed.

Table I. Comparison of the cluster energies (ΔE_{clust}) and enthalpies (ΔH_{clust}) (kcal/mol) of a number of small anion/molecule complexes as obtained by several theoretical and experimental methods.

System	ΔE_{clust}		ΔH_{clust}(298 K)		
	DFT[a]	other calculation	DFT[a,b]	experiment	
ClH•••Cl$^-$	–25.0[c]	–22.3[e]	–22.5	–23.9±2[j]	
FH•••F$^-$	–48.3[c,d]	–43.4[e]	–45.8	–38.7±2[k]	
H_2O•••OH^-	–35.0	–23.1,[f] –28.0[g]	–28.5	–23.9±2,[l]	–35.6±6.9[m]
NH_3•••NH_2^-	–17.6	—	–11.1	–12[n]	
CH_4•••CH_3^-	–6.7	–1.40,[h] –2.35[i]	–0.2	—	

[a]This work; energy calculated with sophisticated density-functionals[21-25] in Xα geometry,[7] double-ζ STO basis with one polarization function on each atom (see text). [b]$\Delta H_{clust}(T) = \Delta E_{clust} + \Delta ZPE + \frac{5}{2}RT$; the difference in zero point vibrational energies between the cluster and the separated fragments, ΔZPE, is estimated from the literature:[32] for ClH•••Cl$^-$ and FH•••F$^-$ ΔZPE ≈ 1 kcal/mol, for the other systems ΔZPE ≈ 5 kcal/mol. [c]Xα geometry optimization yields a $D_{\infty h}$ symmetric "proton bound" halide dimer structure. [d]triple-ζ STO basis with two polarization functions on each atom: 3d and 4f on F and 2p and 3d on H. [e]Minato and Yamabe,[39] HF with double-ζ plus polarization basis. [f]Roos et al.,[33] HF with [541/31] basis. [g]Roos et al.[33], CI with [541/31] basis. [h]Latajka and Scheiner,[34] HF with 6-31G** + p(C) basis ($\zeta_p(H) = 0.15$). [i]Latajka and Scheiner,[34] MP3 with 6-31G** + p(C) basis ($\zeta_p(H) = 0.15$). [j]Caldwell and Bartmess[35]. [k]Larson and McMahon[36]. [l]Payzant et al.[37]. [m]DePaz et al.[38]. [n]Lias et al..[14]

Summarizing, we conclude that with the DF approach interaction energies in anion/molecule complexes are described to an accuracy in the order of 5 kcal/mol, in agreement with previous experience on systems involving main group elements and/or metals.[20,26–31]

Determination of reaction paths

Reaction paths are determined by elongating the bond to be broken in steps of 10 pm (see "theoretical results" in section 5.4). After each step the geometry is allowed to relax; however, the length of the elongated bond is kept fixed. The reaction paths and activation energies are calculated using the Xα exchange-correlation potential.

In a study on the cyanide/isocyanide isomerization of HCN and CH_3CN and the *E/Z* isomerization of N_2H_2, Fan and Ziegler[29] have shown that with this level of density functional theory (DFT) activation energies are obtained which overestimate the barrier by about 5 kcal/mol. Conventional ab initio methods which take to some extent electron correlation into account (for example Hartree-Fock + Many-Body-Perturbation-Theory (HF + MBPT)) afford barriers that are 5 to 10 kcal/mol higher than the DFT values.[29] We have obtained similar results for the activation energy for proton transfer in $CH_4 \cdots CH_3^-$, a system that closely resembles the anion/molecule complexes of present interest. The Xα exchange-correlation potential arrives at a barrier of 3.97 kcal/mol, while with the more sophisticated density-functionals (*vide supra*) the calculated barrier amounts to 9.59 kcal/mol. The latter is only lower by about 3 kcal/mol than the best MP3 value of 12.86 kcal/mol obtained by Latajka and Scheiner[34] with a 6-31G** + p(C) basis set (at the HF level Latajka and Scheiner obtained a barrier of 21.98 kcal/mol).

5.3 Selection of possible reaction mechanisms

In this section several a priori conceivable mechanisms which can lead to the observed formation of the X^- isotope cluster in the reaction system $^AXCH_2^- + CH_3X + NH_3$ are presented. It will be discussed which of them is in principle suitable to be taken into account when an expression is derived which relates the intensity ratio $I(^AX^-)/I(^BX^-)$ to the pressure ratio $p(CH_3X)/p(NH_3)$, and which serves as an instrument for the mechanistic investigation. From the fact that no $^BXCH_2^-$ ions are formed when $^AXCH_2^-$ is isolated and allowed to react in an

atmosphere of CH_3X and NH_3 it is concluded that no measurable thermoneutral proton transfer (PT) occurs in the reactant complex $[^AXCH_2^-\bullet\bullet\bullet CH_3{}^BX]^*$. This point is explained in more detail in the Discussion (section 5.5).

Conceptually the most simple process which results in the formation of the excess of $^AX^-$ is the bimolecularly induced dissociation of the selected halomethyl anion into methylene and the specific isotopomer of the halide anions (Equation 3). However, on the basis of energetic considerations this second step of an α-E1cb elimination can be excluded, as the reaction enthalpy is endothermic by 27.9 and 24.1 kcal/mol for $ClCH_2^-$ and $BrCH_2^-$, respectively (Table II).

$$^AXCH_2^- \xrightarrow{\alpha\text{-Elimination}} CH_2 + {}^AX^- \qquad (3)$$

The next obvious reaction channel is the direct S_N2 substitution of the halomethyl anion on the halomethane (Reaction 4 a). This mechanism leads to the production of the halide anion isotopomers in the proportion of their natural abundance ($I(^{35}Cl^-)/I(^{37}Cl^-)$ = 3.13, $I(^{79}Br^-)/I(^{81}Br^-)$ = 1.03).[6] Thermodynamically, this direct S_N2 substitution is very favorable as it is exothermic by -72.3 and -74.7 kcal/mol for X is Cl and Br, respectively (Table II).

Table II. Overall enthalpies of reaction, ΔH_r (kcal/mol), for some gas-phase processes of the reaction systems $XCH_2^- + CH_3X + NH_3$ (X = Cl, Br).[a]

Equation	process	ΔH_r (X = Cl)	ΔH_r (X = Br)
3	α-elimination	27.9	24.1
4 a	direct S_N2	-72.3	-74.7
4 b	S_N2/E2	-55.1	-56.3
4 c	PT/S_N2	-59.6	-63.4
5	S_N2/S_N2	-72.3	-74.7

[a]Calculated from heats of formation given in reference 14.

Another conceivable mechanism is the proton transfer initiated nucleophilic substitution (PT/S_N2) mechanism of the halomethyl anion and ammonia (Reaction 4c). This PT/S_N2 reaction has first to overcome the phase of endothermic proton transfer, but the overall reaction enthalpy is exothermic by -59.6 and -63.4 kcal/mol for X is Cl and Br, respectively (Table II). The PT/S_N2 process produces pure $^AX^-$ and thus, overall, leads to an excess of the $^AX^-$ isotopomer. The amount with which this process contributes to $I(^AX^-)/I(^BX^-)$ depends linearly on the pressure ratio $p(NH_3)/p(CH_3X)$. Dissociation of the intermediate structure $XCH_3{\bullet\bullet\bullet}NH_2^-$ is thermodynamically inaccessible ($\Delta H_r[XCH_2^- + NH_3 \longrightarrow XCH_3 + NH_2^-] = 7.6$ and 10.9 kcal/mol for X = Cl and Br, respectively).[14]

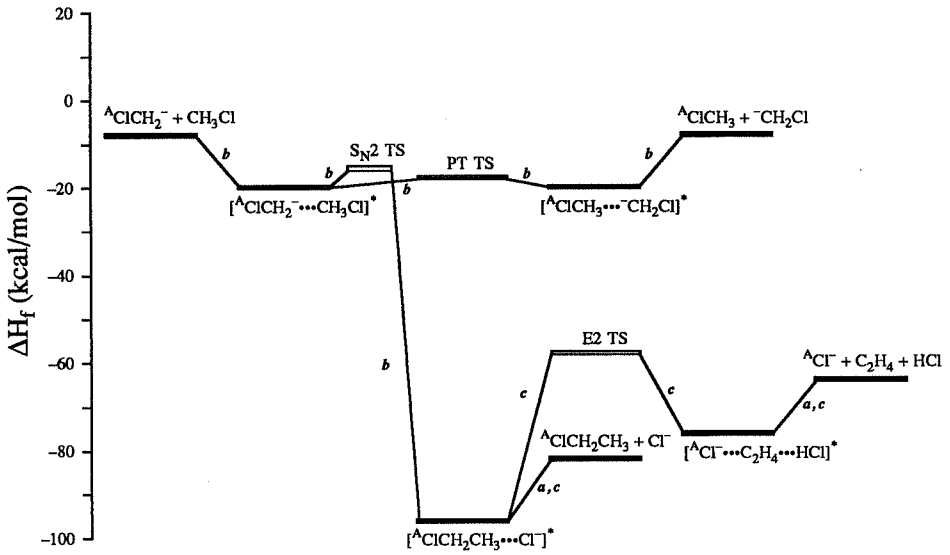

Figure 1. *Schematic energy (kcal/mol) diagram for the thermoneutral proton transfer (PT), the direct S_N2 substitution, and the $S_N2/E2$ process of $ClCH_2^-$ and CH_3Cl. The enthalpies of the separated reactants and products, and enthalpy differences with a label "**a**" have been taken from Lias et al.[14]. The energy differences with a label "**b**" stem from our own calculations (see Table 4). The energy differences with a label "**c**" have been taken from Minato and Yamabe.[39]*

$$^{A}XCH_2^- + CH_3X \rightleftharpoons [^{A}XCH_2^-\cdots CH_3X]^*$$

$$\downarrow S_N2$$

$$[^{A}XCH_2CH_3\cdots X^-]^* \longrightarrow {}^{A}XCH_2CH_3 + X^- \qquad k_1 \quad (4\,a)$$

$$\downarrow E2$$

$$[^{A}X^-\cdots C_2H_4\cdots HX]^* \longrightarrow HX + C_2H_4 + {}^{A}X^- \qquad k_2 \quad (4\,b)$$

$$^{A}XCH_2^- + NH_3 \rightleftharpoons [^{A}XCH_2^-\cdots NH_3]^*$$

$$\downarrow PT$$

$$[^{A}XCH_3\cdots NH_2^-]^*_{labile}$$

$$\downarrow S_N2$$

$$[^{A}X^-\cdots CH_3NH_2]^* \longrightarrow CH_3NH_2 + {}^{A}X^- \qquad k_3 \quad (4\,c)$$

The two above mentioned bimolecular processes (Reaction 4a and 4c) proceed via dissociation of the product ion/molecule complexes $[^{A}XCH_2CH_3\cdots X^-]^*$ and $[CH_3NH_2\cdots {}^{A}X^-]^*$, respectively. While the latter can only dissociate, in the former a secondary E2 elimination could take place in which the halide X^- acts as a base and abstracts a β-proton from the haloethane entity under expulsion of the leaving group $^{A}X^-$ (Reaction 4b). Although this 1,2-elimination step is endothermic (by about 20 kcal/mol for X = Cl[39]), it can proceed as it is fueled by the high exothermicity (Table II) of the foregoing S_N2 step. This can be seen clearly in Figure 1, where the energetics of the reactions between the chloromethyl anion and chloromethane are displayed. The overall S_N2/E2 process is exothermic by –55.1 and –56.3 kcal/mol for X is Cl and Br, respectively (Table II). As the ion/molecule complex $[^{A}XCH_2CH_3\cdots X^-]^*$ is highly (rovibrationally) excited[1], entropic factors are expected to play an important role in determining the competition between

secondary processes that take place from this complex. Therefore, it is expected that the dissociation of this complex to haloethane and halide (Reaction 4a) dominates over the secondary E2 reaction not only due to the more favorable energetics of the former process, but also because of its looser transition state structure. Furthermore, the formation of the $[^AX{\bullet\bullet}H{\bullet\bullet}X]^-$ clusters is *not* observed, i.e. there is *no* indication that the entropically less favorable but 20 kcal/mol[14] more exothermic 1,2-elimination leading to the solvated leaving group takes place.

Analogous considerations lead to the exclusion of another conceivable secondary reaction occurring in the (rovibrationally) excited[1] $[^AXCH_2CH_3{\bullet\bullet\bullet}X^-]^*$ complex, namely the secondary S_N2 substitution of X^- on the haloethane (Reaction 5).

$$[CH_3CH_2{}^AX{\bullet\bullet\bullet}X^-]^* \xrightarrow{S_N2} [CH_3CH_2X{\bullet\bullet\bullet}{}^AX^-]^* \qquad (5)$$

The overall exothermicity of this S_N2/S_N2 reaction is the same as for the direct S_N2 substitution (Table II). In principle, this process could also make a contribution to the excess of the $^AX^-$ isotopomer which is experimentally indistinguishable from the $S_N2/E2$ contribution (Reaction 4b). However, although the activation energy for the secondary S_N2 substitution (14.6 kcal/mol) is 22.7 kcal/mol lower than that of the E2 elimination (37.3 kcal/mol)[39], the latter reaction might be favoured in the highly (rovibrationally) excited[1] $[^AXCH_2CH_3{\bullet\bullet\bullet}X^-]^*$ ion/molecule complex due to the higher density of states in the "loose" E2 transition state.[40] This assumption is confirmed by studies of our group[3-4] on multistep gas-phase reactions, in which an intermediate ion/molecule complex occurred that contained S_N2 as well as E2 reactive sites. In all cases the secondary E2 reactions strongly prevail. The facility of E2 elimination compared to S_N2 substitution has also been noted in other systems.[15] Finally, also the spatial orientation of the Cl^- in the S_N2 product complex $[^AXCH_2CH_3{\bullet\bullet\bullet}X^-]^*$ is in favour of a subsequent E2 reaction. The chloride anion is very close to the CH_3 group of the chloroethane and far away from the proper spatial orientation for a "backside" attack on the chlorine leaving group which would be necessary for a second S_N2 step.

Summarizing, it is concluded that the three processes in Equation 4, i.e., direct S_N2, $S_N2/E2$, and PT/S_N2, can be expected to contribute to the formation of the observed product isotope cluster of halide anions X^- in the reaction system $^AXCH_2^- + CH_3X + NH_3$. On the basis of these possible reactions Equations 6 ($^AX = {}^{35}Cl$), and 7 ($^AX = {}^{79}Br$) can be derived in which the isotope intensity ratio $I(^AX^-)/I(^BX^-)$ is related to the pressure ratio $p(NH_3)/p(CH_3X)$.

$$\frac{I(^{35}Cl^-)}{I(^{37}Cl^-)} = \left[3.13 + \frac{k_2}{k_1}4.13\right] + \left[\frac{k_3}{k_1}4.13\right]\frac{p(NH_3)}{p(CH_3Cl)} \quad (6)$$

$$\frac{I(^{79}Br^-)}{I(^{81}Br^-)} = \left[1.03 + \frac{k_2}{k_1}2.03\right] + \left[\frac{k_3}{k_1}2.03\right]\frac{p(NH_3)}{p(CH_3Br)} \quad (7)$$

As it appears, the relative magnitude of the overall rate constants k_1, k_2, and k_3 (Reactions 4a, 4b, and 4c, respectively) can be obtained from the slope and the intercept of Equations 6 and 7. These can be experimentally obtained by measuring $I(^AX^-)/I(^BX^-)$ as a function of $p(NH_3)/p(CH_3X)$. Finally, one arrives at absolute values for k_1 to k_3 by determining the total rate constant with which the reactant carbanion $^AXCH_2^-$ is transformed to products.

In the case of the chlorine containing reaction system, also the complementary experiment has been carried out with $^{37}ClCH_2^-$ as the reactant carbanion isotopomer ($^AX = {}^{37}Cl$). For this system Equation 8 holds.

$$\frac{I(^{37}Cl^-)}{I(^{35}Cl^-)} = \left[0.320 + \frac{k_2}{k_1}1.32\right] + \left[\frac{k_3}{k_1}1.32\right]\frac{p(NH_3)}{p(CH_3Cl)} \quad (8)$$

5.4 Results

Experimental results

First, in Table III the experimentally obtained rate constants k_1, k_2 and k_3 are presented. For the reaction system $ClCH_2^- + CH_3Cl + NH_3$ these constants amount to $6.5 \cdot 10^{-10}$, $2.0 \cdot 10^{-10}$ and $0.78 \cdot 10^{-10}$ $cm^3molecule^{-1}s^{-1}$, respectively. For the reaction system $BrCH_2^- + CH_3Br + NH_3$ k_1, k_2 and k_3 amount to $7.9 \cdot 10^{-10}$, $1.3 \cdot 10^{-10}$ and $0.32 \cdot 10^{-10}$ $cm^3molecule^{-1}s^{-1}$, respectively.

The relative rate constant values (k_2/k_1 and k_3/k_1) for the reaction system $ClCH_2^- + CH_3Cl + NH_3$ stem from three independent experiments with the isotopomer $^{35}ClCH_2^-$ as the reactant carbanion ($^AX = {}^{35}Cl$; Equation 6) and two complementary experiments with $^{37}ClCH_2^-$ ($^AX =$

^{37}Cl; Equation 8). Figure 2 displays the $I(^{35}Cl^-)/I(^{37}Cl^-)$ versus $p(NH_3)/p(CH_3Cl)$ graph obtained from the combined 21 data points of the three experiments with $^{35}ClCH_2^-$ together with the $I(^{79}Br^-)/I(^{81}Br^-)$ versus $p(NH_3)/p(CH_3Br)$ graph obtained from the 6 data points of the experiment with $^{79}BrCH_2^-$ (see below). The error given in percent of the ratios k_2/k_1 (45%) and k_3/k_1 (18%) represents the standard deviation over the five independent experiments. The absolute rate constant values were obtained from five separate determinations of the overall rate constant with which $^{35}ClCH_2^-$ is transformed to products and using k_2/k_1 and k_3/k_1. The associated standard deviation amounts to 10%.

The relative rate constant values (k_2/k_1 and k_3/k_1) for the reaction system $BrCH_2^-$ + CH_3Br + NH_3 stem from one experiment with the isotopomer $^{79}BrCH_2^-$ as the reactant carbanion ($^AX = {}^{79}Br$; Equation 7; see Figure 2). The error given in percent of the ratios k_2/k_1 and k_3/k_1 is taken from the five independent experiments for X = Cl. The absolute rate constant values were obtained from three separate determinations of the overall rate constant with which $^{79}BrCH_2^-$ is transformed to products and using k_2/k_1 and k_3/k_1. The associated standard deviation amounts to 21%.

Table III. Absolute and relative overall rate constants k_1, k_2, and k_3 (10^{-10} $cm^3molecule^{-1}s^{-1}$) determined for reactions 4 a, 4 b and 4 c, respectively, of the reaction systems XCH_2^- + CH_3X + NH_3 (X = Cl, Br).

Equation	Process	k_i (X = Cl) absolute[a]	relative[b]	k_i (X = Br) absolute[c]	relative[d]
4 a	Direct S_N2: k_1	6.5 ± 0.6	1.0	7.9 ± 1.7	1.0
4 b	$S_N2/E2$: k_2	2.0 ± 0.2	0.34 ± 0.14	1.3 ± 0.3	0.16 ± 0.07
4 c	PT/S_N2: k_3	0.78 ± 0.08	0.12 ± 0.02	0.32 ± 0.07	0.04 ± 0.01

The indicated experimental error corresponds to the standard deviation of: [a]10% over five determinations of the overall rate constant, [b]45% (eq. 4b) and 18% (eq. 4c) over five experiments, [c]21% over three determinations of the overall rate constant, and [d]45% (eq. 4b) and 18% (eq. 4c) taken from the five experiments for the chlorine containing reaction systems (X = Cl). See also the section on the experimental results.

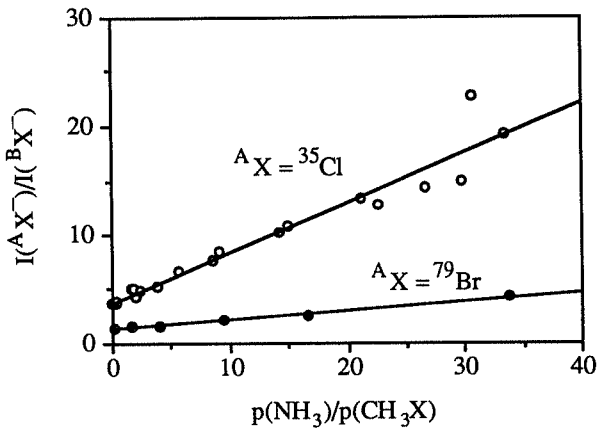

Figure 2. *The intensity ratio* $I(^{35}Cl^-/^{37}Cl^-)$ *as a function of the pressure ratio* $p(NH_3)/pCH_3Cl)$ *for the reaction system* $^{35}ClCH_2^- + CH_3Cl + NH_3$ *(21 data points, 3 independent series of measurements) and the intensity ratio* $I(^{79}Br^-/^{81}Br^-)$ *as a function of the pressure ratio* $p(NH_3)/pCH_3Br)$ *for the reaction system* $^{79}BrCH_2^- + CH_3Br + NH_3$ *(6 data points, 1 independent series of measurements).*

Theoretical results

The theoretical results on the chlorine containing reaction systems are presented in Tables IV (energies, charges) and V (populations), and in Figures 3 (structures) and 4 (reaction profile for the PT/S_N2 reaction taking place from $[ClCH_2^-\bullet\bullet\bullet NH_3]^*$). In Table IV relative energies, ΔE_{rel}, and cluster energies, ΔE_{clust}, are collected. The two reactant anion/molecule complexes $[ClCH_2^-\bullet\bullet\bullet CH_3Cl]^*$ and $[ClCH_2^-\bullet\bullet\bullet NH_3]^*$ appear to have comparable cluster energies of –10.84 and –10.15 kcal/mol, respectively. From a bonding energy analysis[30] it appears that the bonding interactions (electrostatic and orbital interaction) are provided for more than 45% by the orbital interaction. This orbital interaction is mainly attributed to the charge transfer from the lone pair orbital of the carbanion to the $\sigma^*_{C\text{-}H}$ or $\sigma^*_{N\text{-}H}$ MO of the neutral. From Table V it appears that in $[ClCH_2^-\bullet\bullet\bullet NH_3]^*$ the $\sigma^*_{N\text{-}H}$ of NH_3 is populated by 0.19 electrons. Overall, both the NH_3 fragment in $[ClCH_2^-\bullet\bullet\bullet NH_3]^*$ and the CH_3Cl fragment in $[ClCH_2^-\bullet\bullet\bullet CH_3Cl]^*$, have acquired a charge of about –0.2 electrons (Table IV). The population of the anti-bonding $\sigma^*_{C\text{-}H}$ and $\sigma^*_{N\text{-}H}$ MOs is also revealed by the elongation of the corresponding bonds by 5.1 pm to $d(C\text{-}H)_1 = 115.5$

Table IV. Calculated relative energies, ΔE_{rel}, and cluster energies (energy change when the weakly bound (•••) fragments are brought together), ΔE_{clust}, (kcal/mol), and fragment charges, Q(fragment), (electrons) for selected chlorine containing reaction systems. See Figure 3 for structures.

System	ΔE_{rel}[a]	ΔE_{clust}[b]	Q(A$^-$)[c]	Q(M)[c]
Chloromethane clusters				
$[ClCH_2^-\bullet\bullet\bullet CH_3Cl]^*$	0.00	–10.84	–0.80	–0.20
$[ClCH_2^-\bullet\bullet H^+\bullet\bullet{}^-CH_2Cl]^{\neq}$	2.08	—	—	—
Ammonia clusters				
$[ClCH_2^-\bullet\bullet\bullet NH_3]^*$	0.00	–10.15	–0.79	–0.21
$[ClCH_3\bullet\bullet\bullet NH_2^-]^*_{labile}$	4.31	—	–0.65	–0.35
$[ClCH_3\bullet\bullet\bullet NH_2^-]^{\neq}$	7.24	—	–0.74	–0.26
$[CH_3NH_2\bullet\bullet\bullet Cl^-]^*$	–56.01[d]	–6.39	–0.84	–0.16

[a]Calculated with Xα exchange-correlation potential.[7] [b]Calculated with more sophisticated density-functionals[21–25] (see text). [c]Q(A$^-$): charge of anionic fragment, Q(M): charge of molecular fragment. [d]Calculated for the most stable conformation of $[CH_3NH_2\bullet\bullet\bullet Cl^-]^*$ with the sophisticated density-functionals[21–25] (see text).

Table V. Calculated Mulliken MO populations, P(MO), (electrons) for selected chlorine containing reaction systems on the reaction coordinate of the PT/S_N2 process which takes place from the reactant anion/molecule complex $[ClCH_2^-\bullet\bullet\bullet NH_3]^*$. See Figure 3 for structures.

System	$P(C_{LP})$	$P(\sigma^*_{N\text{-}H})$		
$[ClCH_2^-\bullet\bullet\bullet NH_3]^*$	1.78	0.19		
	$P(N_{LP1})$[a]	$P(N_{LP2})$[b]	$P(\sigma^*_{C\text{-}Cl})$	$P(\sigma^*_{C\text{-}H})$
$[ClCH_3\bullet\bullet\bullet NH_2^-]^*_{labile}$	1.76	1.88	0.14	0.14
$[ClCH_3\bullet\bullet\bullet NH_2^-]^{\neq}$	1.78	1.96	0.16	0.05

[a]Nitrogen lone pair (NH_2^- HOMO); points to the C-Cl axis at the "back-side" of the C-Cl bond. [b]Nitrogen lone pair (NH_2^- HOMO-1); points to the hydrogen of the C-H bond.

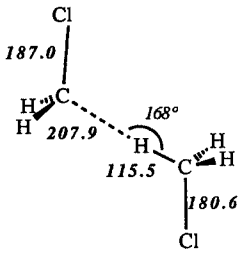

$[ClCH_2^- \cdots CH_3Cl]^*$

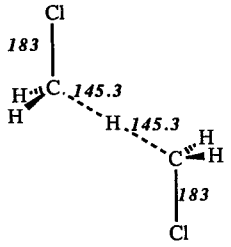

$[ClCH_2^- \cdot\cdot H^+ \cdot\cdot {}^-CH_2Cl]^{\ddagger}$

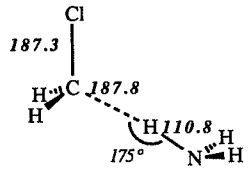

$[ClCH_2^- \cdots NH_3]^*$ (*1*)

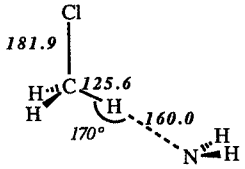

$[ClCH_3 \cdots NH_2^-]^*_{\text{labile}}$ (*3*)

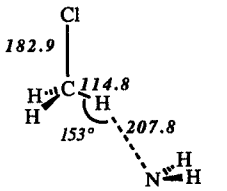

$[ClCH_3 \cdots NH_2^-]^{\ddagger}$ (*4*)

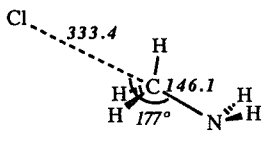

Initial S_N2 product cluster

$[CH_3NH_2 \cdots Cl^-]^*_{S_N2}$ (*5*)

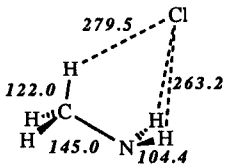

Most stable conformation

$[CH_3NH_2 \cdots Cl^-]^*$

Figure 3. *Calculated structure for selected species with X = Cl. Bond lengthes (pm) are represented in bold/italic, bond angles in italics.*

pm and by 7.5 pm to d(N-H) = 110.8 pm in CH_3Cl and NH_3, respectively (Figure 3), with respect to the isolated fragments. Therefore, it is concluded that the cluster energy for the anion/molecule complexes is provided to a considerable extent by hydrogen bond formation.

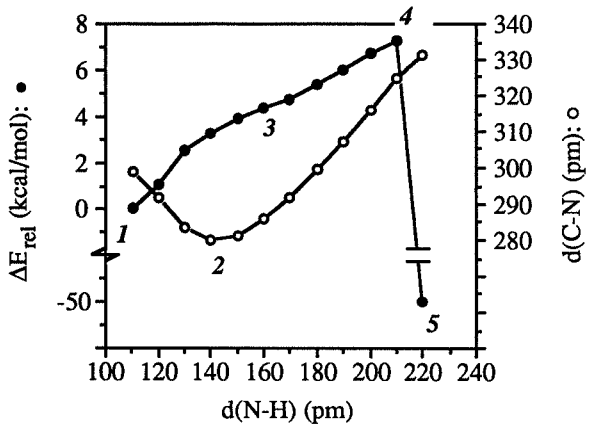

Figure 4. *Calculated reaction profile for the PT/S_N2 reaction which takes place from $[ClCH_2^-\cdots NH_3]^*$. In the diagram the relative energy ΔE_{rel} (kcal/mol) of the system (•) and the distance d(C–N) = d(C–H) + d(N–H) (pm) (o) are displayed as functions of the reaction coordinate d(N–H) (pm). The locations of the following structures are indicated:* ***1****: $[ClCH_2^-\cdots NH_3]^*$,* ***2****: the tight transition structure of the PT phase,* ***3****: $[ClCH_3\cdots NH_2^-]^*_{labile}$,* ***4****: $[ClCH_3\cdots NH_2^-]^{\neq}$, and* ***5****: the initial S_N2 product cluster $[CH_3NH_2\cdots Cl^-]^*_{S_N2}$ (see Figure 3 for structures).*

In Figure 4 the Xα energy profile for the PT/S_N2 reaction which takes place from the $[ClCH_2^-\cdots NH_3]^*$ reactant anion/molecule complex is depicted. This energy profile is obtained by elongation in steps of 10 pm of the N-H bond which participates in the hydrogen bond and which serves as the reaction coordinate; for every step the Xα energy is calculated after the geometry of the complete system, except for the fixed N-H bond, has been allowed to relax. The graphic representation in Figure 4 starts with the equilibrium value of 110.8 pm for d(N–H) in the reactant

anion/molecule complex. When d(N–H) is increased, the (relative) energy ΔE_{rel} rises. Around d(N-H) = 160 pm the *slope* of ΔE_{rel} has a local minimum. At this point the distance d(C–H) amounts to 125.6 pm and the proton can be conceived to be abstracted from ammonia and transferred to the chloromethyl anion. This means that the system now has to be considered as an anion/molecule complex of chloromethane and amide, $[ClCH_3 \bullet\bullet\bullet NH_2^-]^*$, with an energy of +4.31 kcal/mol above that of the original reactant complex. However, no energy barrier has been encountered upon formation of this intermediate complex, i.e. $[ClCH_3 \bullet\bullet\bullet NH_2^-]^*$ is a labile structure without a barrier towards the reformation of the original reactant complex and will therefore be denoted as "$[ClCH_3 \bullet\bullet\bullet NH_2^-]^*_{\textbf{labile}}$". Yet, it is emphasized that there is an entropic bottleneck. This is revealed by the behaviour of the total distance d(C-N) = d(C-H) + d(N-H) which is also represented in Figure 4. In $[ClCH_2^- \bullet\bullet\bullet NH_3]^*$ and $[ClCH_3 \bullet\bullet\bullet NH_2^-]^*_{labile}$, d(C-N) amounts to 298.6 and 285.6 pm, respectively. During the proton transfer (PT) from nitrogen to carbon d(C-N) contracts. On the reaction path, in between the reactant and the intermediate complex (d(N-H) ≈ 140 pm), one arrives at a minimum for d(C-N) of 279.8 pm. This can be conceived as a tight transition structure that corresponds to a situation with a low density of states, i.e., the just mentioned entropic bottleneck.

The bond between the amide anion and the chloromethane fragment in $[ClCH_3 \bullet\bullet\bullet NH_2^-]^*_{labile}$ is, for a considerable part, due to the hydrogen bond between one lone pair (LP1) of NH_2^- and the σ^*_{C-H} of CH_3Cl, which as a result is populated by 0.14 electrons. Simultaneously, however, the second lone pair (LP2) of NH_2^- already exhibits a considerable charge transfer interaction with the anti-bonding σ^*_{C-Cl} of CH_3Cl, resulting in a population of $P(\sigma^*_{C-Cl})$ = 0.14 electrons (Table V). The corresponding bond length, d(C-Cl), has been expanded by 5.6 pm with respect to isolated chloromethane (d(C-Cl) = 176.3 pm) to 181.9 pm.

Upon further elongation of d(N-H) the energy still rises and at about 210 pm the transition state (TS) of the PT/SN2 reaction, $[ClCH_3 \bullet\bullet\bullet NH_2^-]^{\neq}$, is reached, having an activation energy of 7.24 kcal/mol with respect to the reactant anion/molecule complex (Table IV). Simultaneously, the overall charge transfer from NH_2^- to CH_3Cl decreases from 0.35 electrons in the labile intermediate structure, $[ClCH_3 \bullet\bullet\bullet NH_2^-]^*_{labile}$, to 0.26 electrons in the TS (Table IV). From an analysis it follows that this mainly results from the breaking of the hydrogen bond between the amide anion and chloromethane. This is also exhibited by the considerable decrease of the population of σ^*_{C-H} from 0.14 electrons in $[CH_3Cl \bullet\bullet\bullet NH_2^-]^*_{labile}$ to 0.05 electrons in

$[CH_3Cl\bullet\bullet\bullet NH_2^-]^{\neq}$. During the elongation of the bond length d(N-H) the bond angle ∠(CHN) gradually decreases from 175° in $[ClCH_2^-\bullet\bullet\bullet NH_3]^*$ via 170° in $[ClCH_3\bullet\bullet\bullet NH_2^-]^*_{labile}$ to 153° in the TS $[CH_3Cl\bullet\bullet\bullet NH_2^-]^{\neq}$. This bending displays the beginning of the nucleophilic attack of the NH_2^- HOMO lone pair (LP1) on the anti-bonding σ^*_{C-Cl} of CH_3Cl. However, while in $[ClCH_3\bullet\bullet\bullet NH_2^-]^{\neq}$ the hydrogen bond is considerably weakened, the charge transfer to the anti-bonding σ^*_{C-Cl} of chloromethane, i.e. the nucleophilic attack, is only slightly increased to 0.16 electrons. Also d(C-Cl) is only slightly increased to 182.9 pm in the TS. It is interesting to note that already in $[ClCH_3\bullet\bullet\bullet NH_2^-]^{\neq}$ the staggered conformation of the aminomethane fragment in the final product anion/molecule complex $[CH_3NH_2\bullet\bullet\bullet Cl^-]^*$ can be perceived (Figure 3). In this situation the second lone pair (LP2) points away from the chloromethane fragment and is involved only to a minor extent in charge transfer interactions to CH_3Cl (P(LP2) = 1.96 electrons).

When proceeding from $[ClCH_3\bullet\bullet\bullet NH_2^-]^{\neq}$ the N-H bond is increased by another 10 pm to d(N-H) ≈ 220 pm, the transition state is passed and the nucleophilic substitution of NH_2^- on CH_3Cl proceeds without any further barrier towards the initial product anion/molecule complex, indicated as $[CH_3NH_2\bullet\bullet\bullet Cl^-]^*_{S_N2}$ (Figure 3). At this point it is emphasized that the sharp decrease of ΔE_{rel} when the TS is passed (Figure 4) is the result of the choice of d(N-H) as the reaction coordinate throughout the energy profile. If, for example, d(C-N) would have been employed as the reaction coordinate a slighter decrease of ΔE_{rel} when going from the TS to the initial product anion/molecule complex would have been the result. In $[CH_3NH_2\bullet\bullet\bullet Cl^-]^*_{S_N2}$ aminomethane and the chloride anion are rather weakly bound by a cluster energy of –1.96 kcal/mol. However, in the most stable conformation, $[CH_3NH_2\bullet\bullet\bullet Cl^-]^*$ (Figure 3), the cluster energy amounts to –6.39 kcal/mol (Table IV). In $[CH_3NH_2\bullet\bullet\bullet Cl^-]^*$ the orbital interaction between the anion and the neutral only provides 36% of the bonding interactions (electrostatic and orbital interaction). Furthermore, in $[CH_3NH_2\bullet\bullet\bullet Cl^-]^*$ only 0.16 electrons have been tranferred from the anion to the neutral, while in $[ClCH_2^-\bullet\bullet\bullet NH_3]^*$ this number amounts to 0.21 electrons (Table IV). Therefore, it is concluded that hydrogen bonding in $[CH_3NH_2\bullet\bullet\bullet Cl^-]^*$ is clearly less important than in the reactant complex $[ClCH_2^-\bullet\bullet\bullet NH_3]^*$. This result parallels the conclusion of Larson and McMahon[41] that electrostatic effects are far more pronounced in anion/molecule complexes with Cl^- than in anion/molecule complexes with F^-. Overall, the transformation of the reactant complex $[ClCH_2^-\bullet\bullet\bullet NH_3]^*$ to the product complex $[CH_3NH_2\bullet\bullet\bullet Cl^-]^*$ is calculated to be exothermic by –56.01 kcal/mol (Table IV).

Finally, the reaction path for the thermoneutral proton transfer (PT) from chloromethane to the chloromethyl anion in the reactant anion/molecule complex $[ClCH_2^-\bullet\bullet\bullet CH_3Cl]^*$ is considered. In the reactant complex the bond length $d(C\text{-}H)_1$ of the C-H bond in the chloromethane fragment which participates in the hydrogen bond amounts to 115.5 pm, while the hydrogen bond length $d(C\text{-}H)_2$ between the same H-atom and the carbon of the chloromethyl anion comes to 207.9 pm. The C-H-C hydrogen bond is slightly bent, having an angle of $\angle(CHC) = 168°$.

When $d(C\text{-}H)_1$ is enlarged, the energy of the system rises until the transition state (TS) for PT, $[ClCH_2^-\bullet\bullet H^+\bullet\bullet{}^-CH_2Cl]^{\neq}$, is reached at 2.08 kcal/mol above the reactant complex. Going from the reactant complex to the TS, the hydrogen bond becomes linear, and the distance d(C-C) = $d(C\text{-}H)_1 + d(C\text{-}H)_2$ contracts from 323.4 to 290.6 pm. In $[ClCH_2^-\bullet\bullet H^+\bullet\bullet{}^-CH_2Cl]^{\neq}$ the proton which is to be transferred is located symmetrically in between the carbon atoms of both chloromethyl anion fragments ($d(C\text{-}H)_1 = d(C\text{-}H)_2 = 145.3$ pm). The considerable contraction (32.8 pm) of d(C-C) indicates that $[ClCH_2^-\bullet\bullet H^+\bullet\bullet{}^-CH_2Cl]^{\neq}$ represents not only an energetic barrier but also a tight transition structure with a low density of states, i.e. an entropic bottleneck.

For economic reasons, the reaction path for the S_N2 substitution of the chloromethyl anion on chloromethane in $[ClCH_2^-\bullet\bullet\bullet CH_3Cl]^*$ has not been fully explored. However, when $ClCH_2^-$ is placed on the C_{3v} axis of CH_3Cl at the "back-side" of the C-Cl bond, it appears that the nucleophilic substitution proceeds without a barrier, analogously to the situation for the S_N2 reaction of NH_2^- on CH_3Cl. The origin of the barrier for the S_N2 process in $[ClCH_2^-\bullet\bullet\bullet CH_3Cl]^*$ is therefore ascribed to the breaking of the hydrogen bond in order to bring the nucleophile in the right position for the back-side attack on the C-Cl bond in the substrate. As an estimate for this energy barrier one can take the energy difference of 2.93 kcal/mol between $[ClCH_3\bullet\bullet\bullet NH_2^-]^*_{labile}$ and $[ClCH_3\bullet\bullet\bullet NH_2^-]^{\neq}$.

5.5 Discussion

The FT-ICR experiments on the two reaction systems $^AXCH_2^- + CH_3X + NH_3$, with X = Cl or Br, have revealed that three reaction mechanisms are active (Table III):

i) Clearly, the dominating process is the direct S_N2 substitution of the halomethyl anion on

halomethane in the reactant anion/molecule complex $[XCH_2^-\bullet\bullet\bullet CH_3X]^*$ (Reaction 4a), which has an overall rate constant k_1 of $6.5 \cdot 10^{-10}$ and $7.9 \cdot 10^{-10}$ $cm^3molecule^{-1}s^{-1}$ for X = Cl and Br, respectively.

ii) The second process is the $S_N2/E2$ reaction, starting from the same reactant complex (Reaction 4b), and having an overall rate constatnt k_2 of $2.0 \cdot 10^{-10}$ and $1.3 \cdot 10^{-10}$ $cm^3molecule^{-1}s^{-1}$ for X = Cl and Br, respectively.

iii) The third proces, the PT/S_N2 reaction which takes place from the reactant anion/molecule complex $[XCH_2^-\bullet\bullet\bullet NH_3]^*$ (Reaction 4c) is in both reaction systems considerably slower than the two other reactions, having a rate constant k_3 of $0.78 \cdot 10^{-10}$ and $0.32 \cdot 10^{-10}$ $cm^3molecule^{-1}s^{-1}$ for X = Cl and Br, respectively.

In fact, the direct S_N2 (Reaction 4a) and the $S_N2/E2$ process (Reaction 4b) proceed via a common first reaction step, the nucleophilic substitution. Within the steady-state approximation it can be derived that the rate constant k_{nuc} associated wit this elementary reaction is simply given by the sum of the two overall rate constants, i.e. $k_{nuc} = k_1 + k_2$. For X = Cl and Br, k_{nuc} amounts to $8.5 \cdot 10^{-10}$ and $9.2 \cdot 10^{-10}$ $cm^3molecule^{-1}s^{-1}$, respectively. The corresponding average-dipole-orientation (ADO) reaction efficiencies[42-44] (k_{nuc}/k_{ADO}) amount to 0.51 and 0.74, respectively.[45,46] Thus, the S_N2 step proceeds slightly more efficiently for the bromine containing reaction system, in line with the slightly more favorable thermodynamics (Table II) and the better leaving group ability of Br compared to Cl.

The ratio k_2/k_1 displays the efficiency with which the secondary E2 reaction taking place from the S_N2 product complex, $[XCH_2CH_3\bullet\bullet\bullet X^-]^*$, (Equation 4b) competes with the simple dissociation which determines the direct S_N2 process (Equation 4a). From Table III it appears, that this efficiency is significantly higher for X = Cl ($k_2/k_1 = 0.34$) than for X = Br ($k_2/k_1 = 0.16$). The higher efficiency of the secondary E2 reaction in $[XCH_2CH_3\bullet\bullet\bullet X^-]^*$ for the chlorine containing reaction system can be ascribed to the combined effect of: i) Cl^- being a better elimination base than Br^-, and ii) $[ClCH_2CH_3\bullet\bullet\bullet Cl^-]^*$ being a more strongly bound cluster ($\Delta H_{clust} = -14.5$ kcal/mol) than $[BrCH_2CH_3\bullet\bullet\bullet Br^-]^*$ ($\Delta H_{clust} = -11.6$ kcal/mol).[14]

Next, the question is adressed why the (inherently) thermoneutral proton transfer (PT) from CH_3X to $^AXCH_2^-$ (Equation 1b for X = Cl) is *not* observed, as follows from the absence of $^BXCH_2^-$ in the FT-ICR product anion spectra. In principle, the absence of $^BXCH_2^-$ could also be

explained by an alternative mechanistic model: a) PT in $[^AXCH_2^- \cdots CH_3{}^BX]^*$ *does* occur and results in the formation of the metastable intermediate product complex $[^AXCH_3 \cdots {}^-CH_2{}^BX]^*$; b) subsequently, from this intermediate complex only direct S_N2 and S_N2/E2 reactions proceed, i.e. dissociation has no significant contribution. Overall, this model leads to multistep PT/S_N2 and PT/S_N2/E2 mechanisms. However, from the ADO reaction efficiencies (*vide supra*) it follows that this hypothesis is incorrect. For example, in the case of X = Cl about half of the collision complexes dissociates without reaction (k_{nuc}/k_{ADO} = 0.51). This implies that also half of the product complexes $[^{35}ClCH_3 \cdots {}^-CH_2Cl]^*$, possibly formed from $[^{35}ClCH_2^- \cdots CH_3Cl]^*$ by PT, should dissociate. If thermoneutral PT in $[^{35}ClCH_2^- \cdots CH_3Cl]^*$ would occur to a substantial extent, then the formation of $^{37}ClCH_2^-$ should be detectable. As this is *not* the case, it therefore is concluded that indeed this thermoneutral PT cannot effectively compete with the nucleophilic substitution step, i.e. with the direct S_N2 and the S_N2/E2 mechanisms.

From the theoretical calculations on the chlorine containing reaction system (X = Cl) it follows that the energy barrier for PT in (rovibrationally) excited[1] $[ClCH_2^- \cdots CH_3Cl]^*$ amounts to about 2 kcal/mol, which is in principle not very high. However, the energy barrier for the S_N2 reaction is also rather low and is estimated to be only slightly higher (about 3 kcal/mol; see Figure 1 for a schematic overview of the energetics of all processes that take place from $[ClCH_2^- \cdots CH_3Cl]^*$). This means that there is no sharp energy criterion determining which reaction prevails. Therefore, it is concluded that the decisive factor is the entropic bottleneck associated with the PT.

The theoretical calculations have indicated that the origin of the S_N2 energy barrier is the breaking of the hydrogen bond in $[ClCH_2^- \cdots CH_3Cl]^*$ and $[ClCH_3 \cdots NH_2^-]^*$ in order to bring anionic fragment on the right position for a "back-side" nucleophilic attack on CH_3Cl, and that the substitution itself proceeds without an energy barrier (section 5.4). It is interesting to note that this opens the possibility of having anion/molecule collisions between $ClCH_2^-$ and CH_3Cl in which the S_N2 reaction occurs instantaneously without an energy barrier, and without the initial formation of a hydrogen-bonded reactant complex that is necessary for PT. These conclusions are completely in line with a theoretical study of Sheldon et al.[47] on the S_N2 reaction which takes place between CH_3OH and $CH_3OH_2^+$ under formation of protonated dimethylether and H_2O.[48] From this study[47] it follows that the main source of the energy barrier for the S_N2 process taking place from the stable reactant cation/molecule complex $[CH_3OH \cdots {}^+H\text{-}HOCH_3]^*$ is the breaking of the

hydrogen bond between the methanol oxygen and an oxonium hydrogen in order to bring methanol in the right orientation for a "back-side" nucleophilic attack on $CH_3OH_2^+$. However, the substitution itself shows also a small barrier, contrasting the situation for our anionic sytems (*vide supra*).

As the last item, the proton transfer initiated nucleophilic substitution (PT/S_N2) reaction which takes place from the reactant anion/molecule complex $[XCH_2^-\bullet\bullet\bullet NH_3]^*$ is discussed. The rate constant k_3 for the PT/S_N2 reaction has been found to be more than one order of magnitude lower than the rate constant k_{nuc} for the nucleophilic substitution step which takes place in $[XCH_2^-\bullet\bullet\bullet CH_3X]^*$. The theoretical calculations show that this can be connected with the entropic barrier associated with the PT from ammonia to the halomethylanion as well as with the relatively high energy barrier that comprises both the endothermicity of the PT in $[XCH_2^-\bullet\bullet\bullet NH_3]^*$ and the breaking of the hydrogen bond in $[XCH_3\bullet\bullet\bullet NH_2^-]^*_{labile}$ that is neaded to bring NH_2^- on the right location for a "back-side" nucleophilic attack on CH_3X. For the PT/S_N2 reaction which starts from $[ClCH_2^-\bullet\bullet\bullet NH_3]^*$, the energy barrier $\Delta E^{\neq}_{X=Cl}$ is calculated to be +7.24 kcal/mol. The energy barrier $\Delta E^{\neq}_{X=Br}$ for the PT/S_N2 reaction in $[BrCH_2^-\bullet\bullet\bullet NH_3]^*$ has not been calculated. However, as $BrCH_2^-$ has a 3.3 kcal/mol lower proton affinity (PA)[14] than $ClCH_2^-$, $\Delta E^{\neq}_{X=Br}$ is expected to be a few kcal/mol higher than $\Delta E^{\neq}_{X=Cl}$ due to the higher endothermicity of the PT phase of the reaction. This is in accordance with the experimental observation that k_3 for X = Br ($0.32 \cdot 10^{-10}$ $cm^3molecule^{-1}s^{-1}$) is more than two times lower than for X = Cl ($0.78 \cdot 10^{-10}$ $cm^3molecule^{-1}s^{-1}$).

An interesting result is the fact that the PT/S_N2 reaction is a concerted, one-step process. Although it proceeds via two separated phases, namely PT and S_N2, it passes only one energetic transition state. This result parallels the finding of Scheiner[13] that the endothermic transfer of a proton from ammonia (PA = 204.0 kcal/mol[14]) to water (PA = 166.5 kcal/mol[14]) in the cation/molecule complex $[NH_4^+\bullet\bullet\bullet H_2O]^*$ does *not* lead to a stable complex $[NH_3\bullet\bullet\bullet H_3O^+]^*$. From the fact that PT in $[BrCH_2^-\bullet\bullet\bullet NH_3]^*$ is more endothermic than in $[ClCH_2^-\bullet\bullet\bullet NH_3]^*$ it is expected that the resulting intermediate structure on the PT/S_N2 reaction path is also labile. This justifies the general notation $[XCH_3\bullet\bullet\bullet NH_2^-]^*_{labile}$ for X is Cl as well as Br, which has already been employed in the foregoing discussion. Finally, it is pointed out that a concerted PT/S_N2 reaction is in perfect agreement with the previous observation of our group[5] that no H/D exchange is observed when $ClCH_2^-$ or $BrCH_2^-$ are allowed to react with ND_3.

References

1. Nibbering, N.M.M. *Adv. Phys. Org. Chem.* **1988**, 24, 1.
2. Nibbering, N.M.M. *Acc. Chem. Res.* **1990**, 23, 279.
3. Ingemann, S.; Nibbering, N.M.M.; Sullivan, S.A.; DePuy, C.H. *J. Am. Chem.Soc.* **1982**, 104, 6520.
4. Ingemann, S; Nibbering, N.M.M. *J. Org. Chem.* **1983**, 48, 183.
5. Ingemann, S; Nibbering, N.M.M. *J. Chem. Soc., Perkin Trans. 2* **1985**, 837.
6. *'CRC Handbook of Chemistry and Physics'*, 63rd Ed.; Weast, R.C. Ed.; CRC Press, Boca Raton, 1982-1983.
7. Slater, J.C. *Quantum Theory of Molecules and Solids*, Vol. 4; McGraw-Hill: New York, 1974.
8. Parr, R.G; Yang, W. *Density-Functional Theory of Atoms and Molecules*, Oxford University Press: New York 1989.
9. Baerends, E.J.; Ellis, D.E.; Ros, P. *Chem. Phys.* **1973**, 2, 41.
10. Boerrigter, P.M.; Velde, G. te; Baerends, E.J. *Int. J. Quantum Chem.* **1988**, 33, 87.
11. Baerends, E.J; Ros, P. *Chem. Phys.* **1975**, 8, 412.
12. Baerends, E.J; Ros, P. *Int. J. Quantum Chem., Quantum Chem. Symp.* **1978**, S12, 169.
13. Scheiner, S. *Int. J. Quantum Chem.* **1983**, 23, 753.
14. Lias, S.G.; Bartmess, J.E.; Liebman, J.F.; Holmes, J.L.; Levin, R.D.; Mallard, W.G. *J. Phys. Chem. Ref. Data* **1988**, 17, Suppl. Nr. 1.
15. Koning, L.J. de; Nibbering, N.M.M. *J. Am. Chem. Soc.* **1987**, 109, 1715, and references cited therein.
16. Koning, L.J. de; Kort, C.W.F.; Pinkse, F.A.; Nibbering, N.M.M. *Int. J. Mass Spectrom. Ion Processes* **1989**, 95, 71.
17. Huntress, W.T., Jr.; Laudenslager, J.B.; Pinizzotto, R.F., Jr., *Int. J. Mass Spectrom. Ion Physics* **1974**, 13, 331.
18. Bartmess, J.E.; Georgiadis, R.M. *Vacuum* **1983**, 33, 149.
19. Miller, K.J. *J. Am. Chem. Soc.* **1990**, 112, 8533.
20. Versluis, L.; Ziegler, T. *J. Chem. Phys.* **1988**, 88, 322.

21. Becke, A.D. *Int. J. Quantum. Chem.* **1983**, 23, 1915.
22. Becke, A.D. *J. Chem. Phys.* **1986**, 85, 7184.
23. Ziegler, T.; Tschinke, V.; Becke, A. *Polyhedron* **1987**, 6, 685.
24. Stoll, H.; Golka, E.; Preus, H. *Theoret. Chim. Acta* **1980**, 55, 29.
25. Vosko, S.H.; Wilk, L.; Nusair, M. *Can. J. Phys.* **1980**, 58, 1200.
26. Bickelhaupt, F.M.; Fokkens, R.H.; Koning, L.J. de; Nibbering, N.M.M.; Baerends, E.J.; Goede, S.J.; Bickelhaupt, F. *Int. J. Mass Spectrom. Ion Processes* **1991**, 103, 157.
27. Ziegler, T.; Tschinke, V.; Ursenbach, C. *J. Am. Chem. Soc.* **1987**, 109, 4825.
28. Ziegler, T.; Tschinke, V.; Versluis, L.; Baerends, E.J. *Polyhedron* **1988**, 7, 1625.
29. Fan, L.; Ziegler, T. *J. Chem. Phys.* **1990**, 92, 3645.
30. Bickelhaupt, F.M.; Nibbering, N.M.M.; Wezenbeek; E.M. van; Baerends, E.J. *J. Phys. Chem.* **1992**, 96, 4864.
31. Ziegler, T.; Rauk, A. *Theoret. Chim. Acta* **1977**, 46, 1.
32. Støgård, A.; Strich, A.; Almlöf, J.; Roos, B. *Chem. Phys.* **1975**, 8, 405.
33. Roos, B.O.; Kraemer, W.P.; Diercksen, G.H.F. *Theoret. Chim. Acta* **1976**, 42, 77.
34. Latajka, Z.; Scheiner, S. *Int. J. Quantum Chem.* **1986**, 29, 285.
35. Caldwell, G.; Kebarle, P. *Can. J. Chem.* **1985**, 63, 1399.
36. Larson, J.W.; McMahon, T.B. *J. Am. Chem. Soc.* **1983**, 105, 2944.
37. Payzant, J.D.; Yamadagni, R.; Kebarle, P. *Can. J. Chem.* **1971**, 49, 3308.
38. DePaz, M.; Giordini, A.G.; Friedman, L. *Int. J. Mass Spectrom. Ion Phys.* **1970**, 3, 465.
39. Minato, T.; Yamabe, S. *J. Am. Chem. Soc.* **1988**, 110, 4586.
40. Minato, T.; Yamabe, S. *J. Am. Chem. Soc.* **1985**, 107, 4621.
41. Larson, J.W.; McMahon, T.B. *J. Am. Chem. Soc.* **1984**, 106, 517.
42. Su, T.; Bowers, M.T. *J. Chem. Phys.* **1973**, 58, 3027.
43. Su, T.; Bowers, M.T. *Int. J. Mass Spectrom. Ion Phys.* **1973**, 12, 347.
44. Su, T.; Bowers, M.T. *Int. J. Mass Spectrom. Ion Phys.* **1975**, 17, 211.
45. Atomic masses and dipole moments ($\mu_D(CH_3Cl)$ = 1.87 D, $\mu_D(CH_3Br)$ = 1.81 D) used for the ADO calculations were taken from reference 6.
46. Polarizabilities ($\alpha(CH_3Cl)$ = 4.56 Å^3, $\alpha(CH_3Br)$ = 5.61 Å^3) used for the ADO calculations were taken from reference 19.

47. Sheldon, J.C.; Currie, G.J.; Bowie, J.H. *J. Chem. Soc., Perkin Trans. 2* **1986**, 941.

48. Kleingeld, J.C.; Nibbering, N.M.M. *Org. Mass Spectrom.* **1982**, 17, 136.

6 Theoretical Investigation on Base-Induced 1,2-Eliminations in the Model System F^- + CH_3CH_2F. The Role of the Base as Catalyst.

Abstract

The anti-E2 elimination prevails over the syn-E2 elimination. The base has been found to play a key role as a catalyst which strongly influences the competition between anti- and syn-elimination. The thermic elimination of HF from fluoroethane preferentially proceeds via the syn pathway. Upon catalysis by the base, the transition state of the anti-mode is selectively stabilized, leading to the prevalence of anti-E2 over syn-E2 elimination. The main reason for the selective stabilization is the very low energy and, thus, the good acceptor capability of the C_2H_5F-8a' LUMO (σ anti-bonding for CC-H and C^{α}-F; Figure 6b) in the strongly rearranging, loose anti-E2 transition state. This 8a' LUMO effectively relieves the Pauli repulsion that the base-$2p_z$ HOMO has with the C_2H_5F-5a' (σ bonding for CC-H and C^{α}-F; Figure 6b) and has a strong donor/acceptor interaction with the base-$2p_z$ HOMO. However, the anti-mode is also favored for electrostatic reasons, due to the interaction of the F^- base with the C^{α}-F dipole of the substrate.

The anti-E2 elimination prevails over the S_N2 substitution. This is ascribed to the lower energy and entropy barrier for the anti-E2 elimination as well as to the preferential formation of a reactant complex which is predestinated to react further via the anti-E2 pathway. Both anti-E2 and syn-E2 elimination preferentially produce FHF^- and C_2H_4. These results are in excellent agreement with the experimental result that reaction of F^- and C_2H_5F exclusively yields FHF^- and C_2H_4. However, we reinterpret this observation as being the result of anti-E2 and not syn-E2 elimination.

The base-induced eliminations studied are of the E2H category. No E2C-like interactions are present in the transition state. The syn-E2 reaction is slightly E1cb-like, whereas the anti-E2 elimination is virtually ideal E2. Interestingly, there is no distinct channel on the anti-E2 reaction energy surface leading from the reactant complex to the transition state. An important characteristic of the anti-E2 elimination which is not contained in the E2H formalism is the pronounced shift of the abstracted proton from the C^{β} to the C^{α} position in the transition state.

6.1 Introduction

Base-induced 1,2-elimination reactions (E2: Equation 1a) constitute one of the basic types of reaction in organic chemistry.[1,2] They are an important tool to introduce double bonds between carbon and/or heteroatoms in organic synthesis.[1-6] An alternative reaction pathway for a base and a substrate containing a leaving group is the nucleophilic substitution (S_N2: Equation 1b). Therefore, E2 and S_N2 reactions can be in competition and may occur as unwanted side reactions of each other.[1,2]

$$B^- + H\text{-}C^{\beta}H_2\text{-}C^{\alpha}H_2\text{-}L \xrightarrow{E2} B\text{-}H + CH_2{=}CH_2 + L^- \quad (1\,a)$$

$$B^- + H\text{-}C^{\beta}H_2\text{-}C^{\alpha}H_2\text{-}L \xrightarrow{S_N2} CH_3\text{-}CH_2\text{-}B + L^- \quad (1\,b)$$

Extensive experimental investigations on base-induced elimination reactions have been performed in the condensed phase[7-18] as well as in the gas phase[19-33] (cf. Chapters 3 - 5). Considerable experience has been gathered concerning the parameters that determine the reaction rates, the product distribution and the stereochemistry, i.e. syn or anti (coplanar) E2 elimination (Figure 1). An important concept in the description and classification of elimination reactions is the Variable Transition State (VTS).[1,2] In the VTS theory, the reactions are classified according to the geometry of the transition state (TS), which is conceived to be located at one point in a continuous spectrum of mechanistic possibilities. The VTS theory comprises the Bunnett-Cram E2H-spectrum,[12-14] i.e. E1cb(-like), synchronous E2, and E1(-like) eliminations involving linear proton transfer, as well as the Winstein-Parker E2H-E2C-spectrum[15,16] in which bent proton transfer may occur with a certain degree of base/C^{α} covalent interaction (Figure 1).

Gas-phase experiments[19-33] enabled the study of the intrinsic reactivity of reaction systems without the effect of solvent molecules and counter ions.[32,33] An important feature which distinguishes gas-phase from condensed phase reactions is the prominent role that ion/molecule complexes play.[32-34] The double-well potential, first suggested for gas-phase S_N2 reactions on the basis of experiments by Olmstead and Brauman,[35] has been confirmed by *ab initio* calculations[36-45] and is now generally accepted for gas-phase reactions.[32,33] Very recently, the interme-

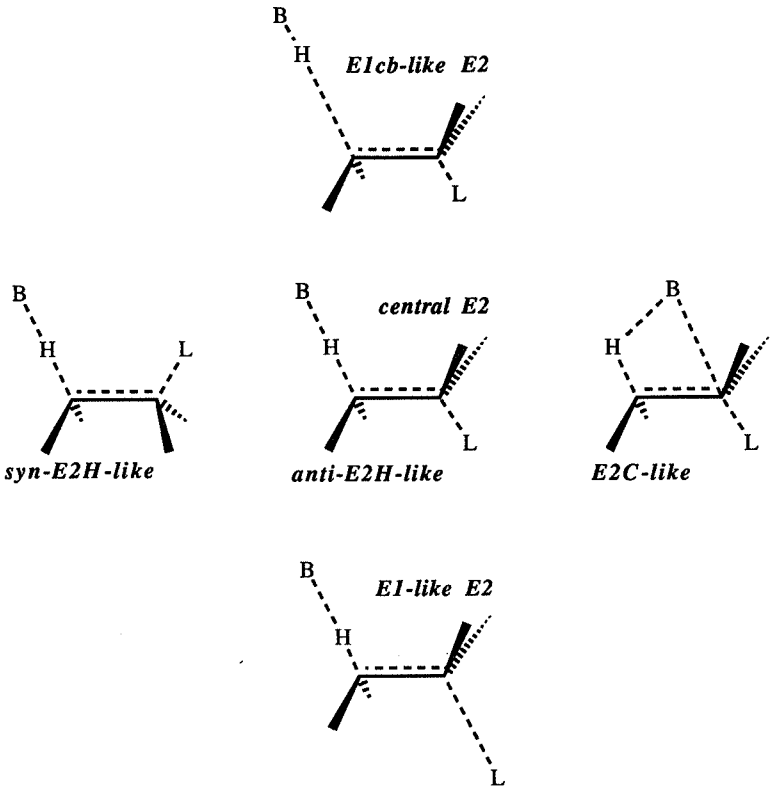

Figure 1. Mechanistic spectrum of transition states of base-induced 1,2-elimination reactions.

diate reactant and product complexes of gas-phase ion/molecule S_N2 reactions were isolated and studied experimentally.[46-48]

Base-induced E2 elimination reactions have received relatively little attention in theoretical studies[38,49-63] if compared to S_N2 substitutions (see, for instance, Refs. 36-45). This may be due to the more extensive and complex reorganization of bond making and bond breaking during the E2 reaction which complicates the finding of the transition state. Early semi-empirical calculations of Fukui et al.[49,50] have shown that the coplanar stereochemistry of E2 reactions can be ascribed to the frontier MO electronic coupling between the leaving group and the H^{β} which has to be abstracted. This is revealed by a higher amplitude on H^{β} and a stronger C^{β}-H anti-bonding

character of the substrate LUMO, which accepts charge from the HOMO of the attacking base, if the H^{β} and the leaving group are anti or syn coplanar. The interdependence of the C^{β}-H and the C^{α}-F bonds via delocalized MOs in E2 reactions has been pointed out by others.[51-58] It appears to be closely related to the mechanism of spin coupling in NMR,[53] and to the phenomena of the anomeric effect and the effect of anionic hyperconjugation on rotational barriers.[64,65] Furthermore, important quantities like E2 reaction and activation energies as well as transition state structures have been determined.

Still, however, a number of interesting questions remain which are not completely understood. Why, in general, does anti-E2 elimination prevail over syn-E2 elimination[1,2] ? In principle, one could expect the TS of the syn-E2 elimination to be more stable than that of the anti-E2 elimination, because of a favorable interaction between the leaving group L^- and the β-proton which is abstracted. Of particular interest is the question on the magnitude and the mechanism of the preferential stabilization of the transition state of the anti-mode by the base in the HL elimination from the C_2H_5L substrate, i.e., what is the catalytic effect of the base in the E2 reaction ?

The purpose of the present paper is to answer these and other questions, in order to arrive at a deeper understanding of the nature of base-induced E2 reactions. To this end, a theoretical investigation on the anti- and syn-E2 reactions of the fluoride/fluoroethane (B^-, $L^- = F^-$ in Equation 1) model reaction system has been carried out. The S_N2 substitution of F^- on C_2H_5F has been included in our study for completeness and for a better comparison with previous theoretical[55,56] and experimental (ICR) gas-phase[22-24] investigations on this reaction system.

In the context of the VTS concept (*vide supra*) it is interesting to know the location of reactant and product complexes as well as transition states on the 2-dimensional reaction energy surface E(d(C^{β}-H), d(C^{α}-F)) of the E2 reaction. Moreover, the shape of this reaction energy surface contains important information on the way that the reaction system can proceed from the reactant configuration to the product configuration, i.e., information on the character of the reaction. Therefore, in the present theoretical study not only stationary points but the complete 2-dimensional reaction energy surface, E(d(C^{β}-H), d(C^{α}-F)), has been determined for the anti-E2 and syn-E2 reaction. Structures and relative energies for the relevant stationary points of the E2 and S_N2 reaction systems have been obtained. The quantitative results, including an estimate of the catalytic effect of the base on the 1,2-elimination, are discussed and explained on the basis of a

detailed analysis of the electronic structure and bonding between the reactants in E2 reactant complexes and transition states.

The calculations were performed using a high-level density-functional (DF) method as implemented in the Amsterdam Density-Functional (ADF) program system.[66-71] Since the one-electron picture is preserved in the Kohn-Sham approach to density-functional theory (DFT),[67] the interpretation of the bonding can be cast in familiar terms such as exchange or Pauli repulsion and donor/acceptor interactions (Chapter 2).[72]

6.2 Method

General

The quantum chemical calculations were performed using a high-level density-functional (DF) method, as implemented in the Amsterdam Density-Functional (ADF) program system.[66-71] The MOs were expanded in a large set of Slater type orbitals (STOs). The basis used in the geometry optimization is of double-ζ quality (two STOs per nl shell), with polarization function added on each atom: 3d on C and F, 2p on H (DZP basis). Geometries were optimized with the simple Xα exchange-correlation potential[66] using gradient techniques[73] for minimum energy structures and for the S_N2 transition state, and a procedure described below for anti- and syn-E2 transition states (Xα/DZP level of theory; Figure 2).

The energy data reported for minimum energy and transition state structures have been obtained in the Xα/DZP optimum geometry with the Xα exchange-correlation functional using the DZP basis (Xα/DZP level) and with more sophisticated density-functionals (DF) for exchange and correlation using the DZP basis (DFT/DZP level) and an extra large TZPP basis (DFT/TZPP level; Table I and Figures 3 and 5). At the DFT level, exchange is described with Slater's $\rho^{1/3}$ potential (Xα with $\alpha = 2/3$), with a non-local correction due to Becke.[74-76] According to the suggestion by Stoll et al.,[77] only correlation between electrons of different spin is introduced, for which electron gas data (in the Vosko-Wilk-Nusair[78] parametrization) are used. The TZPP basis is of triple-ζ basis quality and has been augmented with two polarization functions on each atom (3d and 4f on C and F; 2p and 3d on H). It has been noticed before that the complexation energy of fluorine containing anion/molecule complexes, which depends very critically on the quality of the basis set,

can be described satisfactorily with this basis set (see Chapter 5).[79]

Considerable experience shows that with the DF approach interaction energies in systems involving main group elements and/or metals, including anion/molecule complexes, in general can be calculated with an accuracy in the order of a few tenths of an eV (ca. 5 kcal/mol).[73,79-85]

An analysis of the bonding mechanism[80,86] in F^-/C_2H_5F anti- and syn-E2 reactant complexes and transition states has been performed at the DFT/DZP level (Table II). In this analysis the interaction energy, $\Delta E_{int} = \Delta E^0 + \Delta E_{oi}$, is explicitly split up in the steric repulsion ΔE^0 and the orbital interaction ΔE_{oi}. The steric repulsion, $\Delta E^0 = \Delta E_{elstat} + \Delta E_{Pauli}$, comprises both the classical electrostatic interaction (ΔE_{elstat}) between the unperturbed charge distributions of the fragments and the four-electron destabilizing interactions (Pauli repulsion: ΔE_{Pauli}). The orbital interaction, ΔE_{oi}, accounts for charge transfer and polarization (see Chapter 2, Section 2.3).

2-Dimensional Reaction Energy Surfaces and Transition States

The saddle points on the reaction energy surface, E(d(C^β-H), d(C^α-F)), for the syn-E2 and especially for the anti-E2 reaction of F^- and C_2H_5F appear to be located on extremely shallow saddle regions (Figure 4). This easily leads to an erroneous determination of the position of these saddle points. This problem has been circumvented by the determination of the complete reaction energy surfaces E(d(C^β-H), d(C^α-F)). This allows for a more correct determination of TS structures and, further, leads to a better insight in the nature of the reaction. Starting from the reactant complexes, the reaction energy surfaces are determined by stepwise elongation of d(C^β-H) and d(C^α-F). After each step the geometry is allowed to relax; however, the length of d(C^β-H) and d(C^α-F) is kept fixed and C_S point group symmetry is superimposed. As a result, one acquires a set of energies in a grid of (d(C^β-H), d(C^α-F)) points on the 2-dimensional reaction energy surface (anti-E2 surface: 89 points, syn-E2-surface: 39 points). The reaction energy surfaces are visualized as the contour plots of fifth order polynomials, which have been fitted to the set of points (Figure 4). The saddle point structures determined in this way for the 2-dimensional (2D) reaction energy surface have been subjected to a vibrational analysis. From this it appears that each 2D-saddle point only has one imaginary frequency associated with (Figure 2). Therefore, it corresponds to a first order saddle point in the complete hyper-dimensional energy surface and, thus, represents a proper TS structure.

6.3 Results

The results of the DF calculations are displayed in Tables I and II and in Figures 2 to 8. Table I (energetics) and Figure 2 (structures) summarize the data on the E2 and S_N2 reactions. From Table I it appears that interaction energies decrease when going from the Xα to the DFT level of density-functional theory. This is mainly due to the increasing exchange or Pauli repulsion due to the introduction of non-local corrections for the exchange. The interaction energies further decrease when the basis set increases from DZP to TZPP quality. This is ascribed to a selective stabilization of free F^- ions. The fluoride anions "gain" the most from the introduction of more diffuse basis functions if compared to interacting systems where the charge can be delocalized over the entire F^-/C_2H_5F aggregation.

In the thermic elimination of HF from fluorethane the uncatalysed transition state (UTS) for syn-elimination is considerably lower in energy than that for anti-elimination (Table I). However, upon catalysis by the F^- base the transition state of the anti-elimination is stabilized much (ca. 2 eV) more than that of the syn-elimination. This feature is reproduced at all three levels of theory, i.e. Xα/DZP, DFT/DZP and DFT/TZPP (Table I). An important difference when going from Xα to the more advanced DFT calculations is the crossing of the energy of the TS(anti-E2) and TS(syn-E2), the latter being higher in energy at the DFT level. Apparently, the use of non-local corrections to the exchange is essential in the description of the relative energy of the anti-E2 and syn-E2 transition states. The qualitative features of the DFT/DZP and DFT/TZPP calculations are essentially the same.

Structures (Figure 2) and anti- and syn-E2 reaction energy surfaces (Figure 4) have been obtained at the Xα/DZP level. The discussion on the energetics of the E2 and S_N2 reactions is based on the DFT/TZPP results (Figures 3 and 5), whereas the analysis of the electronic structure and the interaction between the reactants in the reactant complexes and transition states is performed at the DFT/DZP level (Table II and Figures 6 to 8). The C_2H_5F and F^-/C_2H_5F species have closed shells; the valence electron configurations are $(a')^{14}(a'')^6$ and $(a')^{20}(a'')^8$, respectively. Orbital interactions predominantly, i.e., for more than 90 % occur in A' symmetry.

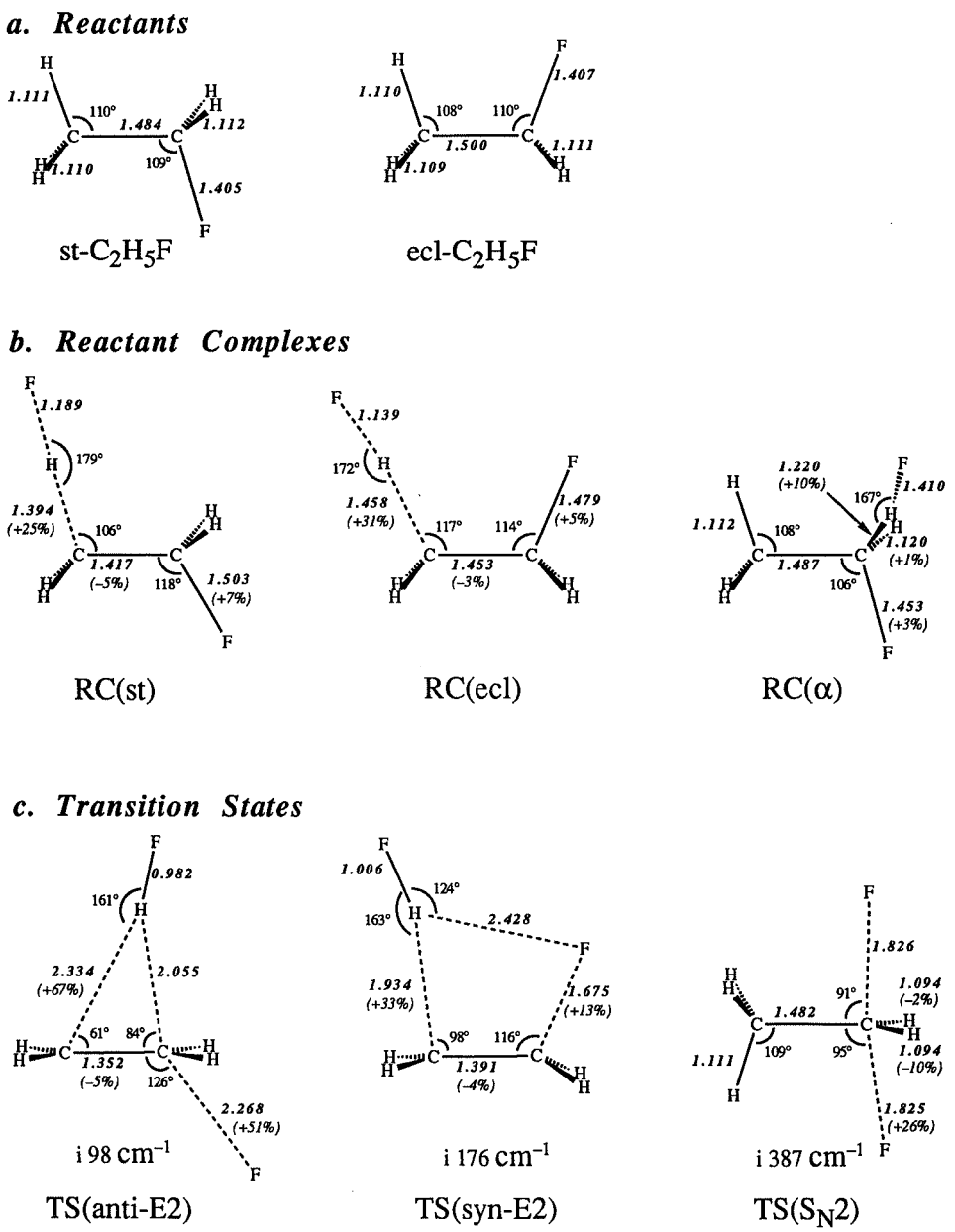

Figure 2. *Calculated structures (Xα/DZP level) for reactants F^- and C_2H_5F (a), reactant complexes (b), transition states (c), product complexes (d) and products (e). Bond lengths (Å) are represented in bold/italic* (Continued overleaf).

d. Product Complexes

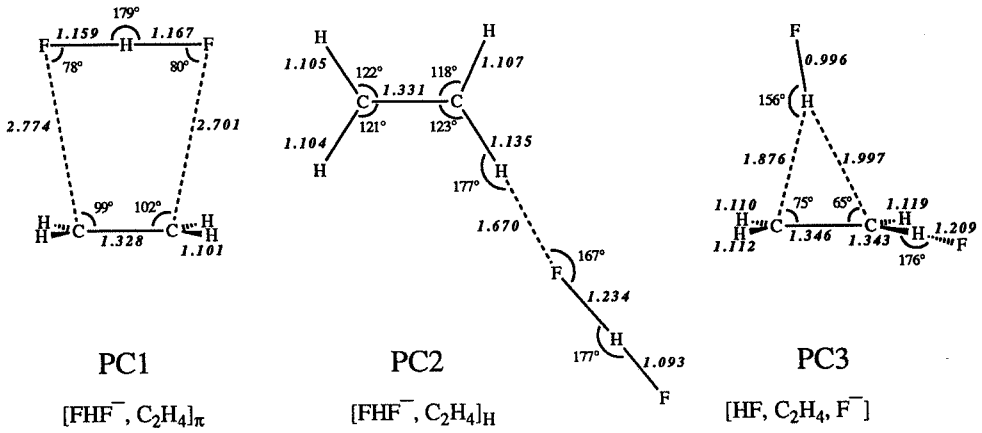

e. Products

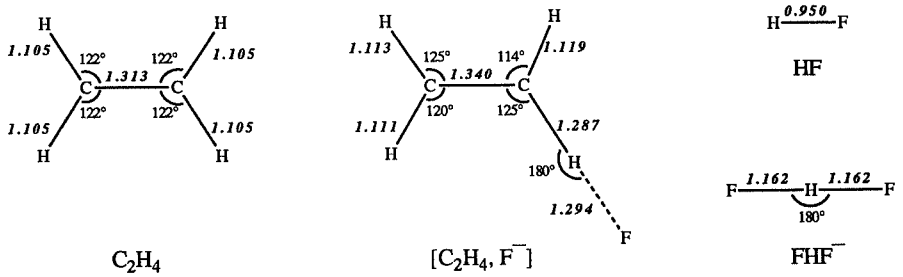

Figure 2. (Continued). *In (b) and (c), the change in the bond length (%) of selected bonds has been displayed for R(st)/R(ecl)/R(st) → RC(st)/RC(ecl)/RC(α) and RC(st)/RC(ecl)/RC(α) → TS(anti-E2)/TS(syn-E2)/TS(S_N2), respectively. In (c), furthermore, the imaginary frequencies associated with the transition states have been displayed.*

Table I. Calculated energies, ΔE (eV), of anti-E2, syn-E2 and S_N2 reaction systems relative to the energy of the separated reactants F^- and staggered CH_3CH_2F (R(st)).[a]

System		ΔE		
		Xα/DZP[b]	DFT/DZP[b]	DFT/TZPP[b]
Reactants				
R(st)	(F^- + st-C_2H_5F)	0.00	0.00	0.00
R(ecl)	(F^- + ecl-C_2H_5F)	0.08	0.07	0.10
Reactant Complexes				
RC(st)	([F^-, st-C_2H_5F])	–1.91	–1.18	–0.46
RC(ecl)	([F^-, ecl-C_2H_5F])	–1.63	–0.87	–0.11
RC(α)	([F^-, st-C_2H_5F]$_\alpha$)	–1.61	–1.03	–0.43
Transition States				
TS(anti-E2)		–0.89	–0.85	–0.41
TS(syn-E2)		–1.29	–0.75	–0.02
TS(S_N2)		–1.06	–0.53	–0.02
UTS(anti-E)[c]		6.20	5.51	5.48
UTS(syn-E)[c]		3.74	3.53	3.60
Product Complexes				
PC1	([FHF^-, C_2H_4]$_\pi$)	–2.31	–2.07	–1.36
PC2	([FHF^-, C_2H_4]$_H$)	–2.66	–2.51	–1.78
PC3	([HF, C_2H_4, F^-])	–1.40	–1.08	–0.37
Products				
P1	(FHF^- + C_2H_4)	–2.05	–2.25	–1.75
P2	(HF + [C_2H_4, F^-])	–0.45	–0.58	–0.02
P3	(HF + C_2H_4 + F^-)	1.22	0.41	0.29

[a] See Figure 2 for structures and Figure 3 for graphical representation of DFT/TZPP[b] results.

[b] Level of theory: "density-functional"/"basis set". The geometries are obtained at the Xα/DZP level (see Method).

[c] Uncatalysed Transition State (UTS): Separate, non-interacting F^- base and C_2H_5F fragment, the latter deformed to its geometry in the corresponding Transition State; i.e. "UTS = TS – F^-".

6.4 Discussion

In the following two subsections the competition between base-induced E2 and S_N2 reactions and between anti- and syn-E2 elimination are discussed in terms of the energetics and structures of the reaction systems and in terms of the shape of the E2 reaction energy surfaces. After this, the question is addressed *why* the base catalyses more effectively the anti-E2 than the syn-E2 elimination. Next, the significance of our results is considered in the context of the Variable Transition State (VTS) concept, i.e. the Bunnet-Cram E2H and the Winstein-Parker E2H/E2C mechanistic spectra. Finally, our results are compared with previous theoretical and experimental gas-phase studies, and it is discussed what differences can be expected when going to the condensed phase.

Anti-E2 versus S_N2

We first consider the competition between the base-induced anti-elimination (anti-E2) and the nucleophilic substitution (S_N2) of F^- and fluoroethane (Equation 1; B^-, $L^- = F^-$). Table I shows the energies of the E2 and S_N2 reaction systems relative to the separated reactants F^- and staggered fluoroethane (F^- + st-C_2H_5F, R(st)). The reactants can combine to form a reactant complex (RC) in which the F^- is hydrogen bonded to st-C_2H_5F either via a β- or via a α-hydrogen: RC(st) and RC(α), respectively (Figure 2). The most stable reactant complex is RC(st) with a complexation energy, $\Delta E_{complex}$, of –0.46 eV, to be compared with –0.43 eV for RC(α) (Table I). In RC(st) the C^{β}-H bond (1.394 Å) and C^{α}-F bond (1.503 Å) have already been elongated considerably by 25% and 7%, respectively, while the C-C bond (1.417 Å) has been contracted by 5% with respect to the reactant st-C_2H_5F (Figure 2). The structural change of the st-C_2H_5F fragment in RC(st) can be understood on the basis of the donor/acceptor interaction between the base-HOMO, i.e. the F^--$2p_z$, and the substrate-LUMO, i.e. the st-C_2H_5F-8a', the latter having σ anti-bonding character in the C^{β}-H and the C^{α}-F bond, and π bonding character in the C-C bond (*vide infra*). The reactant complex RC(st) seems to be predestinated to react further via the TS(anti-E2) (Figure 2), i.e. via the anti-elimination pathway, on the basis of the structural considerations. Nevertheless, in the gas phase the internal rovibrational energy gained upon complexation of F^- and st-C_2H_5F remains available[32,33] (Chapter 2, Section 2.2) for rearrangement to RC(α), from which the S_N2 process may preferentially proceed. It is interesting

to note, however, that preliminary calculations indicate that the F^- is captured only by the C^{α}-H bond to form RC(α) if it approaches in a relatively narrow cone around the C^{α}-H axis.

Comparison of the reaction profiles of the anti-E2 and the S_N2 reaction (Figure 3a, Table I) clearly shows that the transition state for the S_N2 substitution (–0.02 eV relative to R(st)) is considerably higher in energy, i.e. 0.39 eV, than that for the anti-E2 elimination (–0.41 eV relative to R(st)). Furthermore, the imaginary frequency associated with the reaction mode of the TS(anti-E2) (i 98 cm^{-1}) is considerably lower than that of the TS(S_N2) (i 387 cm^{-1}) (Figure 2c). The higher imaginary frequency of the TS(S_N2) corresponds to a "steeper" saddle point on the energy hyper-surface and can be associated with a relatively tight transition state, i.e. a transition state with a low density of states and thus a high activation entropy. This is confirmed by the relatively high frequencies of the normal modes of the TS(S_N2) (86 cm^{-1}, 315 cm^{-1}, 340 cm^{-1}, 361 cm^{-1}, etc...) if compared to those of the TS(anti-E2) (33 cm^{-1}, 83 cm^{-1}, 131 cm^{-1}, 169 cm^{-1}, etc...). A relatively tight transition state for the S_N2 substitution is in agreement with the rigid structure of the TS(S_N2) in which bond breaking occurs to much a lesser extent than in the TS(anti-E2): in TS(S_N2) the C^{α}-F(leaving group) bond has been elongated by only 26%, while the C^{α}-F(base) bond is already equally strong; in contrast to this, in TS(anti-E2) both the C^{β}-H (+67%) and the C^{α}-F (+51%) bond have been expanded considerably, resulting in a relatively loose structure in spite of the formation of the H-F bond (Figure 2c).

Concluding, the base-induced anti-E2 elimination strongly prevails over the S_N2 substitution due to both a lower activation energy and a less negative activation entropy, but also because of the preferential formation of a reaction complex RC(st) which is predetermined to react further via the anti-E2 pathway.

Anti-E2 versus Syn-E2

In this subsection the competition between the base-induced anti-E2 and syn-E2 elimination (Figure 1) of F^- and fluoroethane is discussed. In principle, F^- can also combine with fluoroethane in the eclipsed conformation (F^- + ecl-C_2H_5F, R(ecl)) under formation of the reactant complex RC(ecl) which is 0.35 eV higher in energy than RC(st) (Table I, Figure 3b). In RC(ecl) the C^{β}-H bond (1.458 Å) and the C^{α}-F bond (1.479 Å) have been elongated by 31% and 5%, respectively, while the C-C bond (1.453 Å) has been contracted by 3% with respect to the reactant ecl-C_2H_5F (Figure 2). The higher energy of RC(ecl) can be explained only partly by the energy

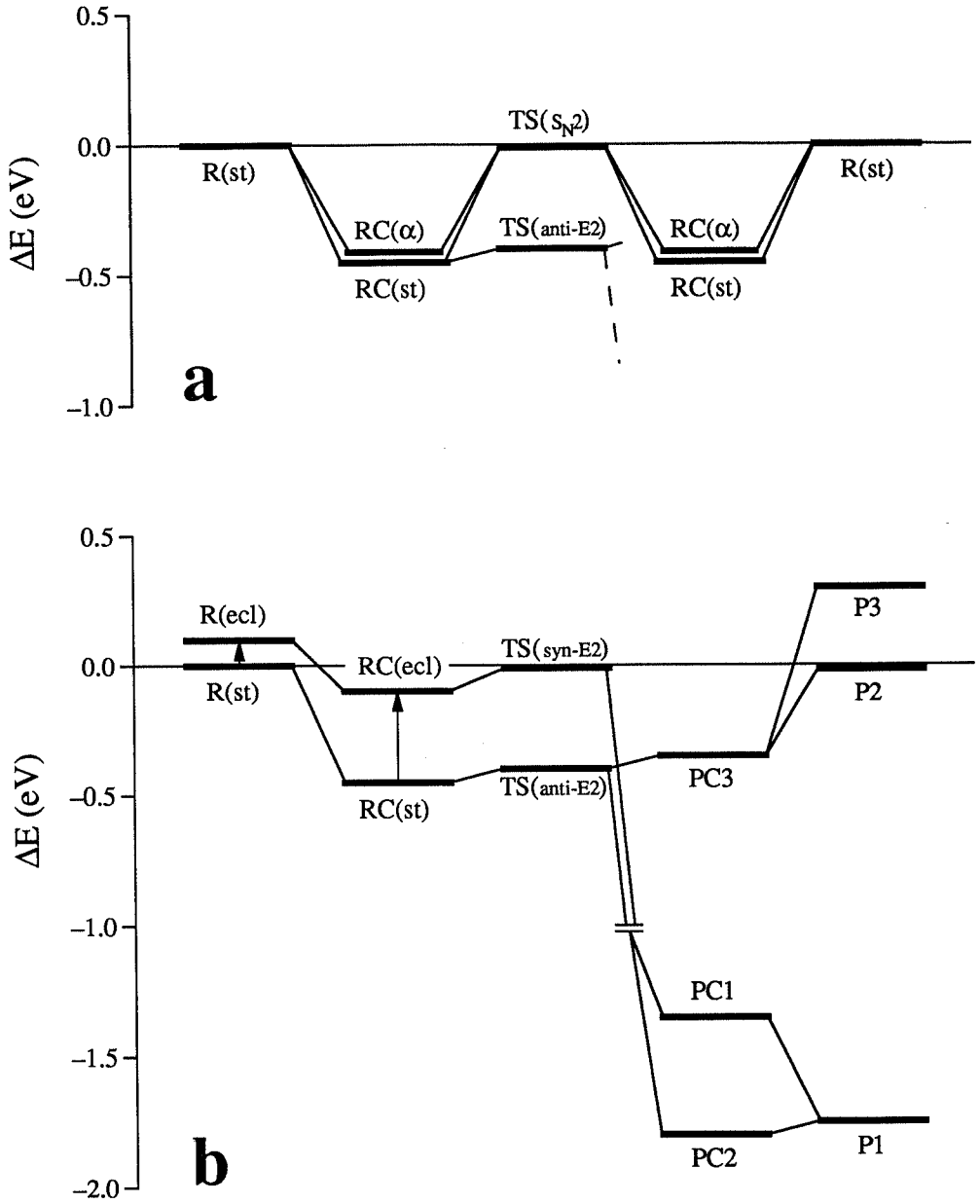

Figure 3. *Schematic reaction energy profiles (DFT/TZPP level) for (part of) the anti-E2 together with the S_N2 reaction (a), and the (complete) anti-E2 together with the syn-E2 reaction (b) of F^- and C_2H_5F.*

difference of 0.10 eV between ecl-C_2H_5F and st-C_2H_5F. The energy difference between RC(ecl) and RC(st) can be followed in detail through the energy contributions in Table II. It appears to be due primarily to a stronger Pauli repulsion between the base-HOMO, i.e. the F^--$2p_z$, and the occupied substrate-6a' (σ bonding for C^β-H). The Pauli repulsion is relieved by a stronger mixing with the ecl-C_2H_5F-8a' LUMO (*vide infra*); the resulting 8a' occupation explains the larger extension of C^β-H in RC(ecl) (+31%) if compared to that in RC(st) (+25%). (Note that such bond elongations raise the energy in free C_2H_5F as reflected in a larger ΔE_{prep} that cancels part of the more favorable ΔE_{oi}). The structural changes upon formation of RC(ecl) indicates the strong tendency of the complex to react further via the syn-E2 pathway. This parallels the behaviour of RC(st) in the anti-E2 reaction. However, an important difference between the two reactant complexes is the fact that RC(st) is a real energy minimum, while RC(ecl) represents a "transition state" of rotation around the C-C axis (imaginary frequency: i 23 cm^{-1}).

Comparison of the reaction profiles of the anti-E2 and the syn-E2 reaction (Figure 3b, Table I) clearly shows that the transition state for the syn-E2 elimination (–0.02 eV relative to R(st)) is considerably higher in energy, i.e. 0.39 eV, than that for the anti-E2 elimination (–0.41 eV relative to R(st)). It is interesting to note, however, that both the anti-E2 and the syn-E2 process have comparably low energy barriers of 0.05 and 0.09 eV, respectively, with respect to the corresponding reactant complexes (RC(st) and RC(ecl)). Furthermore, the imaginary frequency associated with the reaction mode of the TS(syn-E2) (i 176 cm^{-1}) is higher than that of the TS(anti-E2) (i 98 cm^{-1}), but lower than that of TS(S_N2) (i 387 cm^{-1}). This corresponds to a TS(syn-E2) of intermediate tightness (*vide supra*) as is confirmed by the frequencies of the normal modes (93 cm^{-1}, 136 cm^{-1}, 195 cm^{-1}, 382 cm^{-1}, etc...). The tighter transition state for the syn-E2 elimination is in agreement with the much smaller extent of elongation of the C^β-H (1.934 Å, +33%) and the C^α-F (1.675 Å, +13%) bonds in TS(syn-E2) if compared to TS(anti-E2) (Figure 2c; note that percentages are relative to reactant complexes). It is further noted, that dissociation of the C^β-H bond precedes dissociation of the C^α-F bond to a higher extent in TS(syn-E2), i.e. the syn-E2 elimination is more E1cb-like than the anti-E2 elimination. In fact, the structure of the anti-E2 transition state is nearly central E2.

The features of the two base-induced elimination reactions are illustrated by the shape of the 2-dimensional reaction energy surfaces E(d(C^β-H), d(C^α-F)) displayed in Figure 4. The more

rigid structure of the TS(syn-E2) shows up in a less extended saddle region. The syn-E2 saddle region is reached essentially by "going slightly to the right", i.e. moderate C^{β}-H bond expansion, reflecting some E1cb character of the syn-E2 elimination. Most strikingly, there is no distinct channel on the anti-E2 surface leading directly from the reactant complex to the saddle region. Instead, the system displays a weak tendency to elongate initially either the C^{β}-H or the C^{α}-F bond to some extent, before the other bond is expanded, i.e. there is a weak indication of a E1cb-like and a E1-like channel on the anti-E2 surface. It is concluded that the anti-E2 reaction is virtually ideal E2 with respect to the transition state geometry, but that the reaction path toward this transition state cannot be classified in this way, as there is no clear preference on the very shallow slope of the reaction energy surface.

Anti-E2 and syn-E2 elimination result in the exothermic formation (Figure 3b, Table I) of the same product complex PC1 (–1.36 eV relative to R(st), Figure 2d) under the C_S symmetry constraint used in the calculation of the reaction energy surface (Figure 4). PC1 is composed of FHF^- and C_2H_4, and can decompose to the separated products P1 (–1.75 eV relative to R(st), Figure 2e) either directly or via rearrangement to the more stable PC2 (–1.78 eV relative to R(st)) in which FHF^- hydrogen bonds to a C-H bond of ethene. Conceivably, release of the C_S constraint may open the possibility in the *anti*-E2 elimination to lead to the production of the relatively unstable PC3 (–0.37 eV relative to R(st), Figure 2d). The product complex PC3 is composed of rather weakly interacting HF, C_2H_4 and F^-, and may decompose via rearrangement to the more stable PC2. Alternatively, PC3 can separate either partly to HF and the ion/molecule complex [C_2H_4, F^-], i.e. the products P2 (–0.02 eV relative to R(st)), or completely to the products P3 (+0.29 eV relative to R(st)). In principle, the endothermic reaction channel towards P3 is not available under low-pressure conditions in the gas phase.[32,33]

Concluding, the base-induced anti-E2 elimination strongly prevails over the syn-E2 elimination due to both a lower activation energy and a less negative activation entropy, but also because the syn-E2 reactant complex represents a labile structure which tends to rotate around the C-C bond, away from the reactive conformation. Both anti- and syn-E2 reaction preferentially result in the the formation of FHF^- and C_2H_4.

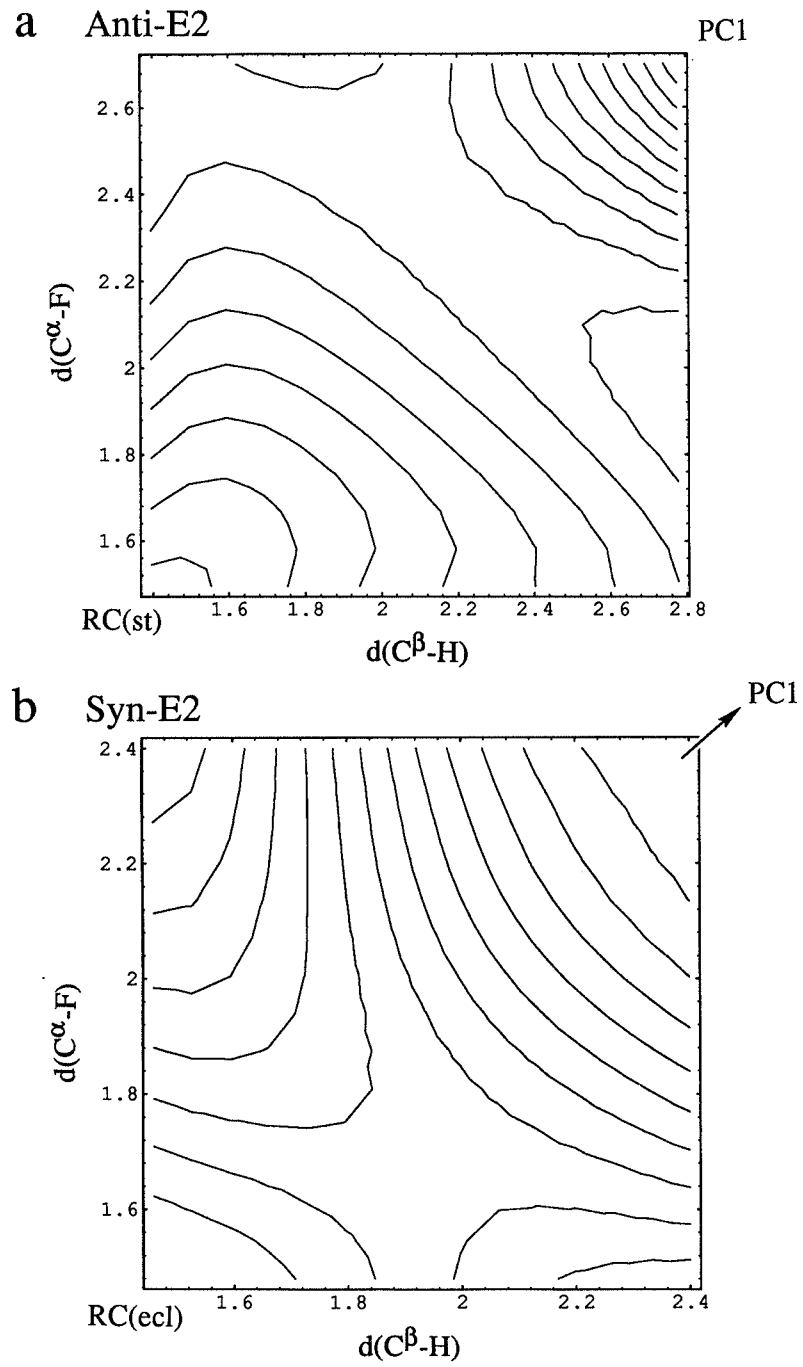

Figure 4. *2-Dimensional reaction energy surface E(d(C$^{\beta}$-H), d(C$^{\alpha}$-F)) (Xα/DZP level) for the anti-E2 reaction (a) and the syn-E2 reaction (b) of F^- and C_2H_5F (contour spacing ca. 0.1 eV).*

Table II. Analysis of the bonding mechanism between F^- and the C_2H_5F fragment in the reaction systems RC(st), TS(anti-E2), RC(ecl) and TS(syn-E2).[a,b]

	RC(st)	TS(anti-E2)	RC(ecl)	TS(syn-E2)
Overlaps $\langle F^- \mid C_2H_5F\rangle$[c]				
$\langle 2p_z \mid 5a'\rangle$	0.08	0.22	0.06	0.08
$\langle 2p_z \mid 6a'\rangle$	0.22	0.16	0.23	0.16
$\langle 2p_z \mid 7a'\rangle$	0.05	0.01	0.06	0.21
$\langle 2p_z \mid 8a'\rangle$	0.19	0.26	0.20	0.24
$\langle 2p_z \mid 9a'\rangle$	0.01	0.05	0.03	0.04
Populations[d] (electrons)				
$P(2p_z)$	1.77	1.62	1.74	1.65
P(5a')	1.99	1.85	1.99	1.99
P(6a')	1.88	1.65	1.86	1.91
P(7a')	1.99	1.99	1.99	1.78
P(8a')	0.27	0.76	0.34	0.56
P(9a')	0.02	0.02	0.00	0.00
Energies[e] (eV)				
ΔE_{elstat}	–2.98	–5.38	–2.98	–4.18
ΔE_{Pauli}	4.65	7.06	5.21	6.87
ΔE^0	1.67	1.68	2.23	2.69
ΔE_{oi}	–3.71	–8.04	–4.34	–6.97
ΔE_{int}	–2.04	–6.36	–2.11	–4.28
ΔE_{prep}	0.86	5.51	1.24	3.53
ΔE	–1.18	–0.85	–0.87	–0.75

[a] Calculated at the DFT/DZP level for Xα/DZP geometries (see Method).

[b] See Figure 2 for structures.

[c] The fluorine z-axis points to the β-hydrogen of the C_2H_5F fragment.

[d] $P(\varphi)$ is the gross Mulliken population that the fragment orbital φ acquires in the complex.

[e] ΔE^0 is the steric repulsion that comprises both the four-electron destabilizing interactions between occupied orbitals (Pauli repulsion: ΔE_{Pauli}) and the classical electrostatic interaction (ΔE_{elstat}) between the electronic and nuclear charge distributions of the fragments. ΔE_{oi} is the orbital interaction, which comes for more than 90% from the A' symmetry. ΔE_{prep} is the energy required to prepare the C_2H_5F fragment in the geometry that it has in the complex from the free, staggered fluoroethane.

Orbital Interactions and the Catalytic Effect of the Base

In this subsection, the magnitude and the origin of the catalytic effect of the base in the anti- and syn-E2 eliminations are investigated. In particular, the question is addressed *why* the transition state is selectively stabilized and *why* this stabilization is more effective for the anti elimination. To this end we consider the thermic, that is the uncatalysed syn and anti elimination (E) of HF from fluoroethane (Equation 2). The structures of the TS(anti-E2) and TS(syn-E2) (Figure 2c) with the base F^- removed serve as model systems for the uncatalysed transition states UTS(anti-E) and UTS(syn-E), respectively. Although artificial to some extent, this choice is plausible and, moreover, allows one to couple the energetics of catalysis with a qualitative picture based on an analysis of the base/substrate interaction in the E2 transition states (Table II). Furthermore, the syn-E barrier of 3.60 eV calculated for our model transition state (Table I) is in reasonable agreement with the SCF/4-31G and CI-SD+QC/4-31G values obtained by Kato and Morokuma[87] which are lower by 10% and 17%, respectively.

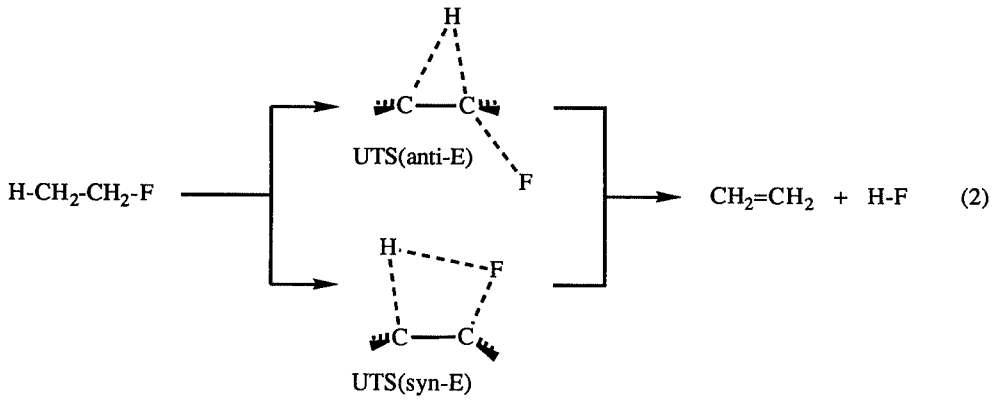

In Figure 5 the energetics of the base-catalysed and the uncatalysed elimination reactions are displayed. In the absence of the F^- catalyst the anti- (+5.48 eV) as well as the syn-elimination (+3.60 eV) of HF from fluoroethane suffers from an enormous activation barrier (Figure 5, Table I). As one might expect intuitively, the uncatalysed syn-E reaction proceeds via a lower energetic transition state due to the onset of a favorable H/F interaction in an early stage of the reaction, associated with a smaller extent of deformation.

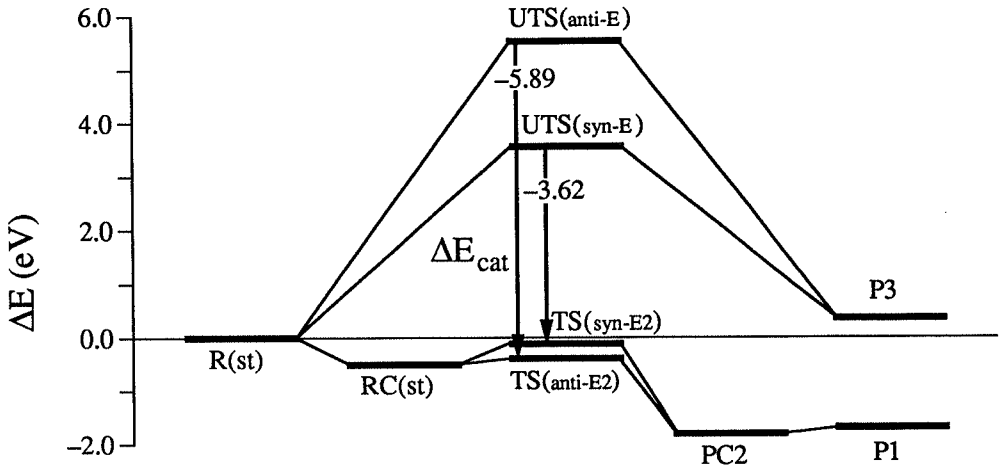

Figure 5. *Catalytic effect of the base F^- on the 1,2-elimination of HF from C_2H_5F (DFT/TZPP energy profile).*

Introduction of the base results in selective stabilization of the transition states (Figure 5, Table I). The catalytic effect for the anti elimination (–5.89 eV) is considerably higher than that for the syn elimination (–3.62 eV). This leads to an inversion of the energetic ordering of transition states resulting in an energetically favored base-catalysed *anti*-E2 reaction. The mechanism of stabilization of the transition state and the high degree of anti/syn-selectivity of the E2 catalyst, i.e. the F^- base, is revealed by a detailed analysis of the electronic structure of and the interaction between the reactants in the E2 reaction complexes and transition states (see Table II and Figures 6 and 7). First the reactant complexes are reviewed in more detail (Figures 6a and 7a). In both RC(st) and RC(ecl) the F^--$2p_z$ (base HOMO) interacts with the 6a' (substrate $\sigma_{C\text{-}H}$) and the 8a' (substrate $\sigma^*_{C\text{-}H}$ and LUMO). The interaction between the occupied $2p_z$ and 6a' leads to Pauli repulsion, which is relieved by the mixing of the $2p_z$ – 6a' combination with the 8a'. This results in a donor/acceptor interaction between the F^--$2p_z$ and the C_2H_5F-8a' and charge transfer within the substrate from the 6a' to the 8a'. The C^β-H and C^α-F bonds are weakened and expand while

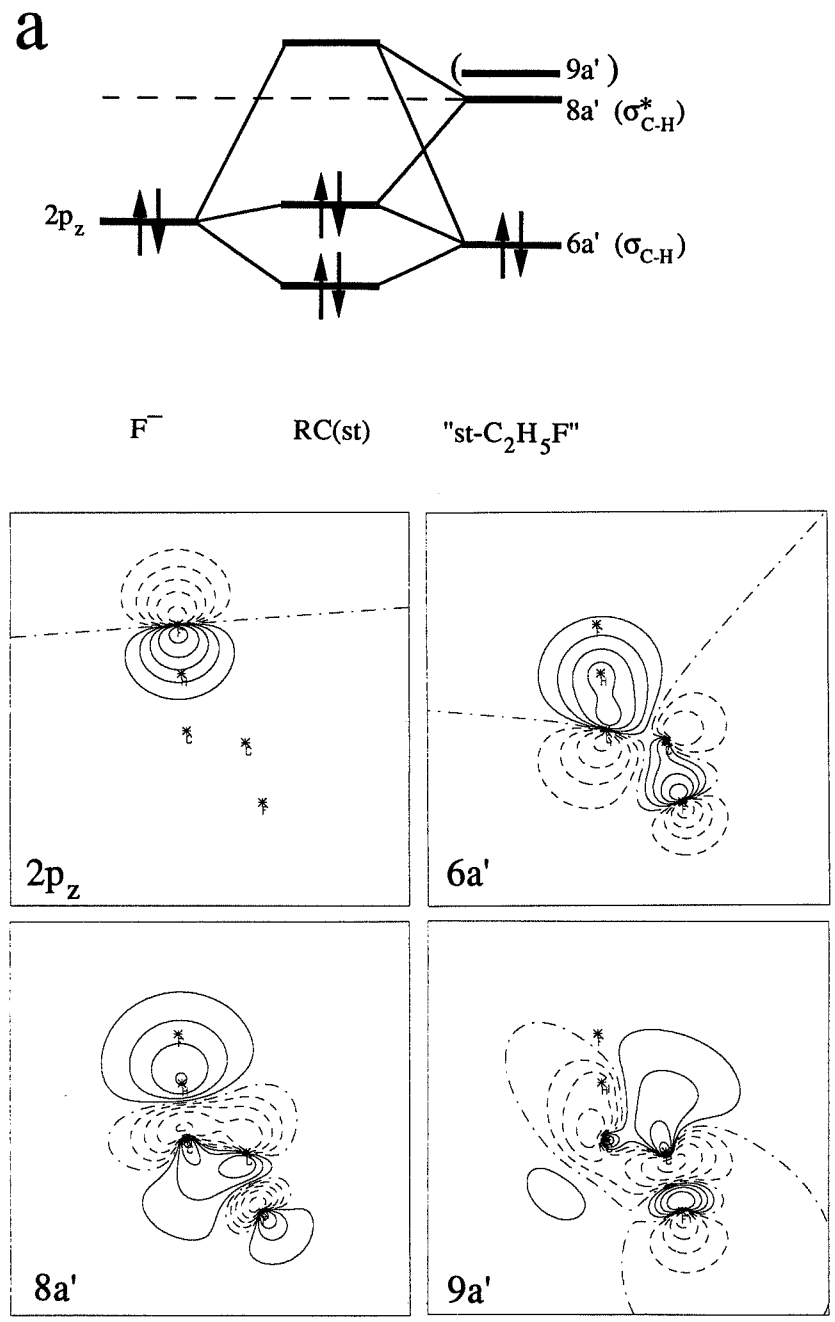

Figure 6. *F^-/C_2H_5F MO interaction scheme and contour plots of selected fragment orbitals for anti-E2 reaction systems* ***RC(st)*** *(a) and* ***TS(anti-E2)*** *(b,* Continued overleaf*). Note, that in the fragment orbital plots also the position of the nuclei of the other fragment are indicated.*

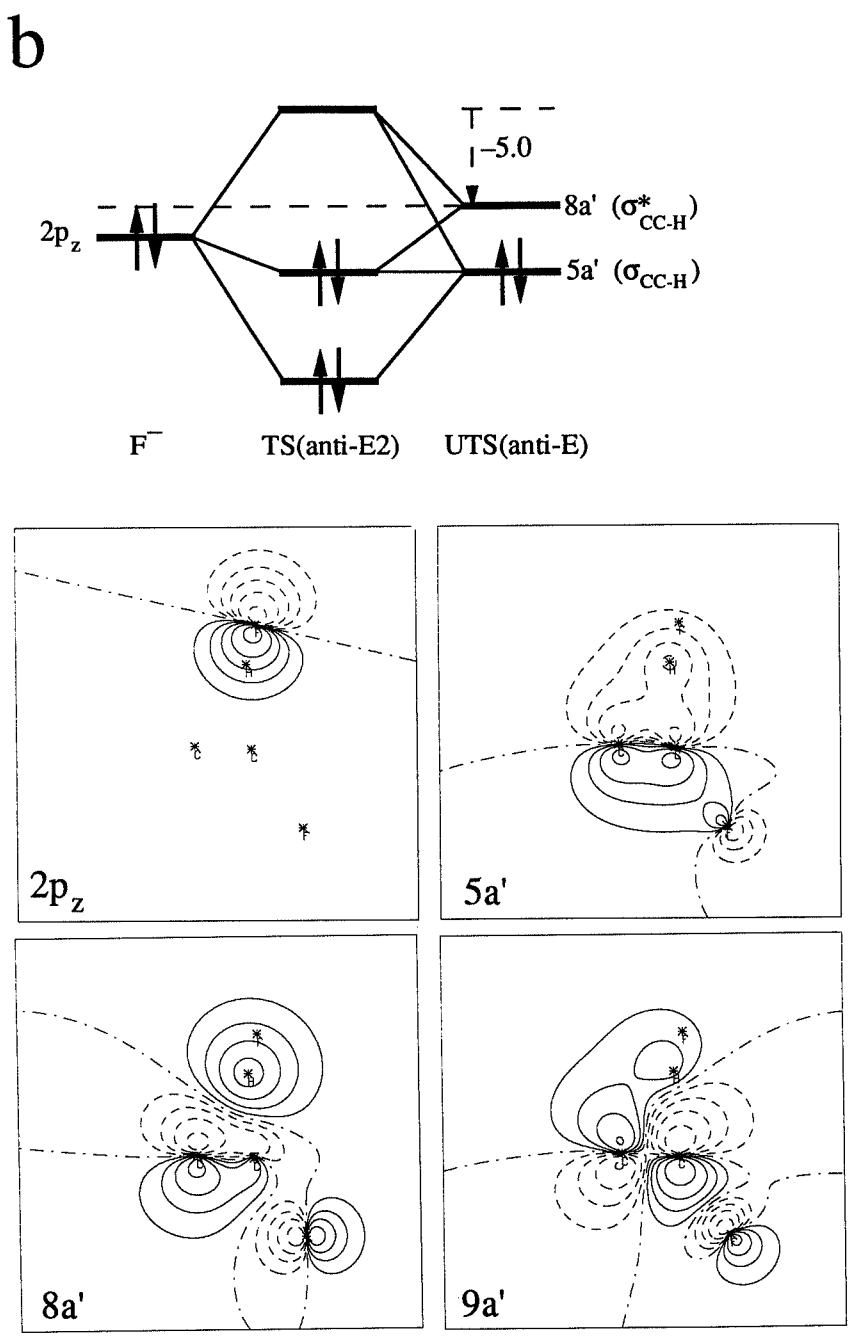

Figure 6. (Continued) *In (b) the stabilization (eV) of the C_2H_5F-8a' is indicated when going from RC(st) to TS(anti-E2).*

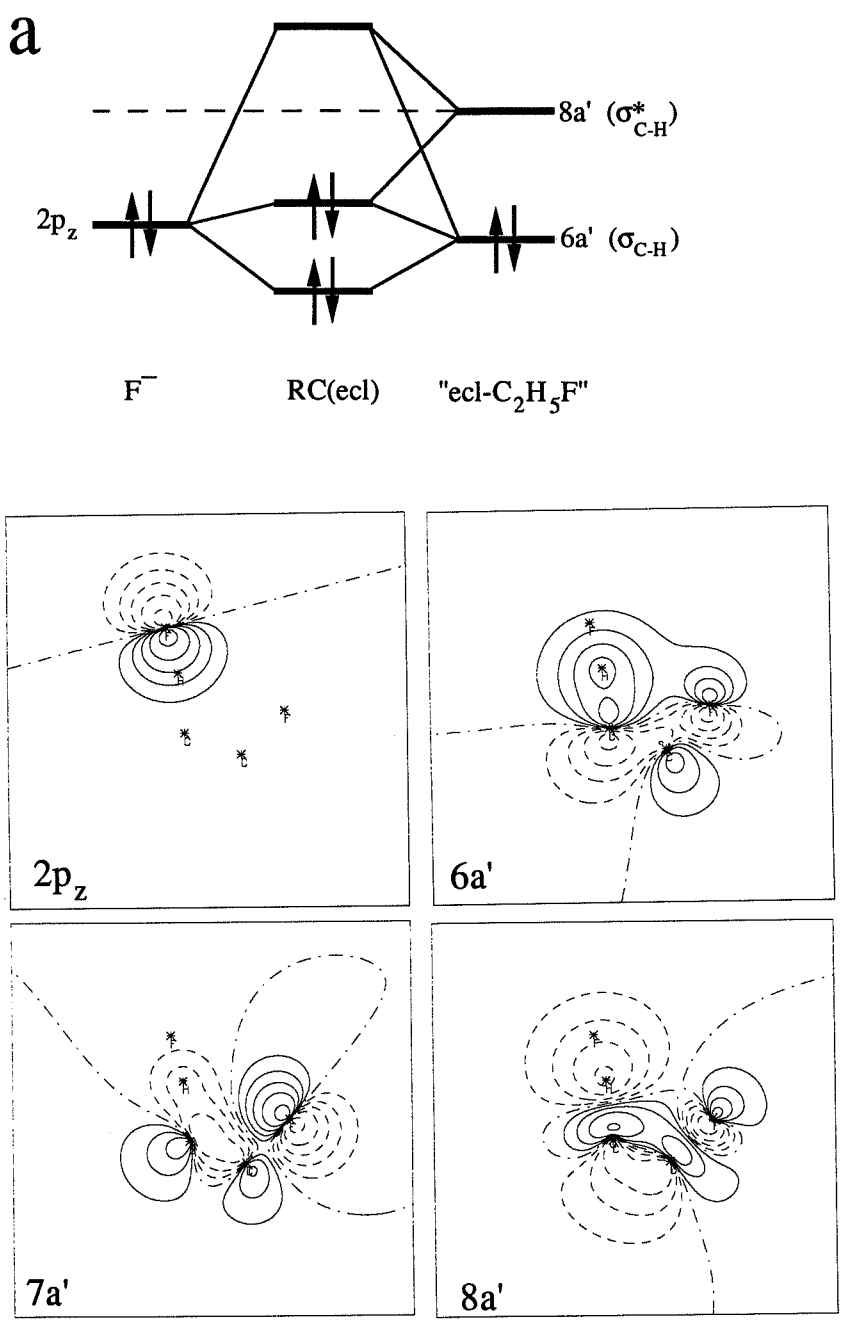

Figure 7. *F^-/C_2H_5F MO interaction scheme and contour plots of selected fragment orbitals for syn-E2 reaction systems* ***RC(ecl)*** *(a) and* ***TS(syn-E2)*** *(b,* Continued overleaf*). Note, that in the fragment orbital plots also the position of the nuclei of the other fragment are indicated.*

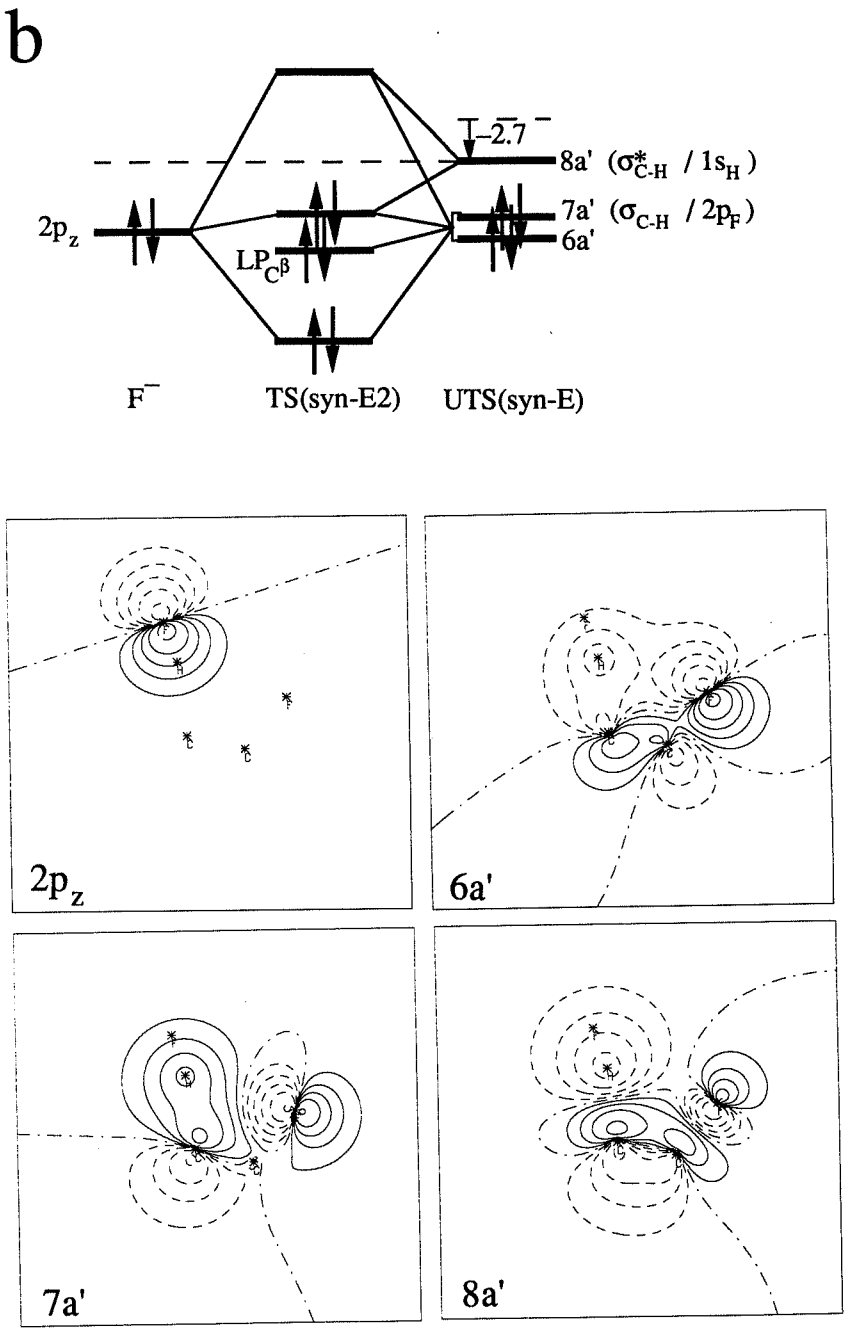

Figure 7. (Continued) *In (b) the stabilization (eV) of the C_2H_5F-8a' is indicated when going from RC(ecl) to TS(syn-E2).*

the C-C bond contracts, mainly due to the donation of charge into the 8a' (σ anti-bonding for C^{β}-H and C^{α}-F, π bonding for C-C), but also because of the depopulation of the 6a' (σ bonding for C^{β}-H and C^{α}-F, π anti-bonding for C-C; Figures 6a and 7a). The C^{β}-H bond expansion is much stronger for R(ecl) which shows up in a higher ΔE_{prep} for the C_2H_5F fragment and a stronger charge transfer from $2p_z$ and 6a' to 8a' (Table II). The reason for this is the larger Pauli repulsion between the $2p_z$ and the 6a' of eclipsed fluoroethane, which is relieved by a stronger mixing with the 8a'. The stronger $2p_z$/6a' interaction is caused by the larger overlap of the $2p_z$ with the rather extended lobe of the 6a' of eclipsed fluoroethane (Figure 7a). Thus, the weaker bonding in the eclipsed reactant complex RC(ecl) (–0.87 eV) relative to the staggered complex RC(st) (–1.18 eV; Table I) is the result of incomplete cancellation of stronger repulsive ($\Delta E^0 + \Delta E_{prep}$) and attractive ($\Delta E_{oi}$) interactions (Table II; see also subsection "Anti-E2 versus Syn-E2").

Next, the transition states are examined. Extension of the C^{β}-H and C^{α}-F bonds in eclipsed fluoroethane relatively early leads to a favorable, i.e. bonding interaction between the H and the leaving group F. This is reflected by the H-F (1s + 2p) bonding character of the 6a' orbital which slightly increases when going from ecl-C_2H_5F in RC(ecl) to UTS(syn-E) in TS(syn-E2) (Figure 7b). (Note that the occupied 7a' (H-F (1s – 2p) anti-bonding) and 8a' LUMO (H-F non-bonding, C-C π-bonding) of the UTS(syn-E) still have to interchange their energetic order and occupation, before a proper ethene + HF configuration is achieved). In the presence of the F^- base, the 6a' and 7a' (Figure 7b) mix to give a fluorine 2p-like combination ($2p_F$) and a combination with more character of a lone pair at C^{β} pointing away from the base ($LP_{C\beta}$), in order to minimize overlap, i.e. Pauli repulsion with the base $2p_z$. The $2p_F$-like combination interacts with the base $2p_z$ and the 8a' (much $1s_H$ character !) in a way that resembles the $2p_z/1s/2p_z$ 3-orbital-4-electron interaction in F-H-F^-. In this interaction the 8a' LUMO accepts 0.56 el., mainly from the base ($P(2p_z)$ = 1.65 el.), but also from the 7a' and to a smaller extent from 6a' (Table II).

A favorable H-F interaction in an early stage of C^{β}-H and C^{α}-F expansion is inherently impossible for the anti-elimination, and the transition state is reached at a point where the C^{β}-H and C^{α}-F bond have been extended to a much higher degree. Consequently, the energy level of the acceptor orbital of C_2H_5F, i.e. the 8a' LUMO, decreases much more for the anti-elimination (–5.0 eV) than for the syn-elimination (–2.7 eV) when proceeding from the reactant complex geometry to the transition state (Figures 6b and 7b). This has the important consequence that the 8a' LUMO of the UTS(anti-E) is much lower in energy and, hence, is a better partner in the donor/acceptor

interaction with the $2p_z$ HOMO of the F^- base. The stronger Pauli repulsion between the F^--$2p_z$ and the relatively high energetic 5a' ($\sigma_{CC\text{-}H}$, Figure 6b) is overcompensated by the very favorable orbital interaction (Table II). This leads to an important extent to the selectively stronger stabilization of the transition state for anti-elimination upon base catalysis (Figure 5). It is emphasized, however, that the electrostatic stabilization by the F^- catalyst is also much larger for UTS(anti-E) than for UTS(syn-E) (compare ΔE_{elstat} of TS(anti-E2) and TS(syn-E2) in Table II). This reflects the favorable orientation of the dipole moment in UTS(anti-E) for interaction with the F^- base in TS(anti-E2). Analogously, the pronounced shift of the abstracted proton from the C^β to the C^α position in the TS(anti-E2) (Figure 2c) can also be ascribed to a favorable interaction between the H-F moiety and the C^α-F dipole. Finally, the high population that the 8a' LUMO acquires in the TS(anti-E2) is also the result of polarization mixing with the 6a' (having proton $1s_H$ and leaving group $2p_F$ character; P(6a') = 1.65el.), besides the donor/acceptor interaction with the base $2p_z$ (P($2p_z$) = 1.62 el.) and the relieve of 5a'/$2p_z$ Pauli repulsion (P(5a') = 1.85 el.; Table II).

Concluding, the syn-mechanism would prevail in the thermic, i.e. uncatalysed elimination of HF from fluoroethane, but a very high barrier precludes this reaction. Preferential stabilization of the loose, highly unsaturated anti-E transition state upon base catalysis reverses this order and makes the anti-mechanism the preferred one for the base-induced elimination. The stabilization has a charge transfer (donor/acceptor) as well as an electrostatic nature.

The E2H and the E2H/E2C Spectrum

The base-induced syn-E2 elimination of F^- and fluoroethane proceeds via a E1cb-like transition state, as appears from the stronger elongation of the C^β-H bond relative to the elongation of the C^α-F bond (Figure 2), the anti-elimination being more central E2. Consequently, the syn-E2 transition state has a much more pronounced charge development on the C^β (–0.41 el.) than the anti-E2 transition state (–0.23 el.; Figure 8). The 1,2-shift of the HF moiety from the C^β to the C^α is an important feature of the TS(anti-E2) which is not accounted for in the formalism of the E2H-spectrum.

There is no indication for an E2C-like interaction, i.e. a (weak) covalent interaction of the base with the C^α-F bond. In the reactant complex RC(st) the base-$2p_z$ has a very poor overlap of 0.01 with the "back-side" lobe of the substrate-9a' which is the $\sigma^*_{C\text{-}F}$ acceptor in the S_N2 reaction and is calculated to be 1.4 eV above the 8a' LUMO (Figure 6a, Table II). This trend continues for

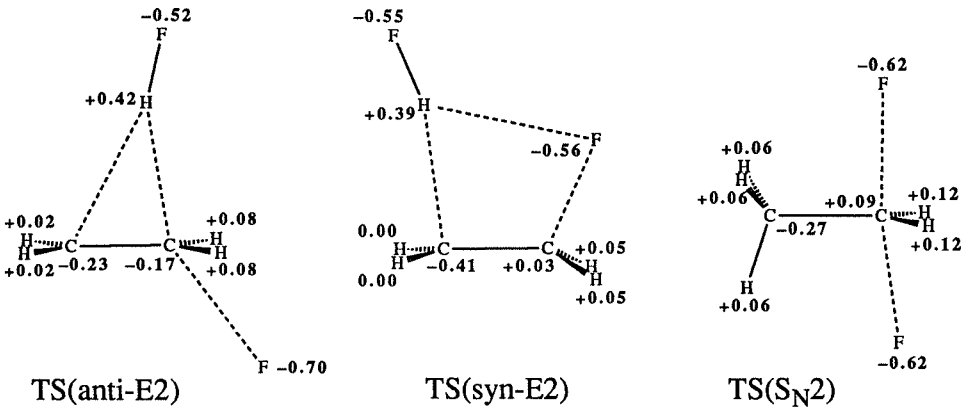

Figure 8. *Gross Mulliken atom charges (in electrons; DFT/DZP level) for the E2 and S_N2 transition states.*

the TS(anti-E2) where $\langle 2p_z | 9a' \rangle$ is only slightly larger and amounts to 0.05 (Figure 6b, Table II). As a result, there is no donor/acceptor interaction with the 9a', and P(9a') amounts to only 0.02 electrons in both RC(st) and TS(anti-E2) (Table II). For comparison, the calculations reveal that in the transition state for S_N2 substitution the F^--$2p_z$ has an overlap of 0.18 with the "back-side" lobe of the substrate $\sigma^*_{C\text{-}F}$ acceptor orbital, which now is populated by 0.33 electrons.

Comparison with Previous Studies

It appears from our results that the C^β-H and the C^α-F bonds expand considerably upon formation of the reactant complexes for elimination, mainly due to charge donation of the base into the delocalized 8a' LUMO of the substrate C_2H_5F (Figures 6a and 7a). This nicely confirms the concept of "electronic coupling", already employed by Fukui et al..[49,50] We have found this donor/acceptor interaction between the base-HOMO (F^--$2p_z$) and the 8a' LUMO of the C_2H_5F fragment to play a key role in the selective stabilization of the transition state for anti-elimination. This picture of selective catalysis principally differs from the concept developed by Bach et al..[54]

In this concept,[54] the elimination is conceived as an internal S_N2 reaction, in which the developing C^β lone pair (or the C^β-H electron pair) performs a back-side attack on the $\sigma^*_{C\text{-}F}$ orbital. Accordingly, the syn-elimination is hampered by the need of an inversion of the configuration at the C^β center, in order to enable the C^β lone pair to interact with the $\sigma^*_{C\text{-}F}$. The simplicity of this view is tempting at first sight. However, the meaning of a back-side attack of the C^β lone pair on the $\sigma^*_{C\text{-}F}$ is rather unclear, as the MOs of the C_2H_5F fragment are highly delocalized (Figures 6 and 7) and orthogonal with respect to each other. Furthermore, the inversion of configuration at C^β in the TS(syn-E2) is not observed in our calculations (Figure 2c; the dihedral angle $HC^\beta C^\alpha$(HF) amounts to 96°, where the first H refers to a C^β-bonded hydrogen atom and the second H refers to the F^- base-bonded proton).

Theoretical investigations on the prevalence of E2 over S_N2 reactions in the gas phase have also been performed for the F^-/C_2H_5F model system by Minato and Yamabe.[55,56] They conclude that preferentially the reactant complex for anti-E2 elimination is formed.[55] Furthermore, they arrive at a more favorable, i.e. less negative activation entropy for the anti-E2 reaction.[55] These results are in nice agreement with our findings. Differences with the present work are the less extensive deformation of the C_2H_5F fragment in the reactant complexes and transition states, and the reversed energetic order of the anti-E2 and S_N2 transition states, respectively, which are calculated to be 0.65 and 0.43 eV above the separated reactants F^- and staggered fluoroethane (RHF/DZP// RHF/3-21G level of theory).[56]

Our results are in excellent agreement with experimental results of low pressure gas-phase studies of Ridge and Beauchamp.[22,23] In the reaction of F^- with fluoroethane the exclusive formation of FHF^- is observed, which has to proceed via elimination (Equation 3).

$$F^- + C_2H_5F \longrightarrow FHF^- + C_2H_4 \qquad (3)$$

This fits in nicely with the strong prevalence of E2 over S_N2 inferred from our calculations. However, the FHF^- complex is not necessarily formed via syn-elimination as suggested by Ridge and Beauchamp.[22,23] From our calculations it follows that the anti-E2 reaction also preferentially leads to the 1.75 eV exothermic FHF^- production and is strongly favored over the syn-E2 reaction (Figure 3b). The absence of F^- ions from anti-E2 is easily explained as this reaction channel is

endothermic by 0.29 eV and, thus, is not available under low pressure conditions (Chapter 2, Section 2.2).[32,33] The nonappearance of [C_2H_4, F^-] is ascribed to the much less favorable reaction energy of the channel leading to products P2 (–0.02 eV, Table I) and is consistent with a preferential collapse of the TS(anti-E2) towards PC1 or PC2 (Figures 3b and 4a).

Expectations for the Condensed Phase

Finally, the relevance of our gas-phase results for condensed phase reactions is qualitatively evaluated. In the condensed phase the reactants are stabilized by solvation. This stabilization is, probably, most pronounced for the separated reactants and products, because the rather compact F^- and FHF^- anions can have a very favorable electrostatic and/or charge transfer (hydrogen bond) interaction with solvent molecules. Both the E2 and S_N2 reaction can only proceed via partial desolvation of reactants in order to form the reactant complex. The change in the mutual competition between E2 and S_N2 upon solvation is difficult to trace. Inspection of the charge distribution of the transition states in Figure 8 shows that the TS(S_N2) contains two relatively "naked" fluorine atoms and may benefit the most by solvation. This would be in agreement with the relative ease of condensed phase S_N2 reactions,[1,2] if compared with the strong prevalence of E2 reactions in the gas phase.[32,33] Nevertheless, this is speculative and more detailed investigations are under way to tackle this problem.

6.5 Conclusion

In this paper we have investigated the nature of the base-induced elimination reaction using F^- and fluoroethane as a model reaction system. The base has been found to play a key role as a catalyst which strongly influences the competition between anti- and syn-elimination. The thermic elimination of HF from fluoroethane preferentially proceeds via the syn pathway. Upon catalysis by the base, the transition states are considerably stabilized. This stabilization, however, selectively favors the anti-mode, leading to the prevalence of anti-E2 over syn-E2 elimination. A main reason for the selective stabilization is the very low energy and, thus, the good acceptor capability of the C_2H_5F-8a' LUMO (σ anti-bonding for CC-H and C^{α}-F; Figure 6b) in the strongly rearranging, loose anti-E2 transition state. This 8a' LUMO effectively relieves the Pauli repulsion that the base-

2pz HOMO has with the C_2H_5F-5a' (σ bonding for CC-H and C^{α}-F; Figure 6b) and has a strong donor/acceptor interaction with the base-$2p_z$ HOMO.

The preference of the gas-phase base-induced elimination over the nucleophilic substitution has several reasons. The base F^- preferentially combines with the C_2H_5F substrate to form a reactant complex that is predestinated to undergo anti-E2 elimination. Furthermore, the activation barrier for elimination is considerably lower (for anti-E2) and the transition states are more loosely bound and thus correspond to a situation with a relatively high density of states, i.e. a less negative and thus favorable activation entropy.

The base-induced syn-E2 elimination is E1cb-like. Nevertheless, the inversion of configuration proposed in the "internal S_N2" concept does not occur. The geometry of the anti-E2 transition state is virtually E2. However, on the reaction energy surface (Figure 4a) there is no direct channel towards the transition state involving synchronous C^{β}-H and C^{α}-F bond breaking. Instead, there is a very weak preference for an asynchronous pathway (either E1cb-like or E1-like). Furthermore it is concluded that the anti-E2 reaction is of the E2H type (Figure 1) as no E2C-like interactions are present in the transition state. Finally, an important characteristic of the anti-E2 elimination is the pronounced shift of the abstracted proton from the C^{β} to the C^{α} position in the transition state. This feature is not contained in the E2H formalism.

References

1. Carey, F.A.; Sundberg, R.J. *Advanced Organic Chemistry*, Part A; Plenum Press: New York, 1984.
2. Lowry, T.H.; Richardson, K.S. *Mechanism and Theory in Organic Chemistry*, 2nd ed.; Harper and Row: New York, 1981.
3. Cockerill, A.F.; Harrison, R.G. in *The Chemistry of Double Bonded Functional Groups*, Supplement A, Part 1; Patai, S., Ed.; Wiley: London, 1977; Chapter 4.
4. Kice, J.L.; Kopczyk-Subotkowska, L. *J. Org. Chem.* **1990**, 55, 1523, and references cited therein.
5. Cullis, C.F.; Fish, A. in *The Chemistry of the Carbonyl Group*; Patai, S., Ed.; Wiley: London, 1966; pp 142-143.

6. *Multiple Bonds and Low Coordination in Phosphorus Chemistry*; Regitz, M.; Scherer, O.J., Eds.; Georg Thieme Verlag: Stuttgart, 1990, in particular Chapter D.4 (Appel, R.), Chapter D.8 (Niecke, E.) and Chapter D.9 (Yoshifuji, M.).
7. Gandler, J.R. in *The Chemistry of Double-Bonded Functional Groups*, Vol. 2, Part I; Patai, S. Ed.; Wiley: New York, 1989.
8. Bartsch, R.A.; Závada, J. *Chem. Rev.* **1980**, 80, 453.
9. Saunders, W.H., Jr. *Acc. Chem. Res.* **1976**, 9, 19.
10. Bartsch, R.A. *Acc. Chem. Res.* **1975**, 8, 239.
11. Saunders, W.H., Jr.; Cockerill, A.F. *Mechanisms of Elimination Reactions*; Wiley: New York, 1973; Chapter 1.
12. Cram, D.J.; Greene, F.D.; DePuy, C.H. *J. Am. Chem. Soc.* **1956**, 78, 790.
13. Bunnett, J.F. *Angew. Chem.* **1962**, 74, 731.
14. Bartsch, R.A.; Bunnett, J.F. *J. Am. Chem. Soc.* **1968**, 90, 408.
15. Parker, A.J.; Ruane, M.; Biale, G.; Winstein, S. *Tetrahedron Lett.* **1968**, 2113.
16. Biale, G.; Cook, D.; Lloyd, D.J.; Parker, A.J.; Stevens, I.D.R.; Takahashi, J.; Winstein, S. *J. Am. Chem. Soc.* **1971**, 93, 4735.
17. McLennan, D.J. *Tetrahedron* **1975**, 31, 2999.
18. Hoffman, R.V.; Bartsch, R.A.; Cho, B.R. *Acc. Chem. Res.* **1989**, 22, 211, and references cited therein.
19. Koning, L.J. de; Nibbering, N.M.M. *J. Am. Chem. Soc.* **1987**, 109, 1715.
20. Berkel, W.W. van; Koning, L.J. de; Nibbering, N.M.M. *J. Am. Chem. Soc.* **1987**, 109, 7602.
21. Koning, L.J. de; Nibbering, N.M.M. *J. Am. Chem. Soc.* **1988**, 110, 2066.
22. Ridge, D.P.; Beauchamp, J.L. *J. Am. Chem. Soc.* **1974**, 96, 637.
23. Ridge, D.P.; Beauchamp, J.L. *J. Am. Chem. Soc.* **1974**, 96, 3595.
24. Sullivan, S.A.; Beauchamp, J.L. *J. Am. Chem. Soc.* **1976**, 98, 1160.
25. Doorn, R. van; Jennings, K.R. *Org. Mass Spectrom.* **1981**, 16, 397.
26. DePuy, C.H.; Bierbaum, V.M. *J. Am. Chem. Soc.* **1981**, 103, 5034.
27. DePuy, C.H.; Beedle, E.C.; Bierbaum, V.M. *J. Am. Chem. Soc.* **1982**, 104, 6483.
28. Bierbaum, V.M.; Filley, J.; DePuy, C.H.; Jarrold, M.F.; Bowers, M.T. *J. Am. Chem. Soc.* **1985**, 107, 2818.

29. Thomas, D.A.; Bloor, J.E.; Bartmess, J.E. *J. Am. Soc. Mass Spectrom.* **1990**, 1, 295.
30. Grabowski, J.J.; Zhang, L. *J. Am. Chem. Soc.* **1989**, 111, 1193.
31. Noest, A.J.; Nibbering, N.M.M. *Adv. Mass Spectrom.* **1980**, 8A, 227.
32. Nibbering, N.M.M. *Acc. Chem. Res.* **1990**, 23, 279.
33. Nibbering, N.M.M. *Adv. Phys. Org. Chem.* **1988**, 24, 1.
34. Lias, S.G.; Ausloos, P. *Ion-Molecule Reactions*, American Chemical Society: Washington, 1975.
35. Olmstead, W.N.; Brauman, J.I. *J. Am. Chem. Soc.* **1977**, 99, 4219.
36. Sini, G.; Shaik, S.; Hiberty, P.C. *J. Chem. Soc., Perkin Trans. 2* **1992**, 1019.
37. Shi, Z.; Boyd, R.J. *J. Am. Chem. Soc.* **1991**, 113, 1072.
38. Zahradník, R.; Hess, B.A., Jr.; *J. Molec. Struct. (Theochem)* **1991**, 230, 387.
39. Zhao, X.G.; Tucker, S.C.; Truhlar, D.G. *J. Am. Chem. Soc.* **1991**, 113, 826.
40. Tucker, S.C.; Truhlar, D.G. *J. Am. Chem. Soc.* **1990**, 112, 3338.
41. Vande Linde, S.R.; Hase, W.L. *J. Phys. Chem.* **1990**, 94, 6148.
42. Ohta, K.; Morokuma, K. *J. Phys. Chem.* **1985**, 89, 5845.
43. Morokuma, K. *J. Am. Chem. Soc.* **1982**, 104, 3732.
44. Wolfe, S.; Mitchell, D.J.; Schlegel, H.B. *J. Am. Chem. Soc.* **1981**, 103, 7692, 7694.
45. Dedieu, A.; Veillard, A. *J. Am. Chem. Soc.* **1972**, 94, 6730.
46. Graul, S.T.; Bowers, M.T. *J. Am. Chem. Soc.* **1991**, 113, 9696.
47. Cyr, D.M.; Posey, L.A.; Bishea, G.A.; Han, C.-C.; Johnson, M.A. *J. Am. Chem. Soc.* **1991**, 113, 9697.
48. Wilbur, J.L.; Brauman, J.I. *J. Am. Chem. Soc.* **1991**, 113, 9699.
49. Fukui, K.; Hao, H.; Fujimoto, H. *Bull. Chem. Soc. Jpn.* **1969**, 42, 348.
50. Fujimoto, H.; Yamabe, S.; Fukui, K. *Bull. Chem. Soc. Jpn.* **1971**, 44, 971.
51. Ito, S.; Kakehi, A. *Bull. Chem. Soc. Jpn.* **1990**, 63, 2850.
52. Hudson, R.F. *J. Molec. Struct. (Theochem)* **1992**, 261, 91.
53. Lowe, J.P. *J. Am. Chem. Soc.* **1972**, 94, 3718.
54. Bach, R.D.; Badger, R.C.; Lang, T.J. *J. Am. Chem. Soc.* **1979**, 101, 2845.
55. Minato, T.; Yamabe, S. *J. Am. Chem. Soc.* **1985**, 107, 4621.
56. Minato, T.; Yamabe, S. *J. Am. Chem. Soc.* **1988**, 110, 4586.

57. Nguyen, M.T.; Clarke, L.F.; Hegarty, A.F. *J. Org. Chem.* **1990**, 55, 6177.
58. Lee, I.; Park, H.Y.; Lee, B.-S.; Kong, B.H.; Lee, B.C. *J. Phys. Org. Chem.* **1992**, 5, 259.
59. Pross, A.; Shaik, S.S. *J. Am. Chem. Soc.* **1982**, 104, 187.
60. Gronert, S. *J. Am. Chem. Soc.* **1991**, 113, 6041.
61. Gronert, S. *J. Am. Chem. Soc.* **1992**, 114, 6041.
62. Dewar, M.J.S.; Yuan, Y.-C. *J. Am. Chem. Soc.* **1990**, 112, 2088.
63. Dewar, M.J.S.; Yuan, Y.-C. *J. Am. Chem. Soc.* **1990**, 112, 2095.
64. Hoffmann, R.; Radom, L.; Pople, J.A.; Schleyer, P. v. R.; Hehre, W.J.; Salem, L. *J. Am. Chem. Soc.* **1972**, 94, 6221.
65. Schleyer, P. v. R.; Kos, A.J. *Tetrahedron* **1983**, 39, 1141.
66. Slater, J.C. *Quantum Theory of Molecules and Solids*, Vol. 4, McGraw-Hill, New York (1974).
67. Parr, R.G.; Yang, W. *Density-Functional Theory of Atoms and Molecules*, Oxford University Press, New York, 1989.
68. Baerends, E.J.; Ellis, D.E.; Ros, P. *Chem. Phys.* **1973**, 2, 41.
69. Boerrigter, P.M.; Velde, G. te; Baerends, E.J. *Int. J. Quantum Chem.* **1988**, 33, 87.
70. Baerends, E.J.; Ros, P. *Chem. Phys.* **1975**, 8, 412.
71. Baerends, E.J.; Ros, P. *Int. J. Quantum Chem., Quantum Chem. Symp.* **1978**, S12, 169.
72. Albright, T.A.; Burdett, J.K.; Whangbo, M.-H. *Orbital Interactions in Chemistry*, Wiley: New York, 1985.
73. Versluis, L.; Ziegler, T. *J. Chem. Phys.* **1988**, 88, 322.
74. Becke, A.D. *Int. J. Quantum. Chem.* **1983**, 23, 1915.
75. Becke, A.D. *J. Chem. Phys.* **1986**, 85, 7184.
76. Ziegler, T.; Tschinke, V.; Becke, A. *Polyhedron* **1987**, 6, 685.
77. Stoll, H.; Golka, E.; Preus, H. *Theoret. Chim. Acta* **1980**, 55, 29.
78. Vosko, S.H.; Wilk, L.; Nusair, M. *Can. J. Phys.* **1980**, 58, 1200.
79. Bickelhaupt, F.M.; Koning, L.J. de; Nibbering, N.M.M.; Baerends, E.J. *J. Phys. Org. Chem.* **1992**, 5, 179.

80. Bickelhaupt, F.M.; Nibbering, N.M.M.; Wezenbeek, E.M. van; Baerends, E.J. *J. Phys. Chem.* **1992**, 96, 4864, and references cited therein.

81. Bickelhaupt, F.M.; Fokkens, R.H.; Koning, L.J. de; Nibbering, N.M.M.; Baerends, E.J.; Goede S.J.; Bickelhaupt, F. *Int. J. Mass Spectrom. Ion Processes* **1991**, 103, 157.

82. Ziegler, T.; Tschinke, V.; Ursenbach, C. *J. Am. Chem. Soc.* **1987**, 109, 4825.

83. Ziegler, T.; Tschinke, V.; Versluis L.; Baerends, E.J. *Polyhedron* **1988**, 7, 1625.

84. Fan, L.; Ziegler, T. *J. Chem. Phys.* **1990**, 92, 3645.

85. Ziegler, T. *Chem. Rev.* **1991**, 91, 651.

86. Ziegler, T.; Rauk, A. *Theoret. Chim. Acta* **1977**, 46, 1.

87. Kato, S.; Morokuma, K. *J. Chem. Phys.* **1980**, 73, 3900.

Samenvatting

In dit proefschrift worden de resultaten van een gecombineerd Fourier Transform Ion Cyclotron Resonantie (FT-ICR) massaspectrometrisch en dichtheidsfunctionaal (DF) theoretisch onderzoek aan basegeïnduceerde eliminatiereacties beschreven (vergelijking 1). Het doel van dit onderzoek is het verkrijgen van een diepergaand begrip van de geaardheid van dit fundamentele reactietype.

$$B^- + H\text{-}C^{\beta}R_2\text{-}C^{\alpha}R_2\text{-}L \longrightarrow B\text{-}H + CR_2{=}CR_2 + L^- \qquad (1)$$

Na een algemene inleiding in hoofdstuk 1 en een beschrijving van de methoden in hoofdstuk 2 wordt in hoofdstuk 3 het effect van de vervanging van de $C^{\alpha}R_2$-groep van het substraat (vergelijking 1) door $N^{\alpha}R$ onderzocht aan de hand van de gasfasereakties van N,O-dimethylhydroxylamine (DHA: $CH_3NH\text{-}O\text{-}CH_3$) met een reeks van anionische basen. De basegeïnduceerde imine-vormende 1,2-eliminatie is het overheersende reactiekanaal, en leidt o.a. tot de vorming van de vrije (CH_3O^-) en de gesolvateerde vertrekkende groep ([CH_3O^-, HB]). De efficiëntie van de imine-vormende eliminatie van $CH_3NH\text{-}O\text{-}CH_3$ is minstens zo hoog als die van alkeen-vormende 1,2-eliminaties van eenvoudige ethers zoals b.v. $CH_3CH_2\text{-}O\text{-}C_2H_5$. De nucleofiele substitutie op stikstof blijkt een relatief effectief, concurrerend proces te zijn, dat kennelijk niet onderhevig is aan een zeer ongunstige activeringsbarriere, in tegenstelling tot de nucleofiele substitutie op koolstof in de gasfase. Dit wordt bevestigd door DF-berekeningen, die op een entropisch gunstige, d.w.z. "losse", S_N1-achtige overgangstoestand wijzen.

In hoofdstuk 4 wordt het effect van de integratie van de C^{α}-L-binding in een cyclische structuur op het reactiviteitspatroon van de basegeïnduceerde alkeen-vormende 1,2-eliminatie onderzocht aan de hand van het substraat tetrahydrofuraan (THF). De anionische basegeïnduceerde reakties van THF verlopen overwegend via de 1,2-eliminatie, welke in eerste instantie tot de

vorming van het rovibrationeel aangeslagen, HB-gesolvateerde but-3-een-1-oxide anion leidt. In afwezigheid van thermische wisselwerking met de omgeving, verdampt HB uit deze aangeslagen gesolvateerde ionen. Afhankelijk van de aard van de base, elimineert een gedeelte van de aangeslagen but-3-een-1-oxide anionen een waterstof molecuul of formaldehyde. Een interessant fenomeen is de efficiente vorming van het gehydrateerde hydroxide-ion, [H_2O, OH^-], in de reactie van het but-3-een-1-oxide anion met water. Het reactiemechanisme omvat een endotherme proton-overdracht van water naar het but-3-een-1-oxide anion, gevolgd door een reversibel hydroxide-geïnduceerd E1cb-proces, en leidt tot de eliminatie van 1,3-butadieen en vorming van het gehydrateerde hydroxide-ion (vergelijking 2). Een interessant aspect van deze 1,2-eliminatiereactie is de onafhankelijke toegang tot een tussenproduct (**I**), dat waarschijnlijk ook in de basegeïnduceerde 1,4-eliminatie optreedt (vergelijking 2).

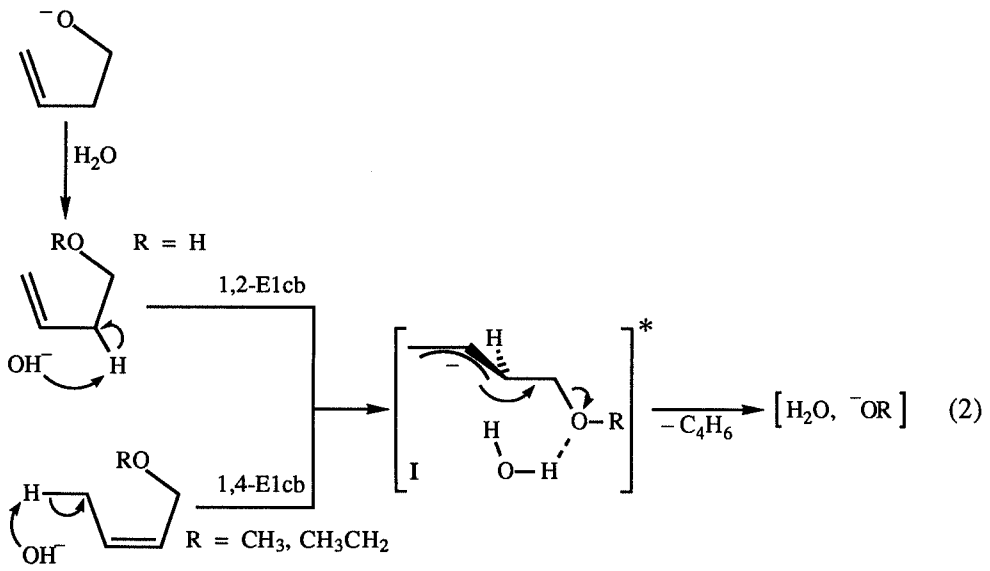

(2)

Vervolgens worden in hoofdstuk 5 de meerstapsprocessen in de gasfase-reacties van halogeenmethyl anionen XCH_2^- (X = Cl, Br) met CH_3X en NH_3 onderzocht. In een atmosfeer van CH_3X en NH_3 reageert XCH_2^- via drie concurrerende reactiemechanismen: i) éénstaps-S_N2-substitutie van XCH_2^- op CH_3X (directe S_N2); ii) als alternatief kan het relatief langlevende producten-complex $[XCH_2CH_3 \bullet\bullet\bullet X^-]^*$ van de S_N2-substitutie in een X^--geïnduceerde 1,2-

eliminatie omgezet worden (tweestaps-S_N2/E2, vergelijking 3), iii) XCH_2^- kan met ammoniak reageren via een endotherme proton-transfer (PT) van NH_3 naar XCH_2^- gevolgt door een zeer exotherme S_N2 substitutie door het resulterende amide-ion op XCH_3 (PT/S_N2). Theoretische berekeningen tonen aan, dat de PT/S_N2-reactie via twee aparte fasen verloopt, echter zonder optreden van een stabiel tussenproduct. Deze reactie is dus *geen* tweestaps- maar een éénstapsproces.

$$XCH_2^- + CH_3X \xrightarrow{S_N2} [XCH_2CH_3 \cdots X^-]^* \xrightarrow{E2} HX + C_2H_4 + X^- \qquad (3)$$

Tenslotte worden in hoofdstuk 6 de resultaten van een theoretisch onderzoek aan de reacties van het modelsysteem $F^- + C_2H_5F$ bechreven. Zoals blijkt, speelt de base een sleutelrol als katalysator, die de anti- en syn-eliminatie sterk beïnvloedt. De thermische eliminatie van HF uit fluorethaan verloopt bij voorkeur met syn-stereochemie. In aanwezigheid van de basische katalysator wordt de overgangstoestand van de anti-eliminatie selectief gestabiliseerd. Dit leidt tot de voorkeur van anti-E2- boven syn-E2-eliminatie. De hoofdreden voor de selectiviteit zijn de lage energie en de daaruit voortvloeiende uitstekende acceptor-eigenschappen van de C_2H_5F-8a' LUMO (σ anti-bindend voor CC-H en C^α-F; Figuur 1) in de sterk gedeformeerde, losse anti-E2-overgangstoestand. De 8a' LUMO heft effectief een gedeelte van de Pauli-repulsie tussende base-$2p_z$ HOMO en de C_2H_5F-5a' (σ bindend voor CC-H en C^α-F) op, en heeft een sterke donor/acceptor-wisselwerking met de base-$2p_z$ HOMO.

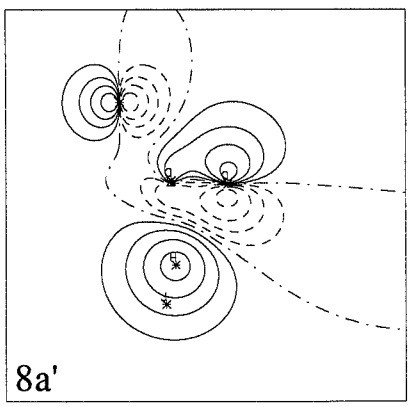

Figuur 1. *De C_2H_5F-8a' LUMO in de overgangstoestand van de anti-E2-eliminatie.*

De voorkeur van de basegeïnduceerde eliminatie boven de nucleofiele substitutie in de gasfase wordt toegeschreven aan de preferentiële vorming van het anti-E2-reactanten-complex, als ook aan de lagere energie- en entropiebarriere voor de anti-E2-eliminatie. De onderzochte basegeïnduceerde eliminaties behoren tot de E2H-categorie. In de overgangstoestand treden geen E2C-achtige interacties op. De syn-E2-eliminatie heeft een E1cb-karakter, terwijl de anti-E2-overgangstoestand in principe de geometrie van een centrale E2-reactie bezit. Een belangrijke karakteristieke eigenschap van de anti-E2-eliminatie is de opvallende migratie van het te abstraheren proton van de C^{β}- naar de C^{α}-positie in de overgangstoestand. Het E2H-formalisme voorziet niet in de beschrijving van zo'n migratie.

Zusammenfassung

Diese Dissertation beschreibt die Resultate einer kombinierten Fouriertransformation-Ionenzyklotronresonanz-(FT-ICR)-massenspektrometrischen und Dichtefunktional-(DF)-theoretischen Untersuchung über baseninduzierte Eliminierungsreaktionen (Gleichung 1). Das Ziel ist die Erlangung eines tiefergehenden Verständnises der Natur dieses fundamentellen Reaktionstyps.

$$B^- + H\text{-}C^{\beta}R_2\text{-}C^{\alpha}R_2\text{-}L \longrightarrow B\text{-}H + CR_2{=}CR_2 + L^- \qquad (1)$$

Nach einer algemeinen Einleitung in Kapitel 1 und einer Beschreibung der Methoden in Kapitel 2 wird in Kapitel 3 der Effekt des Austausches der $C^{\alpha}R_2$-Gruppe des Substrats (Gleichung 1) durch $N^{\alpha}R$ untersucht an Hand der Gasphasenreaktionen von N,O-Dimethylhydroxylamin (DHA: $CH_3NH\text{-}O\text{-}CH_3$) mit einer Reihe anionischer Basen. Die baseninduzierte imin-bildende 1,2-Eliminierung stellt den überwiegenden Reaktionskanal dar und führt u.a. zur Bildung der freien (CH_3O^-) und der solvatierten Abgangsgruppe ([CH_3O^-, HB]). Die Effizienz der imin-bildenden Eliminierung von $CH_3NH\text{-}O\text{-}CH_3$ ist mindestens so hoch wie die von alken-bildenden 1,2-Eliminierungen einfacher Ether wie z.B. $CH_3CH_2\text{-}O\text{-}C_2H_5$. Die nukleophile Substitution an Stickstoff offenbart sich als ein verhältnismäßig effektiver, konkurrierender Prozeß, der offensichtlich keine sehr ungünstige Aktivierungsbarriere hat, im Gegensatz zur nukleophilen Substitution an Kohlenstoff in der Gasphase. Dieses wird bestätigt durch DF-Rechnungen, die auf einen entropisch günstigen, d.h. "losen", S_N1-artigen Übergangszustand deuten.

In Kapitel 4 wird der Effekt der Integration der C^{α}-L-Bindung in eine zyklische Struktur auf das Reaktivitätsmuster der baseninduzierten alken-bildenden 1,2-Eliminierung untersucht am Beispiel des Substrats Tetrahydrofuran (THF). Die anionischen baseninduzierten Reaktionen von THF verlaufen vorwiegend über die 1,2-Eliminierung, welche zuerst zur Bildung des rovibrationel angeregten, HB-solvatierten But-3-en-1-oxid-Anions führt. In Abwesenheit thermischer Wechsel-

wirkung mit der Umgebung, verdampft HB aus diesen angeregten solvatierten Ionen. Abhängig von der Art der Base eliminiert ein Teil der angeregten But-3-en-1-oxid-Anionen molekularen Wasserstof oder Formaldehyd. Interessanterweise führt die Reaktion des But-3-en-1-oxid Anions mit Wasser zur effizienten Bildung des hydratierten Hydroxid-Ions, [H_2O, OH^-]. Der Reaktionsmechanismus umfaßt eine endotherme Protonübertragung von Wasser zum But-3-en-1-oxid-Anion, gefolgt von einem reversiblen hydroxid-induzierten E1cb-Prozeß, und führt zur Eliminierung von 1,3-Butadien und zur Bildung des hydratierten Hydroxid-Ions (Gleichung 2). Ein interessanter Aspekt dieser 1,2-Eliminierungsreaktion ist der unabhängige Zugang zu einem Zwischenprodukt (**I**), welches wahrscheinlich auch in der baseninduzierten 1,4-Eliminierung auftritt (Gleichung 2).

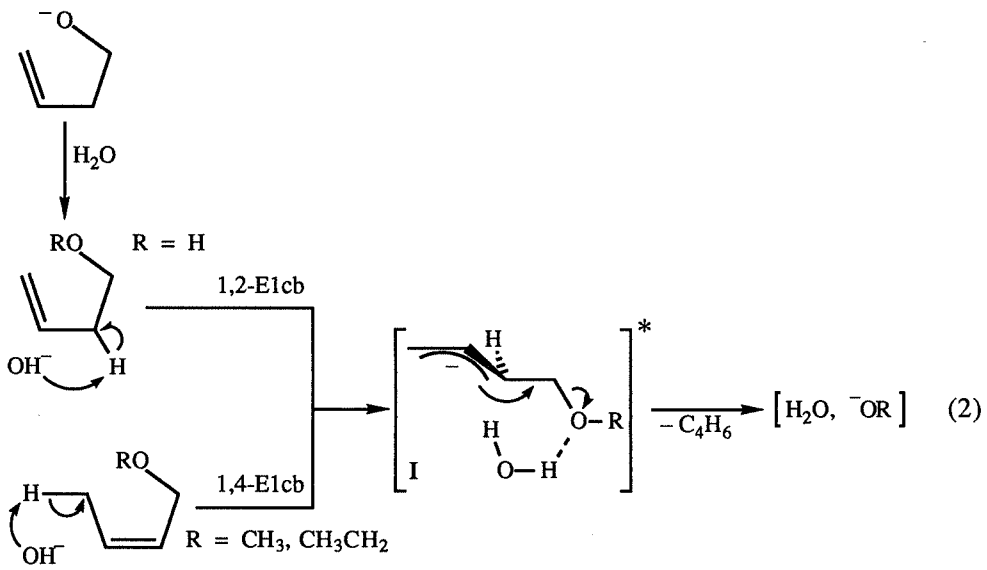

(2)

Im folgenden Kapitel 5 werden die mehrstufigen Prozesse in den Gasphasenreaktionen von Halogenmethyl-Anionen XCH_2^- (X = Cl, Br) mit CH_3X und NH_3 erforscht. In einer Atmosphere von CH_3X und NH_3 reagiert XCH_2^- über drei konkurrierende Reaktionsmechanismen: i) Einschritts-S_N2-Substitution von XCH_2^- an CH_3X (direkte S_N2); ii) als Alternative kann der relativ langlebige Produktkomplex $[XCH_2CH_3 \cdots X^-]^*$ der S_N2-Substitution in einer X^--induzierten 1,2-Eliminierung weiterreagieren (zweistufige S_N2/E2, Gleichung 3); iii) XCH_2^- kann mit Ammoniak

reagieren über einen endothermen Proton-Transfer (PT) von NH_3 zu XCH_2^-, gefolgt von einer sehr exothermen S_N2-Substitution durch das resultierende Amid-Ion am XCH_3 (PT/S_N2). Theoretische Rechnungen zeigen, daß die PT/S_N2-Reaktion in zwei unterschiedlichen Phasen verläuft, jedoch ohne Auftreten eines stabilen Zwischenprodukts. Diese Reaktion ist also *kein* zweistufiger sondern ein einstufiger Prozeß.

$$XCH_2^- + CH_3X \xrightarrow{S_N2} [XCH_2CH_3 \cdots X^-]^* \xrightarrow{E2} HX + C_2H_4 + X^- \qquad (3)$$

Zum Schluß, in Kapitel 6, werden die Resultate einer theoretischen Untersuchung der Reaktionen des Modelsystems $F^- + C_2H_5F$ bechrieben. Wie sich herausstellt, spielt die Base eine Schlüsselrolle als Katalysator, der die anti- und syn-Eliminierung stark beeinflußt. Die thermische Eliminierung von HF aus Fluorethan verläuft vorzugsweise mit syn-Stereochemie. In Anwesenheit des basischen Katalysators wird selektiv der Übergangszustand der anti-Eliminierung stabilisiert. Dieses führt zur Prevalenz von anti-E2- über syn-E2-Eliminierung. Der Hauptgrund für die Selektivität sind die relativ niedrige Energie und, demzufolge, die ausgezeichneten Akzeptor-Eigenschaften des C_2H_5F-8a' LUMO (σ anti-bindend für CC-H und C^{α}-F; Abbildung 1) im stark deformierten, losen anti-E2-Übergangszustand. Der 8a' LUMO hebt effektief einen Teil der Pauli-Repulsion zwischen dem Base-$2p_z$ HOMO und dem C_2H_5F-5a' (σ bindend für CC-H und C^{α}-F) auf, und hat eine starke Donor/Akzeptor-Wechselwirkung mit dem Base-$2p_z$ HOMO.

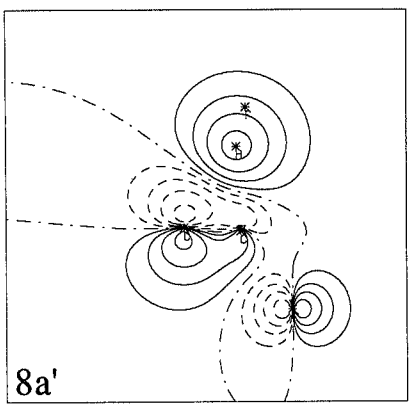

Abbildung 1. *Der C_2H_5F-8a' LUMO im Übergangszustand der Anti-E2-Eliminierung.*

Die Prävalenz der baseninduzierten Eliminierung über die nukleophile Substitution in der Gasphase wird durch die vorzugsweise Bildung des anti-E2-Reaktantkomplexes, sowie die niedrigere Energie- und Entropiebarriere für die anti-E2-Eliminierung erklärt. Die untersuchten basen-induzierten Eliminierungen gehören der E2H-Kategorie an. Im Übergangszustand finden keine E2C-artigen Wechselwirkungen statt. Die syn-E2-Eliminierung hat einen E1cb-Charakter, während der anti-E2-Übergangszustand im Wesentlichen die Geometrie einer zentralen E2-Reaktion aufweist. Ein wichtiges Karakteristikum der anti-E2-Eliminierung, welchem der E2H-Formalismus keine Rechnung trägt, ist die auffallende Wanderung des zu abstrahierenden Protons von der C^{β}- zur C^{α}-Position im Übergangszustand.

Summary

In this thesis, base-induced elimination reactions (Equation 1) have been investigated in a combined Fourier Transform Ion Cyclotron Resonance (FT-ICR) mass spectrometric and high-level density-functional (DF) theoretical approach. The purpose of the investigations is to obtain a deeper understanding of the nature of this fundamental class of reactions.

$$B^- + H\text{-}C^{\beta}R_2\text{-}C^{\alpha}R_2\text{-}L \longrightarrow B\text{-}H + CR_2{=}CR_2 + L^- \quad (1)$$

After a general introduction in chapter 1 and a description of the methods in chapter 2, the effect of replacement of the $C^{\alpha}R_2$ group of the substrate (Equation 1) by $N^{\alpha}R$ is studied in chapter 3 through investigation of the gas-phase reactivity of N,O-dimethylhydroxylamine (DHA: $CH_3NH\text{-}O\text{-}CH_3$) towards a series of anionic bases. Base-induced imine-forming 1,2-elimination constitutes the dominating pathway which, amongst others, results in the production of the free (CH_3O^-) and the solvated leaving group ([CH_3O^-, HB]). The efficiency of the imine-forming elimination reactions of $CH_3NH\text{-}O\text{-}CH_3$ is at least as high as that of base-induced alkene-forming 1,2-elimination reactions of corresponding simple ethers such as $CH_3CH_2\text{-}O\text{-}C_2H_5$. Nucleophilic substitution at the nitrogen atom is found to be a relatively facile, competing process. Apparently, it does not suffer from a very unfavorable activation barrier which is assumed to hamper nucleophilic substitution reactions on carbon atoms in the gas phase. This seems to be supported by DF calculations which indicate that the nucleophilic substitution on the nitrogen atom proceeds via an entropically favored, loose, S_N1-like transition state.

In chapter 4 the effect of integration of the C^{α}-L bond into a cyclic structure on the reactivity pattern of base-induced alkene-forming 1,2-eliminations is investigated using tetrahydrofuran (THF) as the substrate. The anionic base-induced reactions of THF predominantly proceed by 1,2-elimination, initially resulting in rovibrationally excited HB-solvated but-3-ene-1-

oxide anions. In the absence of thermal interaction with the environment, HB is vaporized from these excited solvated ions. Depending on the nature of the base used, a proportion of the excited but-3-ene-1-oxide anions is found to eliminate molecular hydrogen or formaldehyde. Interestingly, reaction between the but-3-ene-1-oxide ion and water results in the very efficient formation of hydrated hydroxide ions, [H_2O, OH^-]. The reaction mechanism involves an endothermic proton transfer from water to the but-3-ene-1-oxide anion which is followed by a reversible hydroxide-induced E1cb process, leading to the elimination of 1,3-butadiene and formation of the hydrated hydroxide ion (Equation 2). An interesting aspect of this 1,2-elimination reaction is that it provides an independent route to a type of intermediate (**I**) which may also occur in base-induced diene-forming 1,4-elimination reactions (Equation 2).

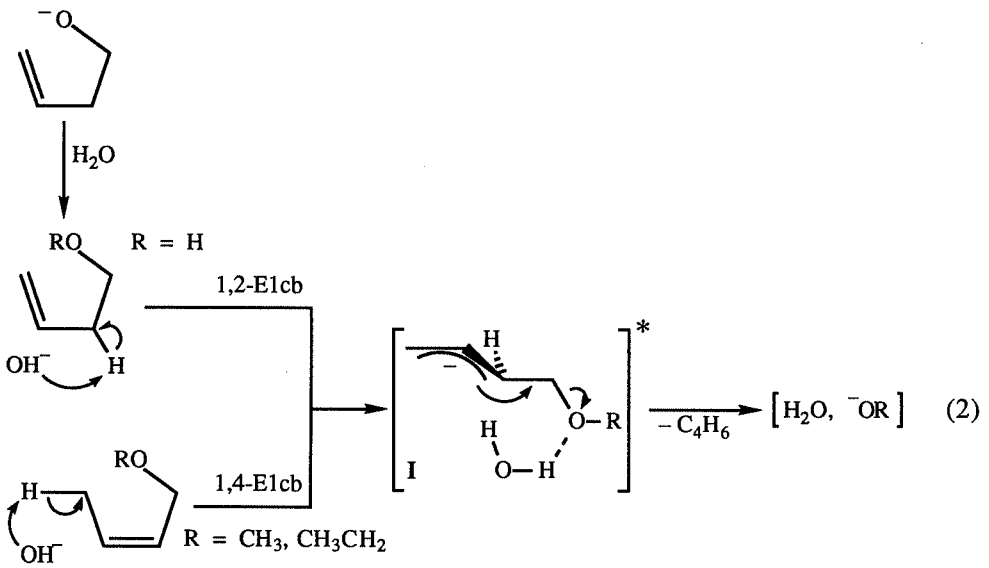

(2)

Next, in chapter 5, the multi-step processes in the gas-phase reactions of halomethyl anions XCH_2^- (X = Cl, Br) with CH_3X and NH_3 are studied. In an atmosphere of CH_3X and NH_3, XCH_2^- reacts via three competing reaction mechanisms: i) one-step S_N2 substitution of XCH_2^- on CH_3X (direct S_N2); ii) alternatively, the relatively long-lived product complex $[XCH_2CH_3 \cdots X^-]^*$ of the S_N2 substitution undergoes X^--induced 1,2-elimination (two-step S_N2/E2, Equation 3); iii) finally, XCH_2^- can react with ammonia by consecutive endothermic proton transfer (PT) from

NH_3 to XCH_2^- and a very exothermic S_N2 substitution of the resulting amide on XCH_3 (PT/S_N2). Theoretical calculations show that the PT/S_N2 reaction proceeds in two distinct phases, but has no stable intermediate. Therefore, this reaction is *not* a two-step, but a one-step process.

$$XCH_2^- + CH_3X \xrightarrow{S_N2} [XCH_2CH_3 \cdots X^-]^* \xrightarrow{E2} HX + C_2H_4 + X^- \quad (3)$$

Finally, in chapter 6, a theoretical investigation has been performed on the reactions of the $F^- + C_2H_5F$ model system. The base has been found to play a key role as a catalyst which strongly influences the competition between anti- and syn-elimination. The thermal elimination of HF from fluoroethane preferentially proceeds via the syn pathway. Upon catalysis by the base, the transition state of the anti-mode is selectively stabilized, leading to the prevalence of anti-E2 over syn-E2 elimination. The main reason for this selective stabilization is the very low energy and, consequently, the good acceptor capability of the C_2H_5F-8a' LUMO (σ anti-bonding for CC-H and C^{α}-F; Figure 1) in the strongly rearranging, loose anti-E2 transition state. This 8a' LUMO effectively relieves the Pauli repulsion which the base-$2p_z$ HOMO has with the C_2H_5F-5a' (σ bonding for CC-H and C^{α}-F) and has a strong donor/acceptor interaction with the base-$2p_z$ HOMO.

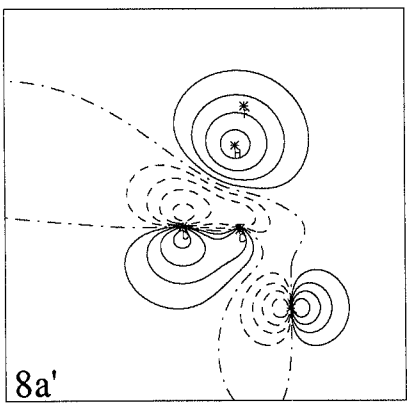

Figure 1. *The C_2H_5F-8a' LUMO in the transition state of the anti-E2 elimination reaction.*

The prevalence of the gas-phase base-induced elimination over the nucleophilic substitution is ascribed to the preferential formation of the anti-E2 reactant complex as well as to the lower energy and entropy barrier for the anti-E2 elimination. The base-induced eliminations studied are of the E2H category. No E2C-like interactions are present in the transition state. The syn-E2 elimination is E1cb-like, whereas the anti-E2 elimination is virtually central E2. An important characteristic of the anti-E2 elimination, which is not contained in the E2H formalism, is the pronounced shift of the abstracted proton from the C^{β} to the C^{α} position in the transition state.

Dankwoord

Tenslotte wil ik iedereen bedanken die aan de totstandkoming van dit proefschrift heeft bijgedragen. Een aantal mensen wil ik met name noemen:

Mijn promotor Nico Nibbering wil ik bedanken voor zijn steun, zijn waardevolle adviezen en de ruimte die hij mij gegeven heeft om zelfstandig onderzoek te doen. Zijn vertrouwen in mij en mijn voornemen om experiment en theorie gecombineerd in te zetten voor het oplossen van chemische problemen was een noodzakelijke voorwaarde voor het welslagen van mijn promotie-onderzoek.

Mijn co-promotor Evert Jan Baerends wil ik eveneens bedanken voor zijn steun en het vertrouwen dat hij in mij gesteld heeft. De vele discussies met hem waren altijd zeer verhelderend en inspirerend. Zijn streven om uit de berekeningen *meer* te verkrijgen dan alleen kwantitatieve resultaten, namelijk kwalitatief inzicht, dus het willen *begrijpen* van chemie, heeft mij zeer aangesproken.

Op deze plaats wil ik ook Leo de Koning noemen. Hij heeft een belangrijke rol gespeeld bij mijn promotieonderzoek.

Met Jaap Snijders heb ik vele waardevolle en leuke discussies gehad op wetenschappelijk gebied, maar ook daarbuiten.

De hulp van Frans Pinkse, Jan Brandt en John Smit bij het draaiende houden van de massaspectrometers en andere apparatuur was van essentiëel belang. Tineke Molenaar heeft mij veel geholpen bij het uitvoeren van organische syntheses. Roel Fokkens wil ik bedanken voor de prettige samenwerking bij het isodicyaan-project. Steen Ingemann heeft mij veel nuttige adviezen gegeven. Piet Kistemaker dank ik voor zijn belangstelling voor mijn werk.

Pieter Vernooijs ben ik zeer erkentelijk voor zijn vele hulp bij het oplossen van technische problemen bij het uitvoeren van ADF-berekeningen op de main frames en supercomputers van SARA.

Godfried Buisman dank ik voor de prettige en succesvolle samenwerking bij het 1,4-eliminatie-project.

Met Egbert van Wezenbeek heb ik een goede en plezierige samenwerking gehad bij het CN-dimeren project.

Klaas Jan van den Berg, Guido U-A-Sai, Ivo Freriks, Albert Heck, Herman Zappey, Astrid Crabbendam en Renée Peerboom wil ik bedanken voor de goede wetenschappelijke en vriendschappelijke samenwerking. Mijn dank gaat verder uit naar Holger von Köding, Margot van Amsterdam, Henri Matimba, Monique Born, Paul Staneke, Lies Hoogeveen, Chris Kort en Han Peeters voor de collegiale sfeer.

Thomas Drewello möchte ich herzlich danken für viele wertvolle Diskussionen, für die Führung im Hahn-Meitner-Institut und für die Einführung ins Nachtleben von Berlin.

Eric Kirchner, Robert van Leeuwen, Ad van Eulem, Erik van Lenthe, Margot Vlot, Marcel Nooijen, Bert te Velde, Paul Nederkoorn, Rob Middelhoek, Walter Ravenek, Gijsbert Wiesenecker en Pier Philipsen dank ik voor hun collegialiteit en hun bijdrage aan de prettige sfeer bij "Theoretisch".

Mijn paranimfen John Groebe en Klaas Jan van den Berg ben ik zeer erkentelijk voor hun hulp bij de voorbereidingen voor de promotie.

Célia ben ik zeer dankbaar voor haar ondersteuning bij mijn werk. Door haar adviezen, maar ook door het inplakken van figuren in het manuscript, heeft zij een directe bijdrage geleverd aan het gereedkomen van dit proefschrift.

Mijn ouders en mijn zusje Christina ben ik veel dank verschuldigd voor hun interesse in en hun steun bij mijn werk. Mede dankzij de goede raad die zij mij altijd gegeven hebben is mijn promotieonderzoek voorspoedig verlopen.

List of Publications

1. Bickelhaupt, F.M.; Baerends, E.J.; Ravenek, W.
   Inorg. Chem. **1990**, 29, 350-354.
   Model Systems for Initial Stages of Oxidative-Addition Reactions. Theoretical Investigation of η^1 and η^2 Coordination of F_2 and H_2 to $PtCl_4^{2-}$ and $Cr(CO)_5$

2. Kraakman, P.A.; Valk, J.-M.; Niederländer, H.A.G.; Brouwer, D.B.E.; Bickelhaupt, F.M.; Wolf, W.H. de; Bickelhaupt, F.; Stam, C.H.
   J. Am. Chem. Soc. **1990**, 112, 6638-6646.
   Unusual Reactivity of Small Cyclophanes: Nucleophilic Attack on 11-Chloro- and 8,11-Dichloro[5]metacyclophane

3. Bickelhaupt, F.M.; Fokkens, R.H.; Koning, L.J. de; Nibbering, N.M.M.; Baerends, E.J.; Goede, S.J.; Bickelhaupt, F.
   Int. J. Mass Spectrom. Ion Processes **1991**, 103, 157-168.
   Isolated Excited Electronic States in the Unimolecular Gas-Phase Ion Dissociation Processes of the Radical Cations of Isocyanogen and Cyanogen

4. Bickelhaupt, F.M.; Koning, L.J. de; Nibbering, N.M.M.; Baerends, E.J.
   J. Phys. Org. Chem. **1992**, 5, 179-190; see **Chapter 5**.
   Multistep Processes in Gas-Phase Reactions of Halomethyl Anions XCH_2^- (X = Cl, Br) with CH_3X and NH_3

5. Bickelhaupt, F.M.; Nibbering, N.M.M.; Wezenbeek, E.M. van; Baerends, E.J.
   J. Phys. Chem. **1992**, 96, 4864-4873.
   Central Bond in the Three $CN^{\bullet}$ Dimers NC-CN, CN-CN and CN-NC: Electron Pair Bonding and Pauli Repulsion Effects

6. Bickelhaupt, F.M.; Koning, L.J. de; Nibbering, N.M.M.
   Submitted for publication; see **Chapter 3.**
   Base-Induced Imine-Forming 1,2-Elimination Reactions in the Gas Phase

7. Bickelhaupt, F.M.; Koning, L.J. de; Nibbering, N.M.M.
   Tetrahedron, accepted for publication; see **Chapter 4.**
   Anionic Ether Cleavage of THF in the Gas Phase

8. Bickelhaupt, F.M.; Baerends, E.J.; Nibbering, N.M.M.; Ziegler, T.
   Submitted for publication; see **Chapter 6.**
   Theoretical Investigation on Base-Induced 1,2-Eliminations in the Model System F^{-} + CH_3CH_2F. The Role of the Base as Catalyst

9. Bickelhaupt, F.M.; Buisman, G.J.H.; Koning, L.J. de; Nibbering, N.M.M.; Baerends, E.J.
   To be submitted for publication.
   Base-Induced Diene-Forming 1,4-Elimination Reactions in the Gas Phase